DEVELOPMENT OF DIGITAL SHEAROGRAPHY FOR COMPLEX DEFECTS INSPECTION

by

BOYANG ZHANG

A dissertation submitted in partial fulfillment of the
requirements for the degree of

DOCTOR OF PHILOSOPHY IN MECHANICAL ENGINEERING

2021

Oakland University
Rochester, Michigan

Doctoral Advisory Committee:

Lianxiang Yang, Ph.D., Chair
Gary Barber, Ph.D.
Hongwei Qu, Ph.D.
Rodrigue Roger Emile Narainen, Ph.D.

I would like to dedicate this dissertation to my parents
for effort and love in bringing me up to be a better individual

ACKNOWLEDGMENTS

I would like to express my special appreciation and thanks to my supervisor, Prof. Lianxiang Yang, who led me on this road of academics and life. Your advice on both research as well as on my career has been invaluable. I would also like to thank my committee members, Professor Gary Barber, Professor Hongwei Qu, Dr. Rodrigue Narainen for serving as my committee members. Your brilliant comments and suggestions gave me so much support on my dissertation. I also want to thank my colleagues, all the professors and other faculties who help me in my work and life. Without help and support from you, I surely will not succeed.

Boyang Zhang

PREFACE

Digital Shearography and other speckle interferometry technologies have been invented for decades, but so far these technologies are still considered to be too advanced in large range applications in industrial situations. I believe the essential issue is that we need to make a wide range of adjustments to the system to complete the measurement work in different conditions, which undoubtedly increases the cost and labor. A series of studies in this paper are aimed at improving the universality of the technology, simplifying the complexity of the equipment, and achieving unified measurements approach for various special conditions. Only by further optimizing this technology can humans truly benefit in the future.

ABSTRACT

DEVELOPMENT OF DIGITAL SHEAROGRAPHY FOR COMPLEX DEFECTS INSPECTION

by

Boyang Zhang

Adviser: Lianxiang Yang, Ph.D.

Digital shearography measures the first derivative of the object surface deformation, which has the advantages of high sensitivity, full field, non-contact, real-time and anti-disturbance. It is widely used in materials inspection in industry. The information acquisition methods of the first derivative distribution are mainly divided into the intensity method and the phase shift method. The intensity method is to directly obtain the first derivative phase distribution by subtracting the light intensity map. The phase shift method to obtain phase information can be divided into temporal phase shift and spatial phase shift. Most digital shearography systems are single camera based and can only capture one image every shoot. However, unpredictable defects like the narrow crack and minor flaws could induce incomplete detection due to some limitations. There are two major issues on the measurement, one is the defect with the irregular shape which is not sensitive to the digital shearography, another is the deformation made of defects that is much smaller than the resolution of cameras. Digital Shearography measures the first derivative of deformation on the object surface Because the shearing direction determines the derivative direction being measured, tests using multiple shearing

directions are sometimes required to detect all kinds of defects. When the deformation is long and narrow as a crack while the shearing direction is perpendicular to the crack growing direction, digital shearography has the best sensitivity. In opposite, if the crack growing direction is parallel to the shearing direction, digital shearography is not able to find it out. Irregular shape defects detection is a tough challenge for digital shearography. Another challenge is the defects that are too small for the field of view. The limited pixels can miss the defects due to the low signal to noise ratio. To increase the sensitivity of detecting minor defects, a small field of view measurement is needed but it is time consuming in a large surface area inspection. The new development can be divided into three categories: 1) Modified Michelson interferometer based dual shearing digital shearography. 2) Spatial light modulator based dual shearing direction shearography. 3) Polarized digital shearography for simultaneous dual sensitive measurement. The basic theory, optical path analysis, preliminary studies, results analysis and research plan are shown in detail in this dissertation.

TABLE OF CONTENTS

TABLE OF CONTENTS—Continued

LIST OF FIGURES

LIST OF ABBREVIATIONS

NDT	Non-Destructive Testing
PSPI	Photographic speckle pattern interferometry
ESPI	Electronic speckle pattern interferometry
DSPI	Digital speckle pattern interferometry
PS	Photographic shearography
ES	Electronic shearography
DS	Digital shearography
DIC	Digital Image correlation
CCD	Charge-Couple Device
CMOS	Complementary metal oxide semiconductor
PZT	Piezoelectric Ceramics
OPD	Optical Path Difference
SLM	Spatial Light Modulator

CHAPTER ONE

INTRODUCTION AND SCOPE OF WORK

New composite materials are becoming more and more popular in practice with the development of science and technology. When the composite material is subjected to external loading, a certain amount of deformation may occur on the outside of the composite material due to defects, design mistakes and delamination [1, 2]. These deformations and defects will have a serious impact on the performance of the material, even damage the equipment, leading to accidents [3]. The conventional contact measurement method is inefficient while the direct contact with the material during the detection process may affect the detection accuracy [4]. In this case, non-contact, full-field, and non-destructive speckle interference technology has become a popular technology in composite material testing [5-7].

The conventional NDT methods for defect testing include X-ray, Ultrasonic testing, etc. However, such NDT methods need to make the light or sound penetrate the object during the inspection which usually has poor performance because a large amount of composite materials like carbon fiber which have irregular clearance inside. The testing results could have a pretty low signal to noise ratio. Speckle pattern interferometry works on the object surface instead of getting into the object. Defects inside the body perform a special deformation under loading. Thus, The speckle pattern techniques have more advantages than the conventional NDT methods [8-10].

Speckle pattern interferometry plays an important role in laser interference technology [11]. In recent decades of development, speckle pattern interferometry can be divided into Photographic speckle pattern interferometry (PSPI), Electronic speckle pattern interferometry (ESPI) and Digital speckle pattern interferometry (DSPI) [11-13]. Similarly, the shearing speckle interferometry can also be divided into shearing Photographic shearography (PS), electronic shearography (ES) and Digital shearography (DS) [14-16].

Among the technologies mentioned above, the latest and most widely used is Digital shearography. Digital shearography directly measures the deformation gradient (strain components). It has the advantages of being full field, non-contact, highly sensitive and robust. Compared to non-coherent measurement methods (such as strain gauge and DIC), it has a much higher measurement resolution. Compared to other coherent measurement methods (such as holographic interferometry or ESPI), it is more robust and applicable for in-field tests [17-18].

However, the unpredictable defects could induce incomplete detection. There are two major issues on the measurement, one is the defect with an irregular shape, which is not sensitive to the digital shearography, another is the deformation made of defects that is much smaller than the resolution of cameras.

Digital shearography is sensitive to its shearing direction. For example, X-direction shearing shearographic system can barely detect the defects which have a large cross section in the X-direction but a small cross section in the Y direction. Similarly, Y-direction shearing shearographic system can barely detect the defects which have a large cross section in the Y-direction but a small cross section in the X-direction. Such defects are very common, such as cracks in pipes, scratches in car shells inner side, and fractures in some composite materials. Two shearographic systems or multi times measurement is needed for avoiding the loss of defects. Two systems are arranged in two orthogonal shear directions to inspect the same object or doing twice tests with a single system in orthogonal shearing directions. Both ways increase the cost and labor but may not obtain consistent results because of accumulated errors in different systems and different testing conditions. This kind of problem puts forward specific measurement requirements for Digital Shearography. When the measurement conditions are known, Customizing the device according to the actual situation is a common approach to solve the issue. In the case defects possible shapes are unknown, the only we can do is multiple attempts of testing. This situation highly limits the development of Digital Shearography. The first thinking is to develop a system that can detect defects of various shapes under limited cost conditions.

The second problem is more complicated. As the Figure. 1.1 shown, it is testing from Optical Measurement Solution Ltd made by D Francis and RP Tatam [20]. A hailstorm damaged aircraft fuselage is detected by Digital Shearography with vibration excitation. The detected plane and the area are shown in (a) and (b), the phase wrapping, and the unwrapping result are shown in (c) and (d). It is very clear to see that there are many shearograms on the detection areas of different sizes. This situation generally indicates that there are deformations of different sizes on the surface, which often comes from the following situations, the size of the defect is different, the depth of the defect from the surface is different, and the sensitivity of the defect to the current load is different. Usually, small size defects could affect small deformation zone and deep defects could generate minor deformation. Besides, loading effects like resonance frequency could be another reason. Because the measurement is not the size of the defect

(a)

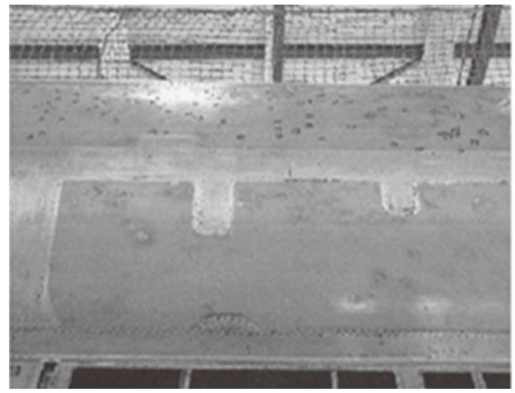

(b)

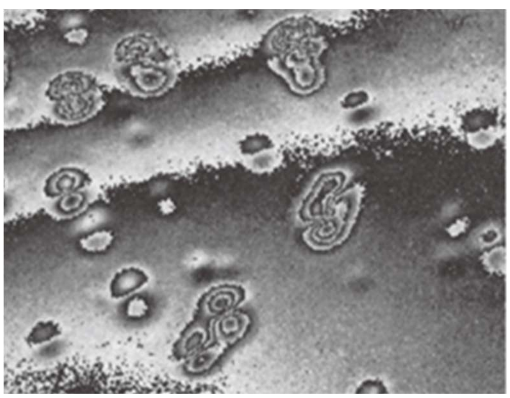

(b)

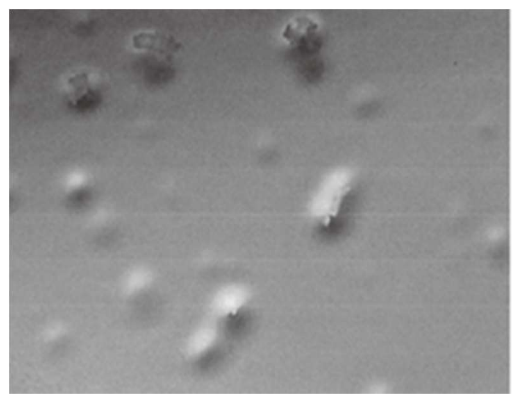

(d)

Figure 1.1. Digital Shearography detection results of a hailstorm damaged aircraft fuselage. (a) The plane suffered from a hailstorm; (b) The area was detected; (c) The phase wrapping map of shearograms; and (d) The unwrapping results

itself, but the size of the deformation caused by the defect. Therefore, it cannot be explained that a smaller shearogram will be relatively safe. It is still necessary to capture all the shearogram on the surface. However, Digital Shearography usually works on a single camera with a single window. As a fulfilled measurement technique, limit resolution means limit data amount. In a fixed field of view test, Digital Shearography is highly possible to lose the small shearograms due to reason of low signal to noise ratio and too large surface deformation which could cover the other small deformation. The conventional solution is the same that multiple device and multiple times testing. When the proposed two problems come together, Digital Shearography may face a huge challenge on the defect detection. The second thinking is to develop a dual resolution Digital Shearography to capture the small shearograms in a large field of view.

This Ph.D. dissertation research introduces a new series of Digital Shearography systems to acquire a utility solution of defects detection problems of different defect shape and shearograms size. With different optical setup and phase shift arrangement, proposed system is capable to achieve a variety of measurement tasks using only a single camera with dynamic test. Catalog by the basic setups, the developments can be divided into three categories: 1) Modified Michelson interferometer based dual shearing digital shearography. 2) Spatial light modulator based dual shearing direction shearography. 3) Dual resolution shearography for small shearograms detection from large field of view.

In this dissertation, Chapter One gives the introduction and scope of works. Chapter Two introduces the basic theory of spatial digital shearography. Chapter Three reviews the phase shift technique. Chapter Four introduces an innovative Modified Michelson interferometer based dual shearing digital shearography. The system can simultaneously measure the X shearing and Y shearing results to capture all the defects in case of the irregular shape that cannot be found by the conventional Digital Shearography. In the Fifth chapter, A spatial light modulator based dual shearing direction shearography is introduced to solve dual shearing issue but with better phase map quality and more compact and simple structure. Chapter Six introduces a novel dual resolution shearography system that can simultaneously acquire two different field of view with different resolution. Using this system, a small filed high-resolution searching can be made with a full large field measurement to avoid miss the small shearograms. In the end, Chapter Seven gives the conclusion.

CHAPTER TWO

THEORY OF DIGITAL SHEAROGRAPHY

2.1 Laser Speckle Pattern

When the laser is projected on an object with a rough surface, light and dark small particle distribution by an image acquisition device or human eyes. At any observation point in space, the coherent light scattered by the rough surface interferes with each other at this point, thereby forming laser speckle [20]. The speckle pattern can be regarded as the interference field of the various scattering points on the observation screen on the surface of the measured object. The Figure. 2.1 shows the speckle field formed by the laser illuminate the measured object. The image contains a large number of light and dark and randomly distributed laser speckles [21].

If the speckle pattern is imaged by cameras or other imaging system, the speckle pattern is observed is called a "subjective speckle pattern". The viewing system parameters determine the detailed structure of the speckle pattern. If a camera is used to record the speckle pattern, the size of the lens aperture determines the size of the speckles. In addition, the speckle pattern will change with the position if the imaging system. Each point in the image can be illuminated by a finite area in the object. The size of this area is decided by the diffraction-limited resolution of the lens. The equation can be written as:

$$\sigma_s = \frac{\lambda f(1+M)}{D} \tag{2.1}$$

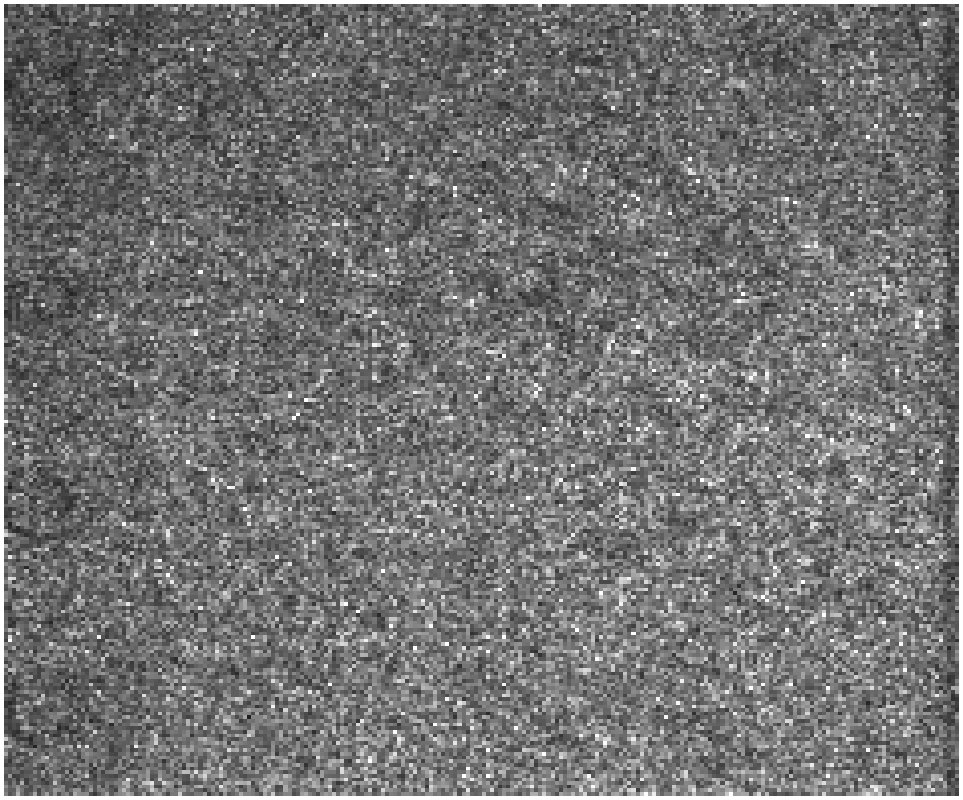

Figure 2.1. The speckle pattern image

where λ is the wavelength of the light, f is the focal length of the lens, and D is the diameter of the lens aperture, M is the amplified ratio.

Another form of the speckle patterns is called objective speckle pattern. When the wavefront which reflected from a rough surface project to another surface. If a photographic plate captures the reflected wavefront without a lens, the speckle pattern's characteristics depend on the geometry of the system and the wavelength of the laser. The speckle size equation can be written as:

$$\sigma_o = \frac{\lambda Z}{L} \tag{2.2}$$

where λ is the wavelength of the light, L is the width of the illuminated area and z is the distance between the object and the location of the speckle pattern. This kind of speckle pattern is formed by the detailed structure of the surface. he relative phases of these scattered waves vary across the scattering surface, so that the resulting phase on each point of the second surface varies randomly. Only the pattern amplified ratio will change with the moving of plane of object, but the pattern is the same.

2.2 The development of shearography

In 1970, Leendertz proposed the basic principle of speckle interference. By using laser to project objects with rough surfaces to generate the speckles. Another reference light is introduced to have interference with the speckles. The speckle interferogram before and after the deformation can obtain the deformation information of the object surface. In 1971, Leendertz and Buttes used a video camera to record speckle interferograms, and processed these speckle interferograms electronically, namely Electronic Speckle Pattern Interferometry (ESPI) [22, 23].

In 1973, Leendertz and Buttes proposed the Speckle Pattern Shearing Interferometry (Shearography) [24]. Unlike the ESPI, the shearography divides the light reflected from the object into two beams. The two beams overlap but with a small shearing amount. By comparing the changes of the speckle interferogram before and after the deformation of the measured object, the first derivative of deformation distribution information on the surface of the measured object is obtained. Since it is a self-interference technology that does not require additional reference light, the shearography has better resistance to external environmental disturbance. In 1982, Y.Y. Hong improved shearography and established a real-time Shearography, which highly improves the resolution but requires a wet chemical development process. This process is time-consuming, which greatly limits the practical application of Shearography. After the 1990s, TV monitor was used to display the real time fringes change, the Shearography in this period was called TV Shearography. In 1990, C. Joenathan used phase shift technology, dual-beam illumination, and used a TV camera to collect images to achieve the measurement of object strain. TV Shearography becomes more mature but it has a disadvantage of low spatial resolution.

After entering the 21st century, with the development of CCD and CMOS camera technology. The shearing speckle interferometry technique that records the image digitally is called the Digital Shearography [25]. By subtracting the speckle intensity information recorded by the camera, the first derivative of deformation of the material can be directly seen on the computer monitor in real time. This method is called the intensity mode. Since the digital recording device digitizes the image, which enables the phase shift technology. It improves the sensitivity of the Digital Shearography and reduces the difficulty of operation. This makes it possible for the united Digital Shearography device to apply on the industry.

2.3 Principles of digital shearography

The principle of the Digital Shearography is to expand the laser beam and project it onto the rough surface of the measured object to form a speckle. The speckle pattern is then reflected back to the shearing device through the image lens. The shearing device equally divide the incident beam into two wavefronts. Some optical components are placed on the optical path of beams to modulate its phase. Usually, one of the beams is concerned as a reference light and the other beam is modulated on shearing and phase.

The two beams of light will interfere on the surface of the image acquisition device to form a speckle interferogram or called shearogram. The surface first derivative of deformation information can be obtained by subtracting the shearograms before and after the deformation. The Classic Digital Shearography system is shown in Figure 2.2 below based on the Michelson Interferometer.

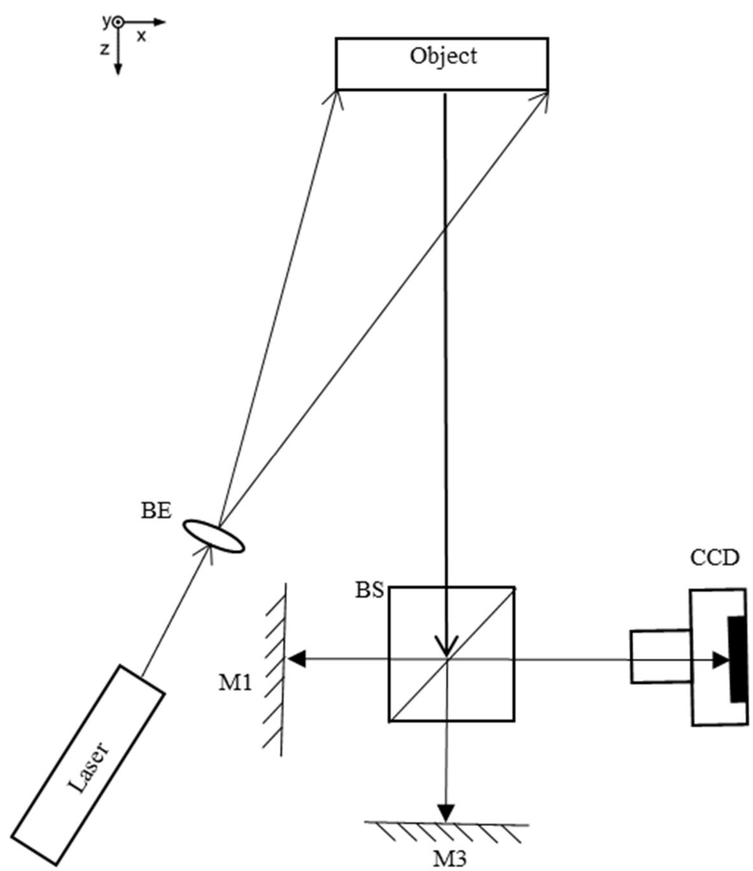

Figure 2.2. The classic Digital Shearography system

As the Figure 2.2, the laser passes through the beam expander and illuminate the object. The light reflected back can be represented as the equation below.

$$U = ae^{i\theta} \tag{2.3}$$

U is the intensity of the light, i is the imaginary number, a is the light amplitudes and θ is the random phase angle of the beam. While the light is divided into two waves by mirrors, the two beams can be written by the following equations.

$$U_1 = a_1 e^{i\theta_1} \tag{2.4}$$

$$U_2 = a_2 e^{i\theta_2} \tag{2.5}$$

θ_1 and θ_2 are the random phase angles and a_1 and a_2 represent the light amplitudes of the two beams. The total light field Ut can be described as:

$$U_t = U_1 + U_2 = a_1 e^{i\theta_1} + a_2 e^{i\theta_2} \tag{2.6}$$

The intensity can be expressed by:

$$I_t = U_t U_t^* = (a_1^2 + a_2^2) + 2a_1 a_2 \cos(\theta_1 - \theta_2) \tag{2.7}$$

U_t^* is the complex-conjugate of U_t. There are two forms to simplify the equations.

$$I_1 = A + Bcos\phi = I_0(1 + \gamma cos\phi) \tag{2.8}$$

ϕ represents the phase difference $(\theta_1 - \theta_2)$ between the light waves. A represent the average intensity or background intensity of the light while B is the term related to the amplitude of the interference. In another form, I_0 is the background intensity and γ is the contrast.

The phase becomes ϕ' while the object is loaded. The new Intensity equation is:

$$I_2 = I_0(1 + \gamma \cos(\phi + \mathit{\Delta})) \tag{2.9}$$

As the recorded intensity is digitized and stored in a computer. It is easy to calculate the intensity subtraction before and after loading. A highly visible fringe pattern can be directly generated and even can be real-time observed from computer screen. The absolute value of intensity subtraction can be expressed by the subtraction from Eq (2.10).

$$I_s = I_0\gamma[\cos(\phi + \Delta) - \cos(\phi)) \tag{2.10}$$

When the Δ=2nπ and n equals to 0, 1, 2, 3..., Is becomes 0, which forms the dark fringes. Hence, a visible shearographic fringe pattern can be generated. Figure 2.3 is the speckle pattern and Figure 2.4 is the corresponded shearogram.

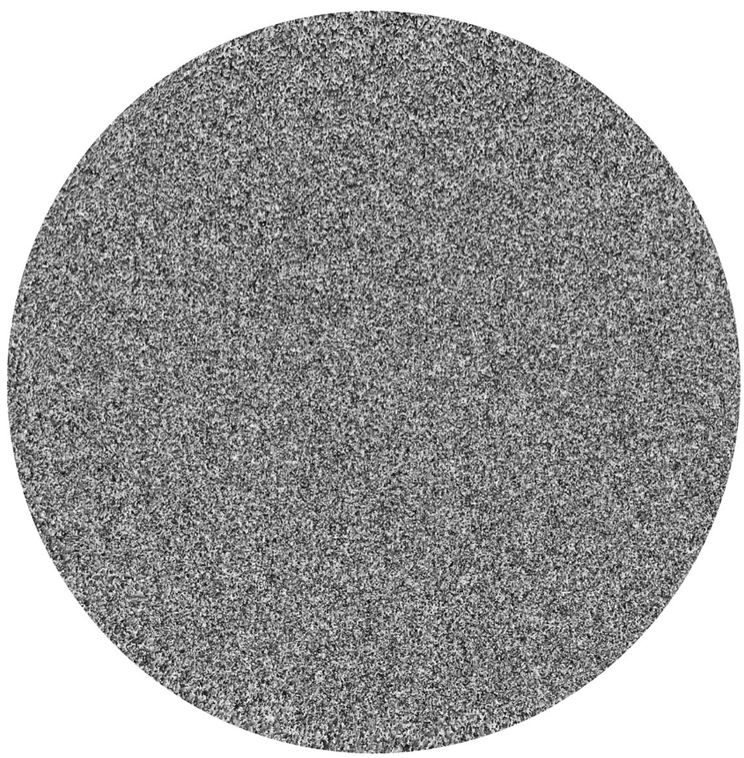

Figure 2.3. The speckle pattern of the Digital Shearography

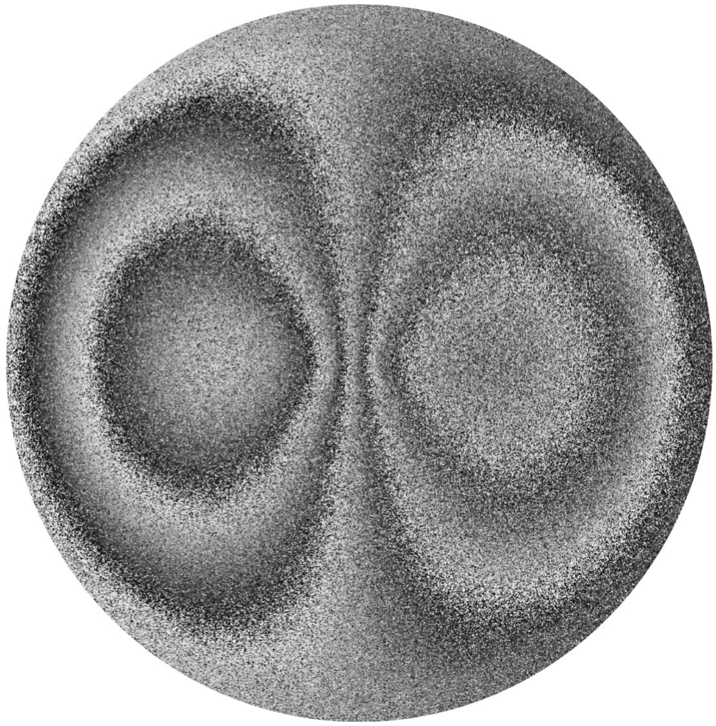

Figure 2.4. The Shearogram

The shearogram pattern looks like a ‘butterfly’, it is also called butterfly pattern. The phase difference of the adjacent fringes is 2π. Based on the optical geometry derivative, the relationship between phase and first derivative of deformation can be figured out as the equation below.

$$\Delta = \frac{2\pi}{\lambda}[(u_1 sina + w_1(1 + cosa)] - [(u_2 sina + w_2(1 + cosa)] \quad (2.11)$$

Simplifying the equation and the new form is as the following.

$$\Delta = \frac{2\pi}{\lambda}[\delta u(sina) + \delta w(1 + cosa)] \quad (2.12)$$

Since, Digital Shearography measures the relative displacement of the adjacent two points. Here, u_1, v_1, w_1 are the displacement components in x, y, z direction respectively on the first point. u_2, v_2, w_2 are the displacement components in x, y, z direction respectively on the second point. δu, δv, δw are the difference of the displacement components in x, y, z direction respectively between two pints. If we assuming the shearing direction is in x-direction with the shearing amount of δx, it divides the both sides of the equation above by δx and δx is very small, the equation above becomes.

$$\Delta_x = \frac{2\pi}{\lambda}[(sina)\frac{\partial u}{\partial x} + (1 + cosa)\frac{\partial w}{\partial x}]\ \delta x \quad (2.13)$$

If the device is in y shearing direction, the equation turns to be the Eq. 2.14.

$$\Delta_y = \frac{2\pi}{\lambda}[(sina)\frac{\partial u}{\partial y} + (1 + cosa)\frac{\partial w}{\partial y}]\ \delta y \quad (2.14)$$

If the angle between the illumination direction and the observation direction is 0, the equations can be shorted as:

$$\Delta_x = \frac{4\pi\delta x}{\lambda}\frac{\partial w}{\partial x} \quad (2.15)$$

$$\Delta_y = \frac{4\pi\delta y}{\lambda}\frac{\partial w}{\partial x} \quad (2.16)$$

Based on the equation, it can be found the phase change and the first derivative of deformation have a linear relationship in ideal assumption. Usually, the illumination angle is very small which can be ignored, so the Eq. 2.15 and Eq. 2.16 are the most common equations used.

Since ESPI is earlier developed than the Shearography, it is necessary to make a comparison between two technologies to explain why the shearography is more popular.

Figure 2.5 shows the difference between the ESPI and Shearography. A loading like thermal method or vacuum will make a buckling on the object surface. Since ESPI detects a defect by looking for displacement anomalies while Shearography looks for the strain anomalies. To demonstrate the concept described above, a square aluminum plate subjected to a point-load at the center of the backside is utilized to test by ESPI and Shearography. Figure 2.6(a) and Figure 2.6(b) show the ESPI fringe pattern and Shearography fringe pattern respectively. Figure 2.7(a) shows the holographic application where some circular anomalous fringes appear at the position of delamination. Figure 2.7(b) shows the shearography application and the shearograms appear at the surface with inner defects.

ESPI measures the deformation directly which is more sensitive but with an independent reference light, which is easily affected by the external vibration. Without a good vibration isolated environment, ESPI cannot be applied. However, vibration isolated device could highly increase the cost and the space of the device, which limit ESPI industrialized process. In opposite, Digital Shearography measures the relative deformation between two adjacent points, and it is a self-interference technology. External disturbance could be cancelled by the two beams with the same vibration mode, which becomes the most important advantages in speckle pattern interferometry in industry application.

2.4 Shearography instrument components

The three key components of Digital Shearography are laser, shearing device and camera. All three components have their own development in recent decades, and each

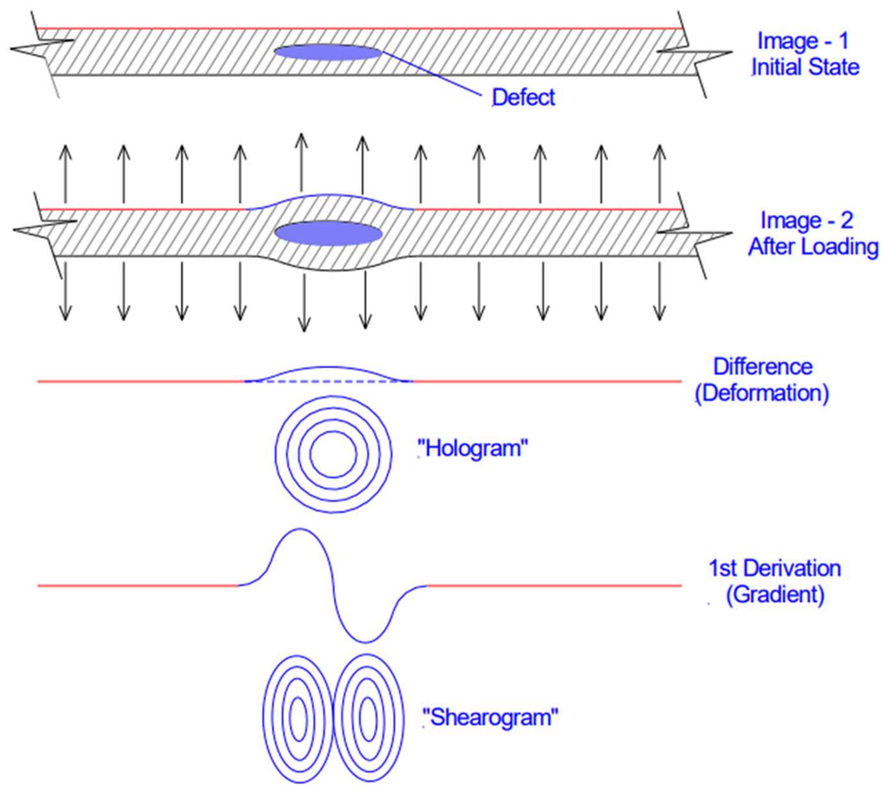

Figure 2.5. The comparison between ESPI and Shearography in NDT

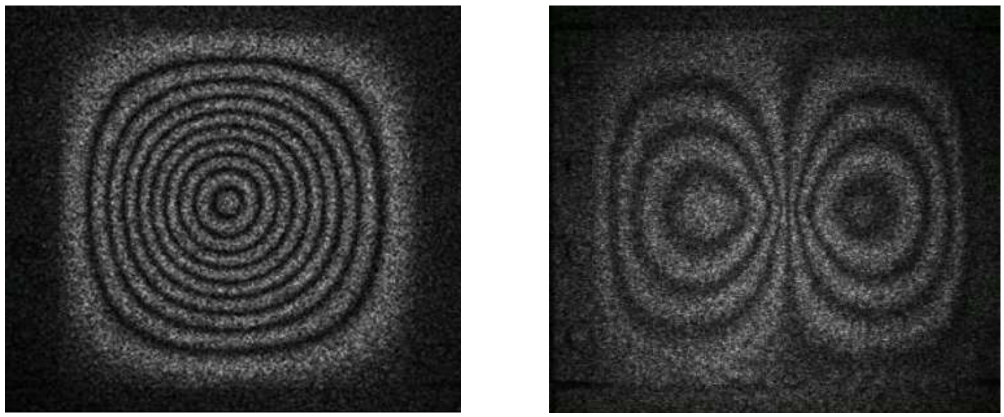

(a) (b)

Figure 2.6. ESPI and Shearography test of a square aluminum plate: (a) Hologram; (b) Shearogram.

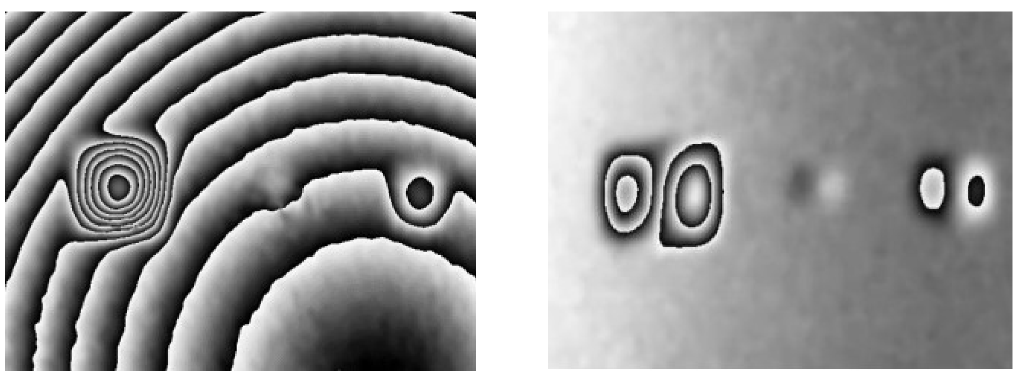

(a) (b)

Figure 2.7. ESPI and Shearography NDT for a composite plate: (a) Hologram; (b) Shearogram.

component has an important effect on the application possibility and result quality of the NDT.

2.4.1 Lasers

Digital Shearography is an interference technology, which can only be achieved by laser illumination at present. The three requirements for interference are the same wavelength, effective coherence length and the same polarization direction. It is difficult for common laser instruments to achieve perfect performance of the above three points. It will be discussed one by one.

Lasers are generally considered to be monochromatic light and exist in both visible and invisible ranges. The choice of laser wavelength will affect some of the parameters of Digital Shearography. In theory, using lasers with different wavelengths for the same measurement will bring different experimental results, because the wavelength is a key parameter. Therefore, if accurate data analysis is required in some kinds multi-wavelength application, the data needs to be compensated. The general Digital Shearography uses lasers in the visible light range, mainly because it is stable, easy to obtain, and economic. The conventional laser sources, such as a He-Ne Laser and a ND: YAG laser. These lasers are commonly used in the laboratory. The 632nm and 532nm wavelength are widely used, which is red and green light. The wavelength of laser also affects the choose of the other optical components like beam splitter and some of lens. Such components usually have coating on its surface which has limited band width. Thus, laser wavelength choosing needs to be careful [26-29].

Coherence length is the propagation distance over which a coherent wave maintains a specified degree of coherence. Interference quality would be better when the paths taken by all of the interfering waves differ by less than the coherence length. The longer coherence length could get a perfect sinusoidal wave [30]. The Digital shearography is not sensitive for the coherence length for self-interference. The two beams joined always have the same distance in optical path. However, other speckle pattern interferometry like ESPI who needs a reference light could suffer from some lasers whose coherence length reducing with the aging of the laser. In that case, object beam and reference beam need to be manipulated to the similar length that smaller the coherence length [31].

Polarization is a property applying to transverse waves that specifies the geometrical orientation of the oscillations. Polarization effect will be detailed discussed in the Chapter 4. In the classic digital shearography technique, polarization of incident beams is not important. The polarized direction could change when a polarized light reflects from the rough surface. The change of the polarization depends on the material, micro-geometry of the surface and some characteristics. Polarization effect has a huge potential in the further development in Digital Shearography application [32].

Digital Shearography does not require a very high-quality laser source. The laser power used for the NDT lies between several decades to hundred milliwatts, depending on the size of object and the light efficiency of the optical device. It is possible for Digital Shearography to use a simple laser diode to illuminate object and a large area with multiple inexpensive laser diodes.

2.4.2 Shearing device

Shearing device is the core system in Digital Shearography, and it is also the basis for the most functions. The basic function of the shearing device is to split the light beam reflected from the object into two beams, and then produce the shearing amount. Besides， the phase shift technique which will be discussed in Chapter three, also need shearing device to introduce the phase change whatever the temporal phase shift or spatial phase shift. Here, some representative shearing devices are the optical glass wedge [33], the bi-angle prism [34], Wollaston prism [35], Mach-Zehnder interferometer and Michelson Interferometer [36].

The first shearing device is an optical wedge. When light pass through the wedge and the lens on the back, the image will be separated to two images in lateral with a shearing amount. The shearing amount is determined by the angle of the wedge. Figure. 2.8 shows a schematic of the optical wedges as a shearing device. The setup has the advantage of only using a few optical components to obtain the shearing, but it is impossible to change the shearing angle and direction once the setup is built. This setup is still used in some application that with a fixed optical design.

The bi-angle prism has a similar characteristic as the optical wedge as shown in the Figure 2.9. The beam passes through the two sides of the bi-angle prism and be divided into two beams. The shearing amount is also decided by the angle of the prism.

The Wollaston prism is another widely used shearing element. Birefringence is the decomposition of a ray of light into two rays when it passes through some special optically anisotropic materials, such as crystals of calcite. These prisms are cemented together on their base to form two right triangle prisms with perpendicular optic axes. Outgoing light beams diverge from the prism as ordinary and extraordinary rays due to the differences in the indexes of refraction, with the angle of divergence determined by

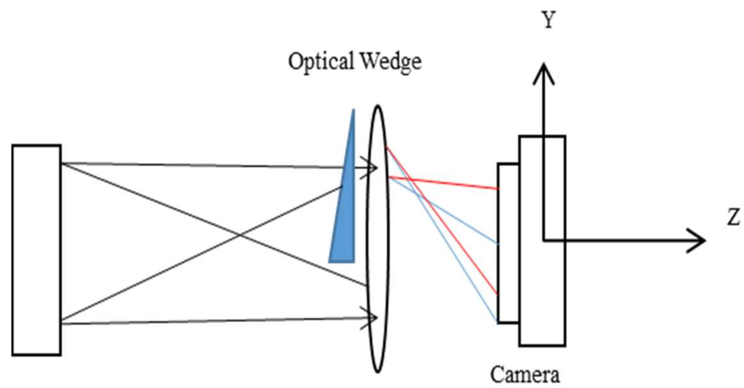

Figure 2.8. The schematic of the optical wedge as a shearing device.

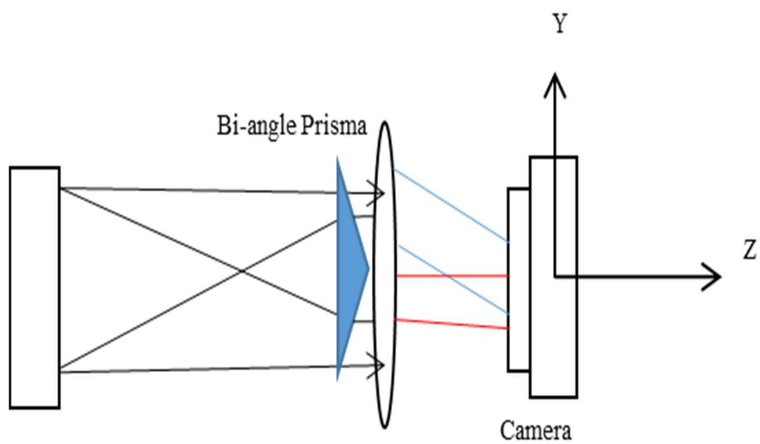

Figure 2.9. The schematic of the Bi-angle Prisma as a shearing device.

the prisms' wedge angle and the wavelength of the light. Commercial prisms are available with divergence angles from less than 1° to about 45°.

Figure 2.10 shows a schematic of Wollaston prism. The incident beam is separated to two beams when it passes through the interface of two angle prisms. In Digital Shearography application, a polarizer with its polarization axis oriented at an azimuth of 45 degree is required to m adjust the two beams to the same polarize directions to realize the interference. The shearing amount is limited by its angle degree as optical glass wedge and the bi-angle prism.

To increase flexibility of adjusting the shearing direction and shearing amount. Interferometers are becoming popular to be used as the shearing device. Mach-Zehnder and Michelson interferometer are the two representative interferometers that applied in Digital Shearography.

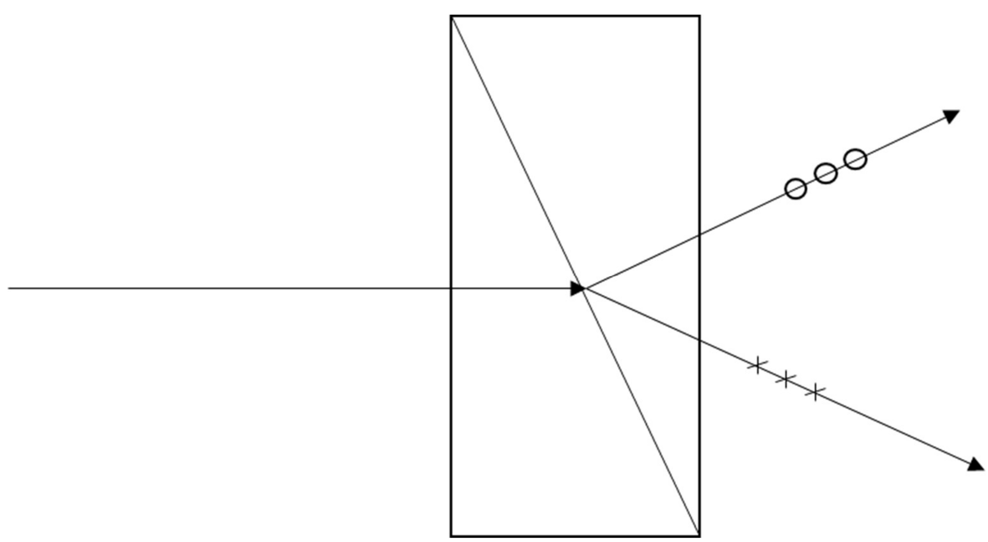

Figure 2.10. The schematic of the Wollaston prism.

The Mach–Zehnder interferometer is a highly configurable instrument. Each of the well-separated light paths is traversed only once as shown in the Figure 2.11. The incident beam passes through a cubic beam splitter and divided into two beams toward two directions with 90-degree angle. Two beams hit two mirrors independently and combined by the second beam splitter. In this process, all the beams are one way transmit which is good for independent modulation.

The Michelson interferometer is the most compact shearing device as shown in Figure 2.12. Two mirrors are arranged on the side of the beam splitter. When the incident beam is separated and two mirror will reflect back and combined to project on the CCD.

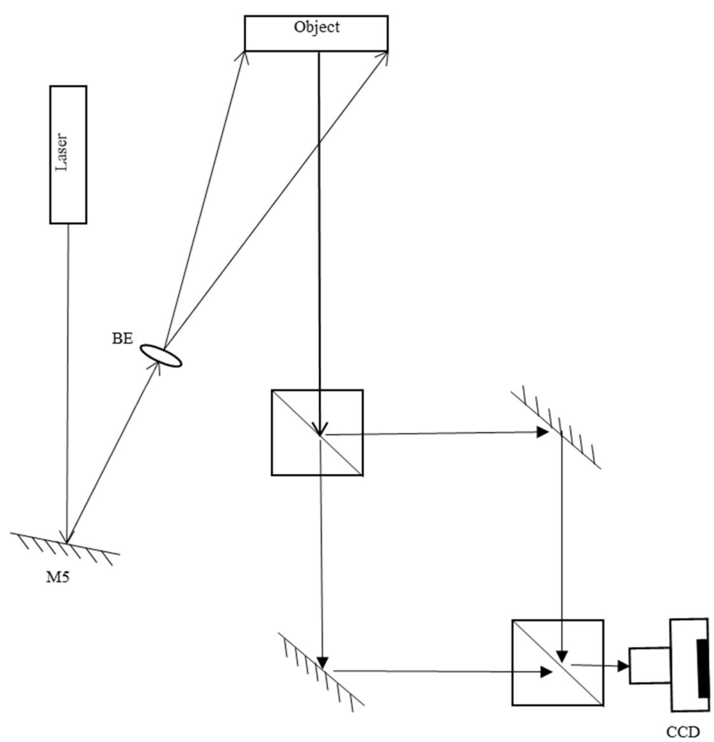

Figure 2.11. The schematic of Mach–Zehnder interferometer.

By tilting one of the mirrors of a small angle, the shearing can be generated. The Michelson interferometer help Digital Shearography to simply the setup while increase its flexibility of adjusting shearing and generating the phase change.

In addition, some lateral shearing units have been invented and applied such as: Savart Plate [37] and circular polarization gratings made in liquid crystal polymers [38-39]. Besides, Digital optical modular are also applied as the shearing device recently. Spatial light modular which can modulate the shearing amount and direction precisely by programming does need any special optical treatment or manually or mechanically adjusting. This new shearing device will be discussed in detail in Chapter Five from theory to structure.

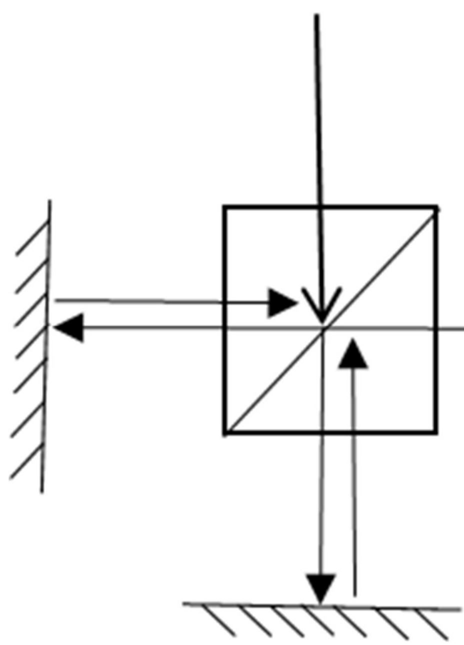

Figure 2.12. The schematic of Michelson interferometer.

The shearing device is important because Digital Shearography is shearing sensitive. There are two parameters in shearing, shearing amount and shearing direction. It is clear from the Eq. 2.13 to 2.16, shearing amount determine the distance between two adjacent point. When a small shearing amount is adopted, the relative deformation is also small which results in a low measuring sensitivity. In this case, the result is close to the first derivative or strain information. In opposite, adjusting the shearing amount to a large number, the visible change is the shearograms is expanding with the increasing of the shearing amount, at the meantime, the sensitivity increases. To better understand this concept, a relationship among the deformation, the relative deformation, and the shearing amount over a defect are is shown in Figure 2.13. Before the shearing amount increase over half of the are deformation, the relative deformation increases with the shearing amount increase. At this moment, the maximum relative sharing amount is equal to

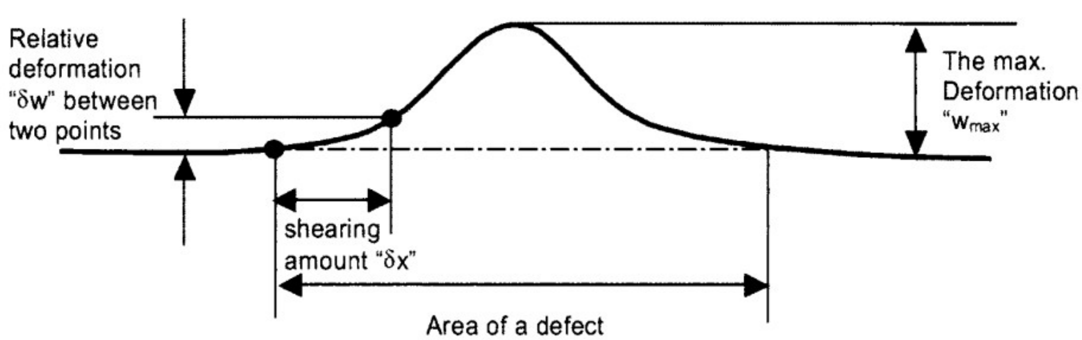

Figure 2.13. The shearing amount expression in a defect.

maximum deformation. The half diameter of the minimal defect is the best selection for shearing amount. To determine this value, the minimum defect size needs to know in first. In the case of the technician who did the measurement cannot acknowledge the size of defect, a minimum safe size will be proposed to set as the shearing amount.

There are two forms of shearing, lateral shearing and radial shearing. The most famous radial shearing device is diffractive holograph elements which was introduced by Albertazzi's research group from Santa Catarina University in Brazil [40]. This method uses a diffractive holographic element to generate double illumination and radial in-plane sensitivity which make the in-plane strain component measurement available [41-44]. However, radial shearing usually needs special equipment and is not ideal to measure the out of surface strain on the surface.

The lateral shearing is more direct and easier to implement. Shearing directions exist in lateral shearing and determine the surface deformation gradient directions. As the topic of the dissertation, the defects own many shapes. The circular shape defect is the most common. The deformation made of such defects usually is a regular circle convex shape. The gradients of deformation are the same of such uniform appearance in any directions, which mean shearing direction plays no role on it. However, some defects like cracks or narrowly rectangular foreign matter could bring a deformation irregular. Figure 2.14 shows a quadratic plate with one round grove and three narrow rectangular grooves oriented in different direction on the back side. Figure 2.4 (a) is measured in horizontal shearing direction while Figure 2.4 (b) is measured in vertical direction. For the circular shearograms, shearing direction switching changes the pattern direction but the relative deformation is the same in each direction if the deformation is uniform. The rectangle

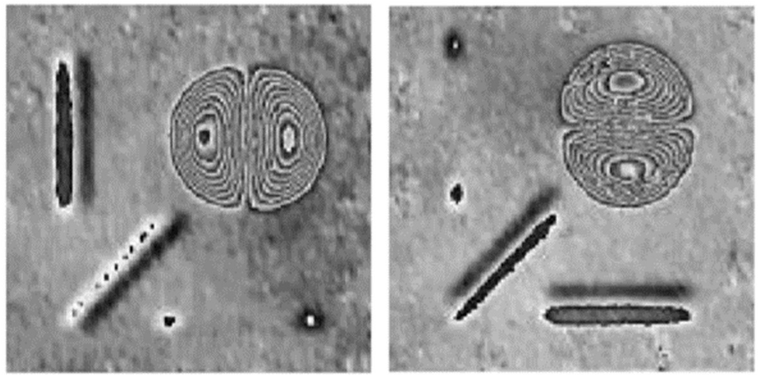

(a) (b)

Figure 2.14. Digital shearograms with different shearing direction: (a) Digital shearogram with a horizontal shearing direction; (b) Digital shearogram with a vertical shearing direction.

Grooves in 45-degree directions can be detected either in both shearing direction for the same reason that the gradient of the deformation is the same in horizontal shearing direction and vertical direction. However, if the shearing direction is parallel to the grove's growing direction, the gradient of deformation would be very small on the defects. In opposite, if the shearing direction is perpendicular to the grove direction, the gradient of deformation would be large to see just as the result of horizonal and vertical groove of the Figure 2.4.

Digital shearography is sensitive to its shearing direction. Two shearographic systems or multi times measurement are needed for comprehensive inspection, which highly increases the cost and produces additional problems, for instance, poor phase map quality, low power efficiency and cumulative error. Thus, A simultaneous dual shearing directions measurement is necessary for the fast and precise inspections. The dual channel system will be a good solution.

2.4.3 Camera

Camera is the tool to record the interference pattern. Charge-Couple Device (CCD) and Complementary metal oxide semiconductor (CMOS) are the two main kind camera core unit [45-46]. In past decades, CCD has a better performance than CMOS. CMOS gets a fast development in recent years and becomes the most widely used in camera production for its economic advantage. Both cameras can be used in Digital Shearography.

Camera has the following characteristic that can affect the measurement of Digital shearography, pixel number and size, spatial resolution and acquisition rate. Pixel size could affect the quality of spatial phase shift which will be discussed in the next chapter. Acquisition rate could determine the dynamic measurement limitation. Without a high-speed camera, some loading as the shock wave is unable to measure. Spatial resolution is a critical issue for Digital Shearography. High resolution camera is usually expensive which is not good for industry application. One time test with a camera with a limited resolution could miss some minor defects. We can adjust the lens of the camera to zoom to a small area to solve the issue. However, it needs multi-times test which increase the cost and labor. The way that simultaneously measure minor shearograms with a large filed measurement is necessary to be developed. This development will be discussed in details in Chapter Six.

CHAPTER THREE

PHASE EXTRACTION TECHNOLOGIES

In the Digital Shearography, the phase keeps changing during the measurement. To measure the deformation of the surface, first is to obtain its phase information. Therefore, obtaining the phase information from the speckle is a key part of Digital Shearography. According to the different phase extraction technologies, the commonly used methods mainly include real-time intensity subtraction technology, temporal phase shift technology, spatial phase shift technology.

3.1 Real-time intensity subtraction technology

The simplest and most direct way of phase extraction is to directly subtract the intensity map collected by the camera. By this way, butterfly pattern can be directly observed on the monitor. With the software development, it is able to observe the deformation change with the loading process. The phase difference is then calculated by counting fringes. Real time subtraction Digital Shearography only reach a 2π phase measurement sensitivity. In general, real-time intensity subtraction technology is very practical, reliable, but a relative low deformation measurement sensitivity.

However, as the Figure 3.1, the intensity subtraction map has various noise errors, the obtained fringe resolution is low. Even if some image processing methods are used to eliminate some noises, some new errors will be introduced during the image processing. For example, the skeleton line of the stripe after filtering may shift away the original position, which brings the incorrect phase information. Therefore, this method is generally only used for qualitative detection during defect detection.

Figure 3.1. Shearogram by real-time intensity subtraction

3.2 Temporal phase shift technology

In order to obtain a higher quality shearogram and increase the measurement sensitivity, the phase is generally obtained by phase shift technique. Catalog by phase-shift techniques, the phase shift shearography can be divided into temporal phase shift shearography and spatial phase shift shearography. Among them, the temporal phase shift technology uses error averaging in time and in the actual measurement system, the aperture is relatively large, and the amount of information acquired by the camera is more, so it has better fringe quality.

3.2.1 Introduction of temporal phase shift technology

The temporal phase shift technology is the most widely used and the most precise technology in the phase extraction of Digital Shearography. This method introduces a fixed phase value to the image in sequence while the object under test remains stable and unchanging, and then collects the image. This method was first proposed by Carré in 1966 and introduced to optical inspection by Bruning. At present, the most commonly used method is to connect piezoelectric ceramics (PZT) with a mirror in the shearing device and input a fixed voltage to control the movement of the piezoelectric ceramics to introduce a fixed phase shift value. The piezoelectric ceramic drive device has the advantages of high displacement resolution, fast response, small size, relatively low price, and no heat generation. It is a material that can mutually convert mechanical energy and electrical energy. Its single-step displacement can reach the nanometer level [47-50].

Figure 3.2 below shows a typical Michelson interferometer based Digital Shearography that uses piezoelectric ceramics to introduce a temporal phase shift. The object is illuminated by the laser expanded using a beam expander. The speckle caused by the diffuse reflection of the rough surface is reflected into the shearing system. In the shearing system, a mirror deflects slightly, introducing the shearing amount and controlling the shearing direction, and the two misaligned images interfere on the imaging plane of the camera to form a new speckle pattern. The piezoelectric ceramic is connected to one of the mirrors, and a computer is used to control the voltage input to the piezoelectric ceramic.

PZT is a key component to achieve phase shift. It is a voltage control device which can generate a nanometer displacement. By changing the optical path, a certain phase value will be introduced. For each specific PZT component, a voltage to displacement relationship as shown in Figure 3.3. The relationship between the movable

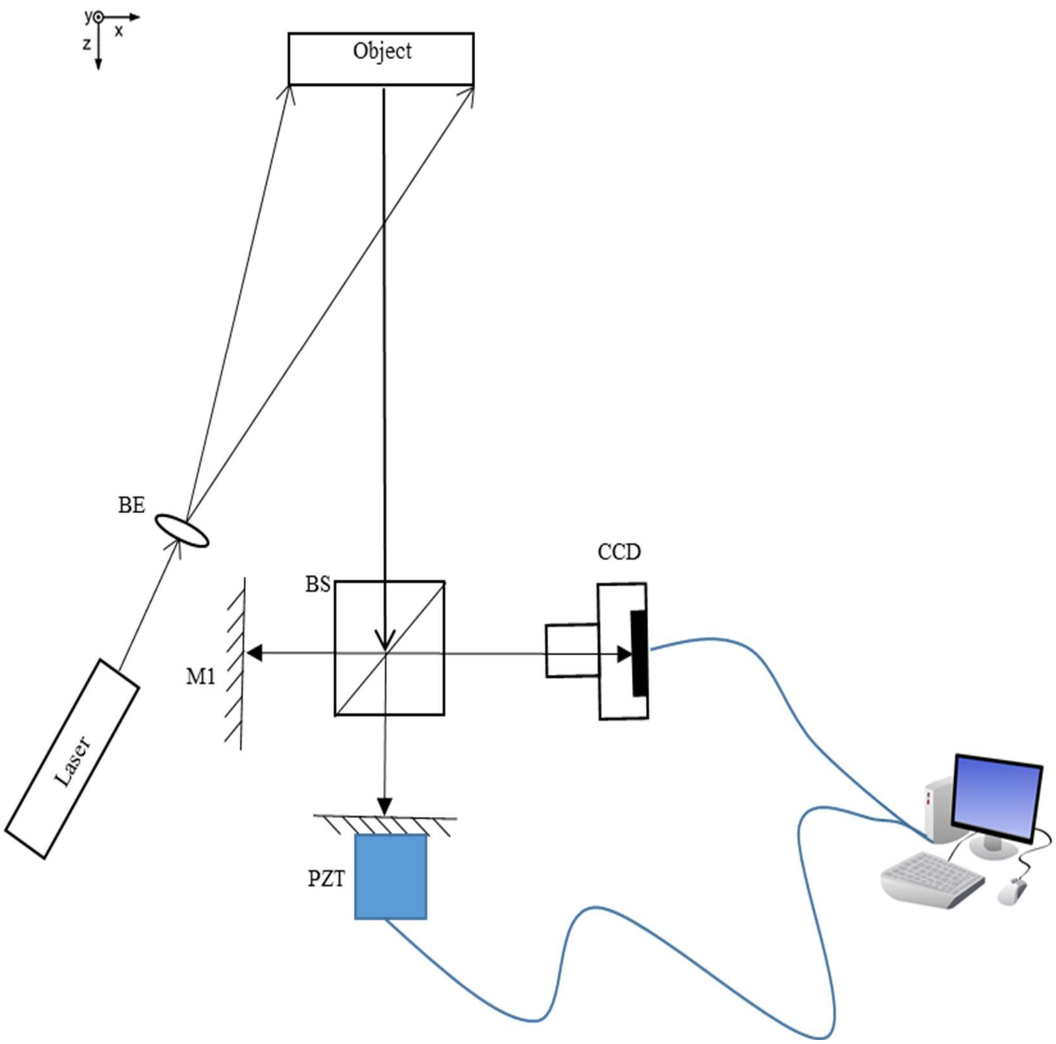

Figure 3.2. The schematic of Digital Shearography with PZT

distance and the voltage is not liner. A part of curve can be recognized as the linear line which can be used.

A sensitivity factor of PZT can be expressed as:

$$k = \frac{x_2 - x_1}{\Delta U} \tag{3.1}$$

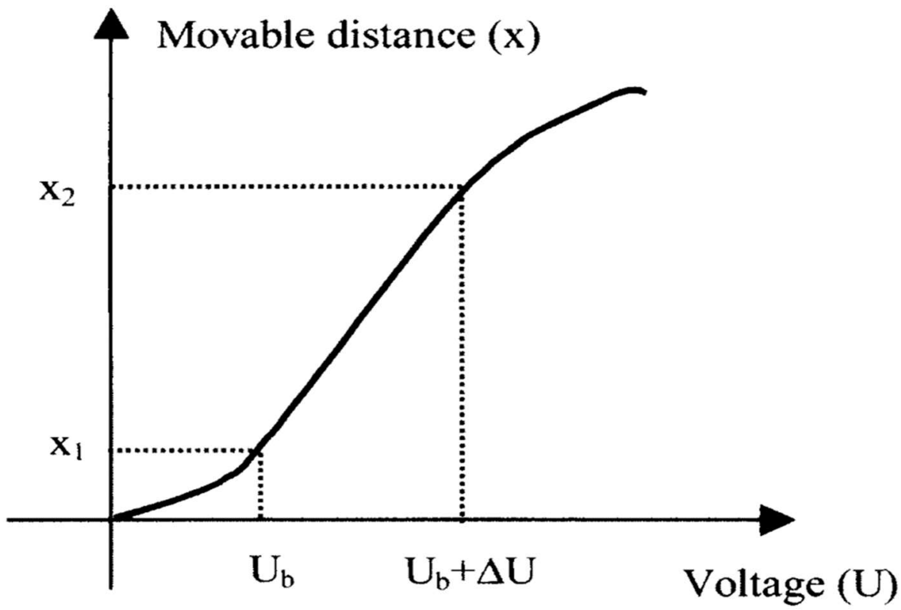

Figure 3.3. Voltage-to-displacement relationship o f a PZT mirror

Where, x_1 is the origin position of the PZT and x_2 is the position after PZT moving. ΔU is the volage change to make this movement.

With this factor k, the displacement of PZT under given voltage increment can be calculated by:

$$d = k\Delta U \tag{3.2}$$

As shown in Figure 3.4, assuming the incident light reach the PZT mirrors with an incident angle of α. The displacement d is achieved with a ΔU voltage applied on the PZT. The displacement d brings the optical path change ΔL which can be written as:

$$\Delta L = \frac{2dn}{cos\alpha} = \frac{2nk}{cos\alpha}\Delta U \tag{3.3}$$

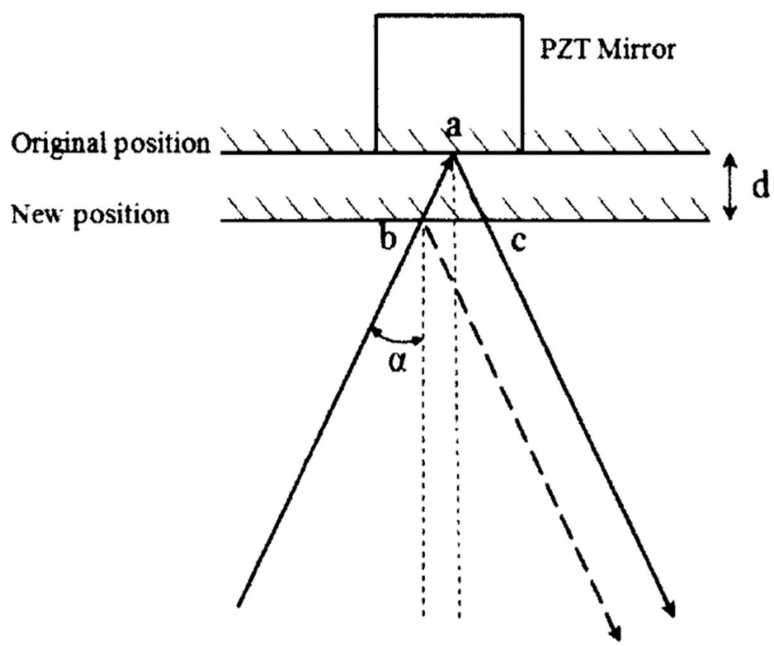

Figure 3.4. Optical path analyses on PZT mirror

The phase value can be extracted from the optical path difference by the following equation.

$$\Delta\phi = \frac{2\pi}{\lambda}(\frac{2nk}{cos\alpha}\Delta U) = \frac{4\pi nk}{\lambda cos\alpha}\Delta U \tag{3.4}$$

In a real setup as the Michelson Interferometer shearing device, the PZT is perpendicular to the incident light, thus angle of mirror equals to 0 while the air index number n=1. The final equation can be written below:

$$\Delta\phi = \frac{4\pi k}{\lambda}\Delta U \tag{3.5}$$

Besides the PZT method, there are some other devices also can introduce the phase like polarizer. In practice, circularly polarized light is produced by passing linearly polarized light at the horizontally polarized light through a quarter wave plate whose fast axis is oriented at 45°. The output beam is right circularly polarized. If the input light is polarized at vertically polarized light, then the output beam is left circularly polarized. A rotatable polarizer placed after the quarter wave plate acts as a phase shifter whose azimuth will directly give the phase of the output beam [51-53].

3.2.2 3+3 temporal phase-shift algorithm

In order to obtain better phase quality, phase subtraction is used instead of direct light intensity subtraction before and after loading. There are multiple algorithms to extract the phase from the equation which are derive from the speckle pattern equation below.

$$I = A + Bcos\phi \tag{3.6}$$

The equation has been discussed in the section of the principles of Digital Shearography. Here, we can find A, B and ϕ are three unknowns to be solved, thus, at least three equations are needed to solve Equ 3.5. PZT can introduce a known phase value to help to solve the equation. If a 120-degree phase difference is introduced to the three images with the same loading state, an equation group can be written as:

$$I_1 = A + Bcos\phi$$
$$I_2 = A + Bcos(\phi + 120^{\circ}) = A - B(\frac{\sqrt{3}sin\phi + \cos\phi}{2}) \quad (3.7)$$
$$I_3 = A + Bcos(\phi + 240^{\circ}) = A + B(\frac{\sqrt{3}sin\phi - \cos\phi}{2})$$

If the PZT move the distance L, the introduced phase is represented by:

$$\varphi = \frac{2\pi}{\lambda}2L \quad (3.8)$$

Inversely, the phase difference of three speckle pattern image can be expressed as

$$\phi = arctan\frac{\sqrt{3}(I_3 - I_2)}{2I_1 - I_2 - I_3} \quad (3.9)$$

This algorithm needs to consider its final phase position because the same arctan value could result two answers range from 0 to 2π. The signs of the numerator and denominator should be considered separately to determine the exact phase value. The rule is When the numerator and denominator are positive, the phase values are in the first quadrant; for a positive numerator and a negative denominator it lies in the second quadrant; a negative numerator and a negative denominator lies in the third quadrant; and a negative numerator and positive denominator, results in phase values which lie in the fourth quadrant.

After the loading, the phase shift procedure will be processed again and the following equations can represent the new three image.

$$I_1' = A + Bcos\phi'$$

$$I_2' = A + Bcos(\phi' + 120^\circ) = A - B(\frac{\sqrt{3}sin\phi' + \cos\phi'}{2}) \quad (3.10)$$

$$I_3' = A + Bcos(\phi' + 240^\circ) = A + B(\frac{\sqrt{3}sin\phi' - \cos\phi'}{2})$$

The phase-difference after deformation can be calculated as:

$$\phi' = arctan\frac{\sqrt{3}(I_3' - I_2')}{2I_1' - I_2' - I_3'} \quad (3.11)$$

Then the relative phase change caused by deformation can be calculated by:

$$\Delta = \phi' - \phi \qquad for\ \phi' > \phi$$

$$\Delta = \phi' - \phi + 2\pi \quad for\ \phi > \phi' \quad (3.12)$$

As we get the phase value, the first derivative of deformation can be calculated by the Eq. 2.15

If we put a phase value of the whole image into a new image, the gray levels from 0 to 255 correspond with the phase values between 0 and 2π. When subtracting ϕ digitally from ϕ', a negative value will be transformed into a positive value for the 2π periodic function.

3.2.3 4+4 temporal phase shift algorithm

Three equations are the basic requirement to solve the three unknowns but not the best way to extract phase due to it’s a little bit complicated calculation. Currently, 4+4 temporal phase shift algorithm is the most popular phase shift method. It has the advantages of fast and simple calculation procedure [54-57]. As the name ‘4+4’, it requires 4 phase shift steps for each phase calculation and each phase step is 90 degree. The four intensity maps are now recorded before deformation:

$$I_1 = A + B\cos\phi$$
$$I_2 = A + B\cos(\phi + \tfrac{\pi}{2}) = A - B\sin\phi$$
$$I_3 = A + B\cos(\phi + \pi) = A - B\cos\phi \qquad (3.13)$$
$$I_4 = A + B\cos(\phi + \tfrac{3\pi}{2}) = A + B\sin\phi$$

The phase value can be written as:

$$\phi = arctan(\frac{I_4 - I_2}{I_1 - I_3}) \qquad (3.14)$$

Similarly, another four phase shift steps are taken while their corresponded speckle pattern images can be expressed as:

$$I_1' = A + B\cos\phi'$$
$$I_2' = A + B\cos(\phi' + \tfrac{\pi}{2}) = A - B\sin\phi'$$
$$I_3' = A + B\cos(\phi' + \pi) = A - B\cos\phi' \qquad (3.15)$$
$$I_4' = A + B\cos(\phi' + \tfrac{3\pi}{2}) = A + B\sin\phi'$$

The phase value after loading can be written as:

$$\phi' = arctan(\frac{I_4' - I_2'}{I_1' - I_3'}) \qquad (3.16)$$

The phase difference map which describes the surface deformation distribution is shown as the Eq. 3.12. The detailed process can be explained in the Figure 3.5, the speckle patterns and shearogram are displayed individually. Four speckle patterns are required for calculation of a phase map before and after loading. The subtraction of the phase instead of the intensity maps can obtain higher sensitivity phase map. 4+4 temporal phase shift method is the most commonly used temporal phase shift method in Digital Shearography because of its simple calculation.

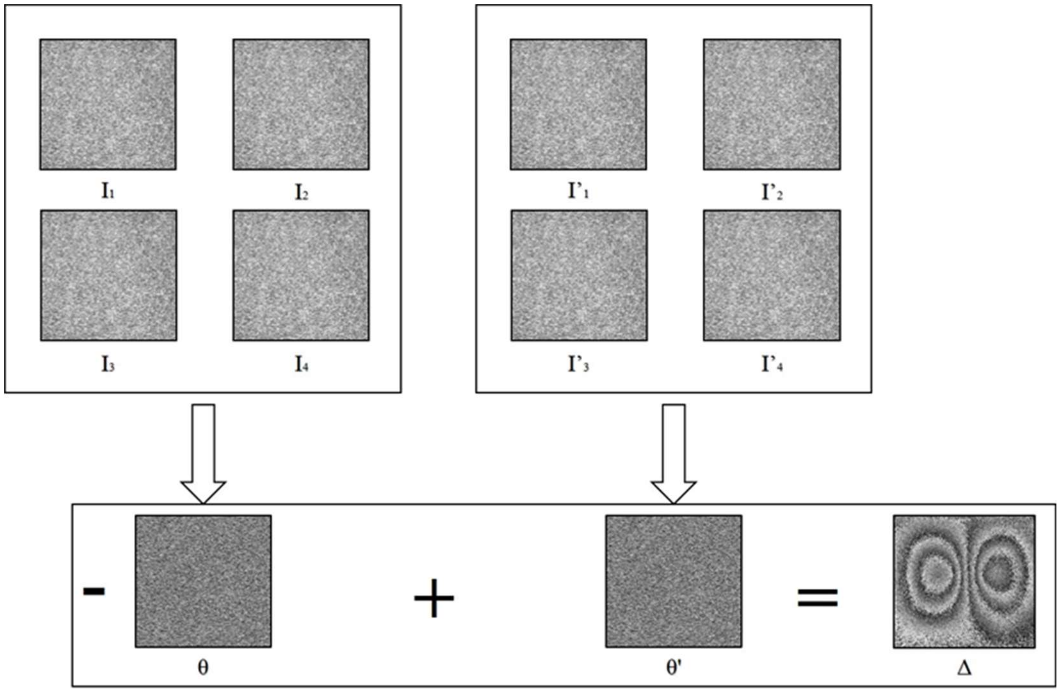

Figure 3.5. 4 +4 temporal phase shift process

3.2.4 Fast temporal phase shift algorithm

3+3 and 4+4 temporal phase shift can satisfy the state loading test. It requires enough time for multi steps phase shift. Different phase shift device has their own running speed. For the most mechanism based phase shift device, the phase shift speed is a challenge for the dynamic or continuous loading. There are some methods developed to improve the testing quality in dynamic loading [58-60].

In recent years, a variety of fast temporal phase shift algorithms have been developed, including 3+2, 3+1, 4+2 and 4+1 fast temporal phase-shift algorithms. For simplicity, in this dissertation, they are all cataloged as N+i fast temporal phase-shift algorithms, where N represents the number of phase-shift steps before loading, and I represent the number of phase-shift steps after or during the loading. N steps phase shift is taken before the loading which is used as the basic parameters' calculation. Following the theory of intensity formula, N is at least 3 while bigger can improve the phase map quality. The i value has a great influence on the dynamic measurement capability. When i=1, there is no phase shift during the loading which is the real dynamic measurement. However, the assumption of N+1 method is based on the other parameter not changing during the loading process, which results in poor phase map quality. An alternative way is to set i=2. In this case, only one phase shift step is required for each picture frame. Compared to the 4+4 temporal phase shift algorithm, the N+2 algorithm uses the cost o f a reasonable decrease of phase-map quality to get a significant increase in acquisition rate, resulting in a dynamic measurement capability at a low dynamic range.

Some common N+i methods are shown in detail respectively. The first method is 3+2 method, which has 3 images before loading and two images after loading. The equation is described below.

$$I_1 = A + Bcos\phi$$

$$I_2 = A + Bcos(\phi + 120^{\circ})$$

$$I_3 = A + Bcos(\phi + 240^{\circ})$$

(3.17)

$$I_1' = A + Bcos\phi' = A + Bcos(\phi + \Delta)$$

$$I_2' = A + Bcos(\phi' + 120^{\circ}) = A - Bcos(\phi + \Delta + 120^{\circ})$$

From the images taken before loading, the phase can be determined using Eq. 3.11. In addition, the parameter A can also be solved:

$$A = \frac{I_1 + I_2 + I_3}{3} \tag{3.18}$$

The phase $\phi + \Delta$ can be solved as:

$$\phi + \Delta = arctan\frac{\sqrt{3}(I_1 + I_2 + I_3 - 2I_2' - I_1')}{3I_1' - (I_1 + I_2 + I_3)} \tag{3.19}$$

At the same time, Δ can be calculated by subtraction before and after loading.

$$\Delta = arctan\frac{\sqrt{3}(I_1 + I_2 + I_3 - 2I_2' - I_1')}{3I_1' - (I_1 + I_2 + I_3)} - arctan\frac{\sqrt{3}(I_3 - I_2)}{2I_1 - I_2 - I_3} \tag{3.20}$$

The 3+2 method assumes that A and B in Eq. 3.17 remains constant before and after loading. However, A and B may not be identical due to decorrelation of some speckles, which results in more noise. To achieve higher speed of phase shift, 3+1 temporal phase shift introduced. Three images are recorded before loading and only one image is recorded after loading as shown below.

$$I_1 = A + Bcos\phi$$

$$I_2 = A + Bcos(\phi + 120^{\circ})$$

$$I_3 = A + Bcos(\phi + 240^{\circ}) \tag{3.21}$$

$$I' = A + Bcos\phi' = A + Bcos(\phi + \Delta)$$

To calculate the phase difference Δ, the following equations need to be processed.

$$(I_1 - I')^2 = 4B^2\sin^2(\phi + \Delta/2)\sin^2(\Delta/2)$$

$$(I_2 - I')^2 = 4B^2\sin^2(\phi + \frac{\Delta}{2} + \pi/2)\sin^2(\frac{\Delta}{2} - \pi/2) \tag{3.22}$$

$$(I_3 - I')^2 = 4B^2\sin^2(\phi + \frac{\Delta}{2} + 2\pi/3)\sin^2(\frac{\Delta}{2} - \pi/2)$$

$\frac{\Delta}{2}$ is a low-frequency component, the phase is ϕ is a high frequency component related to the surface microstructure. The terms $(\phi+\frac{\Delta}{2})$, $(\phi+\frac{\Delta}{2}+\pi/2)$, and $(\phi+\frac{\Delta}{2}+2\pi/3)$ are also high frequency components. A detector captures the average value of the high frequency terms within each speckle. The following equation can be obtained with this assumption.

$$\sin^2\left(\phi+\frac{\Delta}{2}\right)\approx\frac{1}{2n\pi}\int_0^{2n\pi} sin^2\left(\phi+\frac{\Delta}{2}\right)d\left(\phi+\frac{\Delta}{2}\right)=\frac{1}{2} \tag{3.23}$$

where n is an integer number. The feasibility of the equation is based on the assumption that the speckle size is smaller than the pixel size, so a pixel will cover several speckles.

With the result shown in Eq. 3.23, Eq. 3.22 can be simplified as follows

$$\begin{aligned}(I_1-I')^2&=B^2[1-\cos(\Delta)]\\(I_2-I')^2&=B^2[1-\cos(\Delta-2\pi/3)]\\(I_3-I')^2&=B^2[1-\cos(\Delta-4\pi/3)]\end{aligned} \tag{3.24}$$

Then the phase can be determined by

$$\Delta=arctan\frac{\sqrt{3}((I_3-I')^2-(I_2-I')^2)}{2(I_1-I')^2-(I_2-I')^2-(I_3-I')^2} \tag{3.25}$$

The fast temporal phase shift algorithm does increase the measurement speed and brings the possibility of dynamic measurement. Similar algorithms are 4+2 and 4+1, but this kind of method greatly reduces the quality of the phase image. The relevant comparison is shown in the Figure 3.6

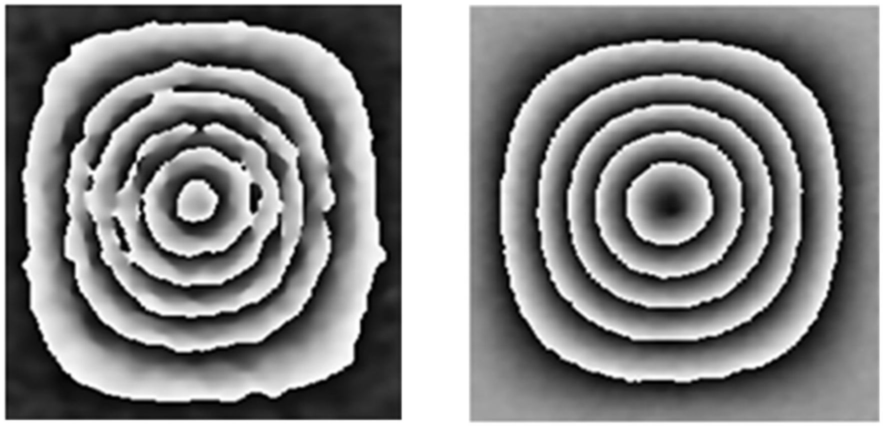

(a) (b)

Figure 3.6. Comparison of phase maps by different algorithms: (a) 3+2 Fast temporal phase shift (b) 3+3 temporal phase shift.

3.3 Spatial phase shift technology

Temporal phase shift method increases the measurement sensitivity about 10 to 30 times higher than the conventional intensity subtraction method. However, the temporal phase-shift shearography technique assumes the phase distribution of the speckle pattern image remains static during the multiple phases stepping procedure. This brings low acquisition rate and low phase map quality [61-65]. Spatial phase shift is a brand-new method that only requires a single image to create the phase map. Thus, the acquisition rate will only be limited by the camera's acquisition rate [66-71].

Spatial phase shift was developed to quantitatively determine phase difference using a single intensity image. There are two major methods to reach this goal. One is known as the multichannel spatial phase-shift approach, and the other called the frequency carrier spatial phase shift method. In recent decades, the frequency carrier method is more popular that a Fourier transform method provides a way to extract and separate each phase information from a single image. The earlier approach to solve dynamical loading problem was to use multichannel spatial phase shift method. Multiple channel spatial phase-shift method it to create a spatial phase shift between several adjacent pixels by adjusting the reference beam. Each pixel is like a channel with a particular phase difference. By setting the reference beam an appropriate angle α, an optical path difference between two adjacent pixels is created. The premise of this technology is that a speckle needs to cover the corresponding number of pixels [72-77].

<u>3.3.1 The multichannel spatial phase shift method</u>

To extracting the phase by multichannel spatial phase shift method, there are several algorithms to select. The basic algorithms are similar to the temporal phase shift method that can be roughly divided to three steps, four steps and five arbitrary steps. The difference is that three steps and four steps method require a specific phase value difference (120 degrees for three steps method and 90 degrees for four steps method) between all the adjacent two pixels while five arbitrary steps method only requires that the two adjacent pixels have the same phase value difference but not particular value. It brings about a difference in optical layout and image quality. Besides, the traditional multi-channel method considers that speckles exist without overlapping, so the phase information of the same pixel value is not calculated repeatedly. However, recent studies have shown that the speckle arrangement is randomness and overlapping, which means it is feasible to extract the phase pixel by pixel. This possibility can overcome the limitations of the spatial resolution of the multichannel spatial phase shift algorithm. In the past, it took three pixels at least to calculate a phase value, but now we can get a phase value amount equivalent to the number of CCD pixels. However, it also shows that the measurement result contains multiple speckle information and contains a lot of noise.

Figure 3.7 shows the schematic of the multichannel method for generating a spatial phase shift among pixels. An appropriate angle α between object beam and reference beam can generate an optical path difference (OPD). Eq. 3.24 describes the relationship between OPD and pixel size S and illumination angle α.

$$OPD = S \cdot sin\alpha \tag{3.26}$$

If a laser wavelength used is λ, a phase shift is obtained by

$$\Delta = (S \cdot sin\alpha/\lambda)2\pi \tag{3.27}$$

Because the basic principles of the three steps phase shift method and the four steps phase shift method are similar, the more popular and simpler, four steps phase shift method is introduced here. Using intensity data of Four adjacent pixels, the phase distribution can be calculated as presented

$$\begin{aligned} I_1 &= A + B\cos\theta \\ I_2 &= A + B\cos(\theta + \frac{\pi}{2}) \\ I_3 &= A + B\cos(\theta + \pi) \\ I_4 &= A + B\cos(\theta + \frac{3}{2}\pi) \end{aligned} \tag{3.28}$$

Where I_1 to I_4 represent the intensity of four pixels. A and B are parameters related to the background information. θ is the phase information of the corresponded speckle pattern. By adjusting a proper angle α, the π/2 phase difference can be achieved. In order to obtain a precise π/2 phase difference, the angle α needs to be calculated based on the configurations of the optical layout. The phase θ can be calculated as

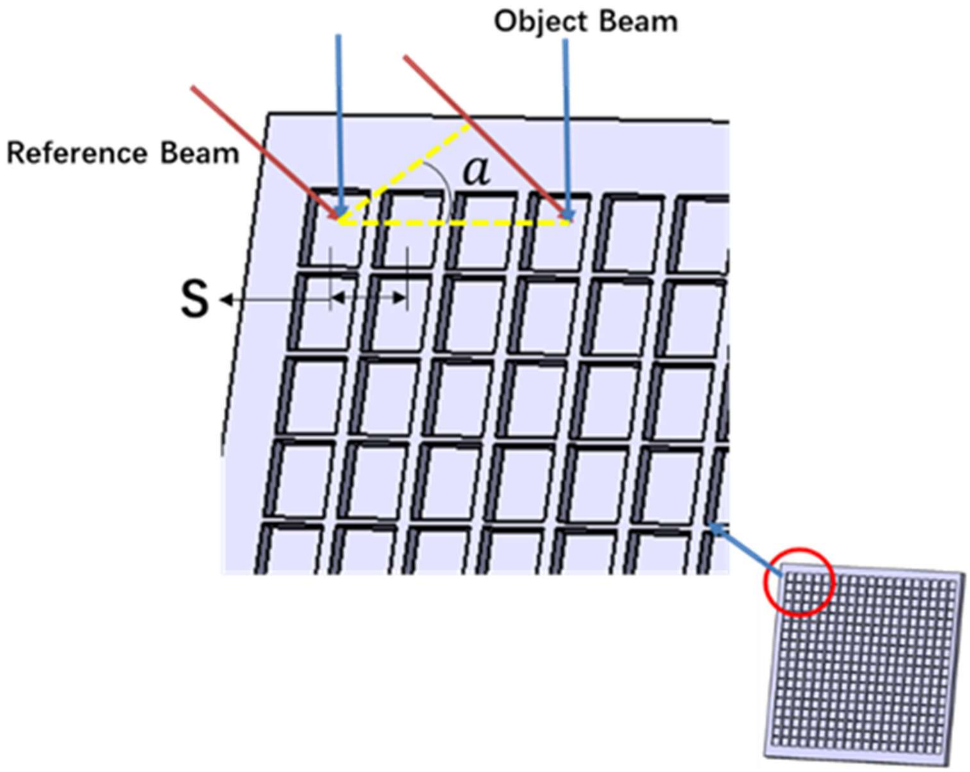

Figure 3.7. The schematic of the multichannel method for generating a spatial phase shift among pixels

$$\theta = \arctan(\frac{I_4 - I_2}{I_1 - I_3}) \tag{3.29}$$

In arbitrary five steps phase shift method, five adjacent pixels are used to solve a single phase. The intensity of five pixels can be written as

$$\begin{aligned} I_0 &= A + B\,cos(\theta - 2\Delta) \\ I_1 &= A + B\,cos(\theta - \Delta) \\ I_2 &= A + B\,cos(\theta) \\ I_3 &= A + B\,cos(\theta + \Delta) \\ I_4 &= A + B\,cos(\theta + 2\Delta) \end{aligned} \tag{3.30}$$

Δ can be any phase value except zero in arbitrary five steps method, which means it is flexible to arrange the angle α. The phase θ can be calculated as

$$\theta = \arctan\left(\frac{2(I_1 - I_3)}{2I_2 - I_0 - I_4} \frac{1}{\sqrt{1 - \left[\frac{I_0 - I_4}{2(I_1 - I_3)}\right]^2}}\right) \tag{3.31}$$

Compared with the four steps phase shift algorithm, arbitrary five steps algorithm is simpler and more convenient in optical setup arrangement. However, it uses some approximate trigonometric transformations and has lower calculation speed. The comparison between two methods is shown in the Figure 3.8.

Both the four steps phase shift and the arbitrary five steps phase shift can be used to calculate the phase value in the multichannel spatial phase shift algorithm. The difference is that when building the optical path, the four steps phase shift requires very

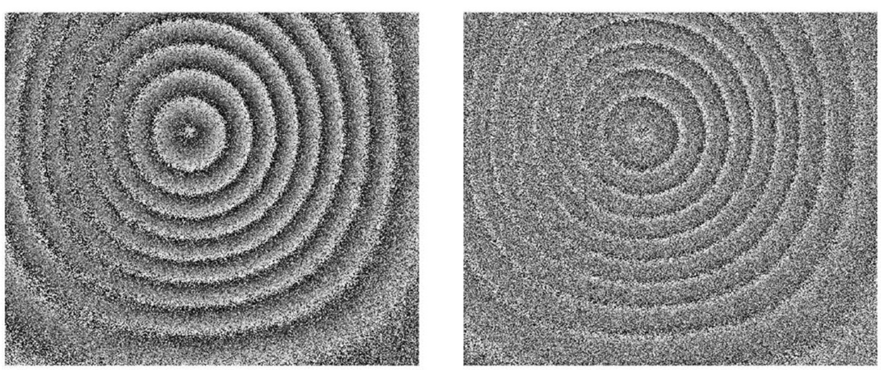

(a) (b)

Figure 3.8. Phase map of multichannel spatial phase shift method (a) 4 steps phase shift method (b) arbitrary five steps method.

precise angle control to ensure that the phase difference between adjacent pixels is 90 degrees, which puts higher requirements on the modulation and accuracy of the equipment. Besides, the parallelism of the reference light also has a certain impact on the phase map quality. The bad parallelism of the reference light can bring the different levels of noise in different positions of the same phase image. The arbitrary five steps phase shift method does not have such strict modulation requirements. The phase value can be obtained without knowing the specific angle relationship between the reference light and the object light. However, arbitrary five steps phase shift method uses a certain degree of approximation algorithm in the calculation process, which results in the noise.. Therefore, when choosing these two algorithms, it needs to consider the requirements. When the equipment is integrated into the instrument through precise optical path design, the four steps algorithm has the advantages of simplicity, fast calculation speed and high accuracy. When the experimental conditions cannot achieve the corresponding accuracy, the five-step algorithm is also a good choice to obtain a decent result.

3.3.2 The frequency carrier phase shift method

Carrier frequency technique is used in telecommunication first. The useful signal is modulated by a high-frequency carrier and transmitted through space as an electromagnetic wave. After receiving, the modulated signal is demodulated for separating the useful signal and carrier frequency. This method is applied in speckle pattern interferometry since 1996, introduced by G Pedrini. A setup based on Mach-Zehnder Interferometer is built to realize the spatial phase shift shearography. Here, we use Pedrini's setup as an example to show the fundamentals of frequency carrier spatial-phase-shift technique. In this configuration, Figure 3.9, a Mach-Zehnder Interferometer is used as a shearing device. The shearing amount and carrier frequency are determined by the angle of mirrors. A CCD camera records the final two images. Mach-Zehnder Interferometer is a very symmetry interferometer whose two beams has no intersection before the combination. The individual two beams provide the potential for Mach-Zehnder interferometer to do some comparison tests.

In Mach-Zehnder interferometer, the shear is not only generated by the tilting of mirrors, but also by the moving of the mirror. Mirrors move along the horizontal or vertical direction can result in the movement of the image in the CCD plane. The operation of moving mirror has the similar function as tilting mirror. The difference is tilting mirror introduces in an angle of the beam but moving mirror not. In other interference research, even in temporal phase shift method, the effect of this difference is minor. However, this characteristic is very important in the spatial phase shift method. Because the angle by tilting mirror will bring the spatial frequency for the evaluation process. The details will be explained by the equations.

The equations of sheared and unsheared images can be expressed as below:

$$u_1(x,y) = |u_1(x,y)|\, exp[i\varphi(x,y)] \tag{3.32}$$

$$u_2(x,y) = |u_2(x+\Delta x,y)|\, exp\{i\varphi(x+\Delta x,y) + 2\pi i f_0 \cdot x\} \tag{3.33}$$

Here, only single x direction shearing is concerned. U1 and U2 are the two components of the reference and real object. Δx is the shearing distance in x shearing direction. The value represents the component of carrier frequency introduced by tilting angle.

$$f_0 = (sin\,\beta\,/\lambda) \tag{3.34}$$

The intensity of the two images can be expressed as

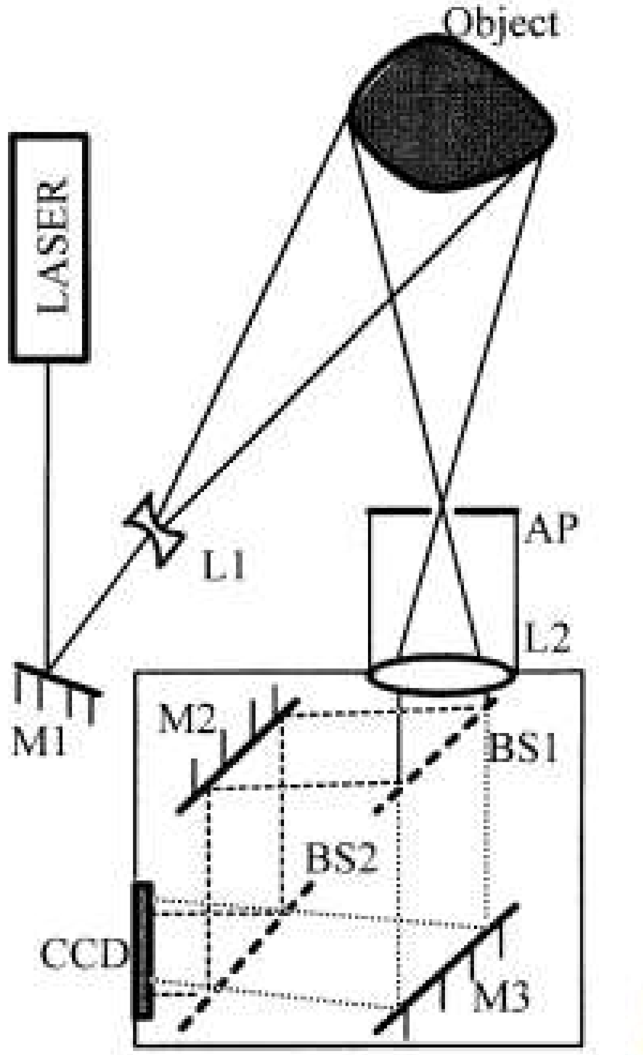

Figure 3.9 Schematic of shearography using Mach-Zehnder Interferometer

$$I = (u_1 + u_2)(u_1{}^* + u_2{}^*) = u_1 u_1{}^* + u_2 u_2{}^* + u_1 u_2{}^* + u_2 u_1{}^* \tag{3.35}$$

The Fourier Transform is used to converts the image from a spatial domain to the Fourier domain.

$$\begin{aligned} FT(I) = {} & U_1(f_x, f_y) \otimes U_1{}^*(f_x, f_y) + U_2(f_x + f_0, f_y) \\ & \otimes U_2(f_x + f_0, f_y) + U_1(f_x, f_y) \otimes U_2{}^*(f_x + f_0, f_y) \\ & + U_2(f_x + f_0, f_y) \otimes U_1{}^*(f_x, f_y) \end{aligned} \tag{3.36}$$

Terms which contain the useful information are $U_1 \otimes U_2^*$ and $U_2 \otimes U_1^*$. The two spectra are located at $(f_0, 0\ )$ and $(-f_0, 0)$ as shown in Figure 3.10. Windowed Inverse Fourier Transform (WIFT) is used to calculate the phase distribution. Area of $(-f_0, 0)$ can be transformed by WIFT as:

$$[\theta + 2\pi x f_0] = arctan \frac{Im[u_2 u_1{}^*]}{Re[u_2 u_1{}^*]} \tag{3.37}$$

Same as the temporal phase shift method, the phase difference can be calculated by the phase after load to subtract the phase before load. The equation is written as:

$$\Delta\theta = \theta - \theta' \tag{3.38}$$

Spatial phase shift method only needs a single image to calculate the phase distribution, which means the acquisition rate is no longer limited by the phase shift steps. The dynamic test becomes possible by the application of a high-speed camera.

In recent years, Xin proposed a new Michelson Interferometer based single carrier frequency spatial phase shift shearography [78]. Compared with the Pedrini's setup, Xin's setup has a much larger field of view. Figure 3.11 shows the schematic of the Michelson Interferometer based spatial phase-shift shearography setup.

Tilting Ml shifts the spatial spectrum on the spatial frequency domain while generating the shearing amount. A circular shaped aperture is placed in front of the

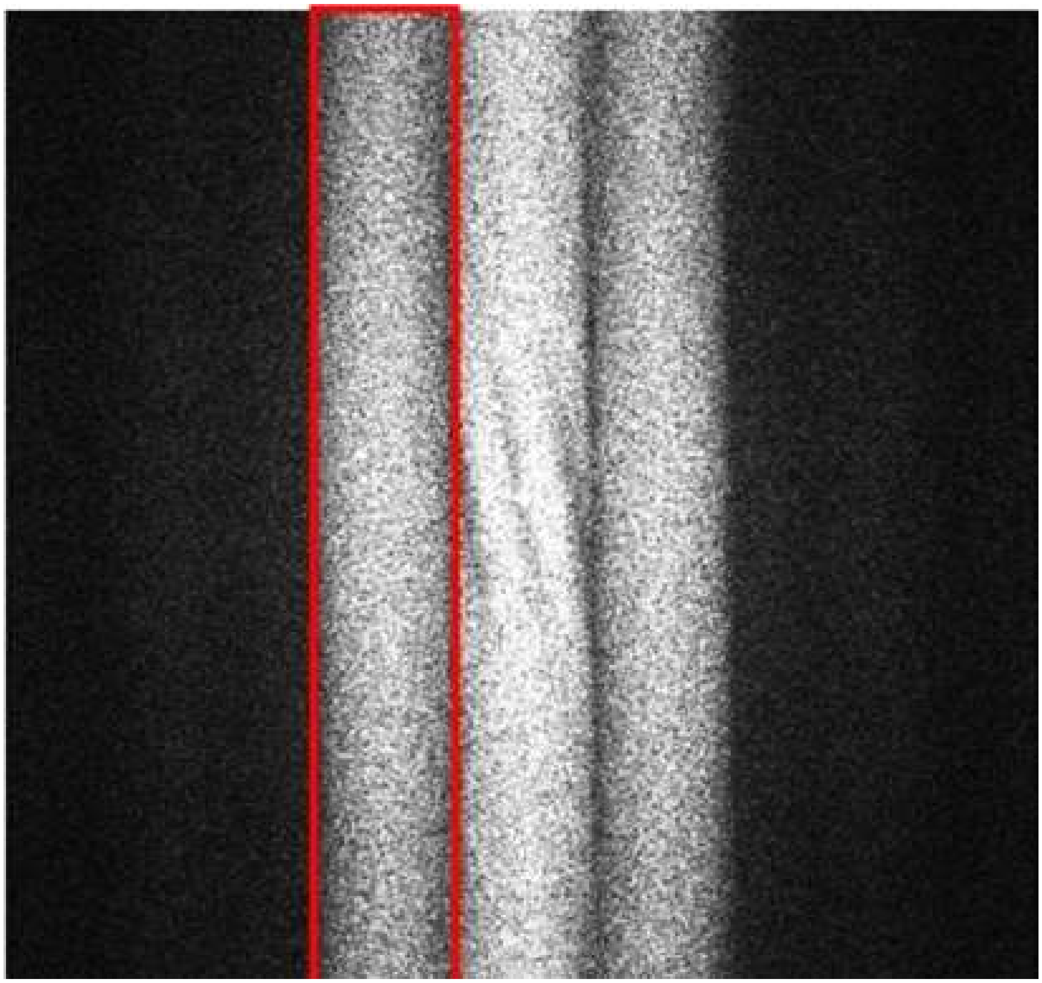

Figure 3.10 Spectrum after Fourier transform

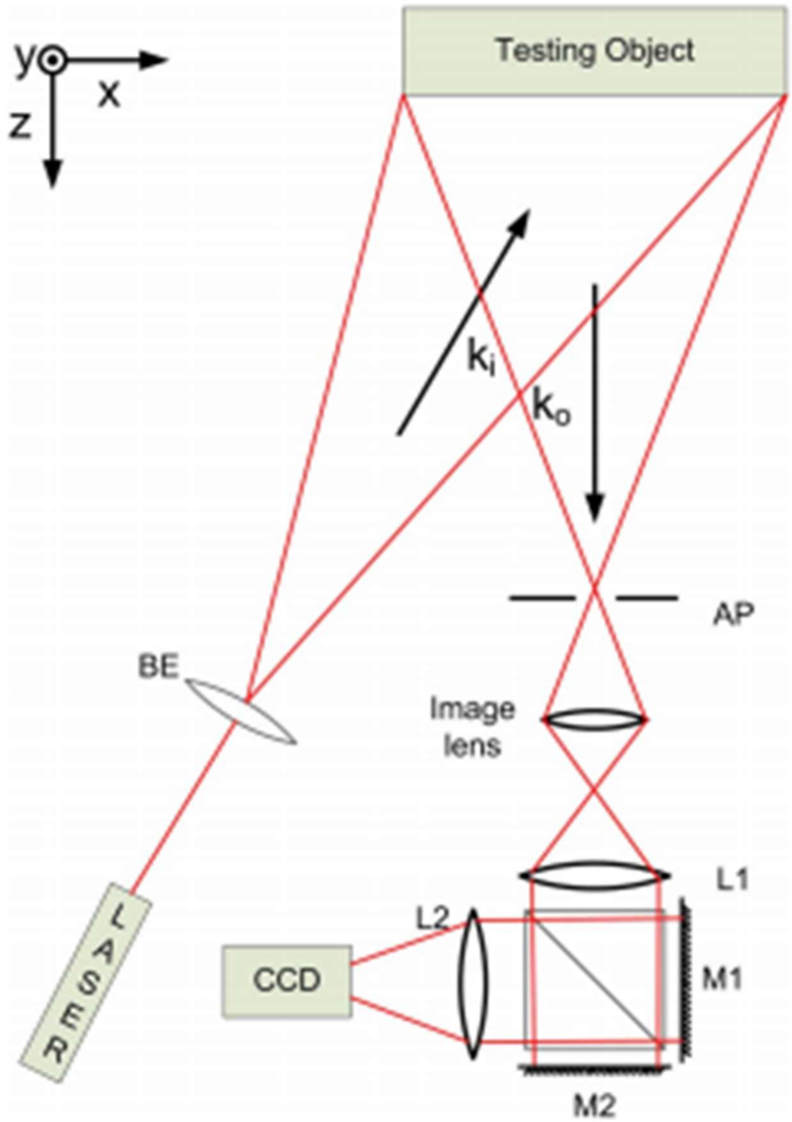

Figure 3.11 Michelson Interferometer based shearography setup

imaging lens at the Fourier plane to control the spectrum size on the spatial frequency domain. Through the Fourier Transform, the speckle pattern image is transferred into a spectrum on the Fourier domain. The two parts of the spectrum that contain the phase information of the recorded shearogram are also separated when a spatial frequency shift is introduced by the shearing. The phase differences can then be calculated from the complex amplitude by applying a properly selected Windowed Inverse Fourier Transform. By analyzing the phase difference of the laser before and after loading, the out-of-plane deformation gradient of the testing object due to the loading can be evaluated.

The modified Michelson interferometer has the advantage of ease of changing the shearing amount and shearing direction, simple and reliable structure and adjustable field of view because of a 4f system.

The 4f system consists of two lenses with the same focus length. The optical path length between the two lenses is equal to double the focus length of the lenses axis in the system. The 4f system transmits the images from the image plane of the image lens to the sensor inside the camera. It rotates the image 180° with an image size magnification of 1：1.

3.4 The filtering method of the phase map

Digital shearography uses the characteristics of random distribution of speckles to encode the surface information of the object to be measured and obtain it by calculation. During this process, various systems or random errors are also introduced. For subsequent processing, it is generally necessary to filter the resulting phase map.

Commonly used filtering methods are mean filtering, median filtering, phase filtering and frequency domain low-pass filtering [79-81].

Mean filtering is a typical linear filtering method. This method replaces the original value of the point with the average value of the surrounding points of the center pixel. This method has the advantages of simple and fast calculation, which is good for high-frequency noise filtering. This method could make the image blurry while the image details are largely lost in the filtering process. For the phase image of speckle interference, the position of the fringe jump directly affects the accuracy of the subsequent processing. Therefore, it is not possible to obtain an ideal speckle interference phase map using only the mean filtering.

Median filtering is a non-linear signal processing technology based on sorting statistical theory. This method considers the gray value of each pixel as the median value of all pixels in a certain neighborhood window of that point. This method can eliminate isolated noise points. In the process of filtering, the median filter does not need to perform statistical analysis on the image and does not make the image blurred. However, this method has poor filtering ability for Gaussian noise, and is mostly used to remove salt and pepper noise. However, the ability of median filtering to preserve the linear phase information of the speckle interference phase map is poor, the filtering result is less smooth than other methods, and the calculation speed of this method is slow.

Gaussian filtering is also a linear filtering. Like mean filtering, Gaussian filtering is also a process of weighted averaging over the entire image, and the result of weighted averaging the values of other pixels in the surrounding area is used as the value of the target pixel. However, Gaussian smoothing has the characteristics of homogeneity. After filtering, the characteristic information of the image will be lost.

Frequency-domain low-pass filtering is to perform Fourier transform on the shearography. By controlling the transfer function of the filter, low-frequency components can be extracted from the frequency spectrum. preserving the overall image information, filtering out some high-frequency noise is possible. According to the transfer function of the filter, the frequency domain low-pass filter can be further subdivided into ideal low-pass filter, exponential low-pass filter and Butterworth low-pass filter. The filtering ability of the frequency domain low-pass filter is proportional to the cut-off frequency, but the corresponding details are seriously lost.

The phase filtering technology is a method to pre-process the image to ensure the jump information of the speckle interferogram in response to the loss of the peak information of the phase map caused by other filtering technologies. Because the information at the jumps of the speckle interferogram is discontinuous, the phase filtering technology needs to convert the discontinuous information into continuous information before processing. This technique expands the phase information of the phase map on the unit circle of the complex plane through Euler's formula, so that the discontinuous transitions become continuous information. Then filtering the real and imaginary parts of the complex plane separately (such as mean filtering, median filtering, etc.) to obtain new complex information. By restoring the filtered new information, the filtered phase map can be obtained. This technology will not affect the jump information of the speckle interferometric phase map and can effectively filter the noise information of the phase map. In the actual filtering process, phase technology is often used to save the jump information of the speckle interferogram, and then different filtering techniques are used as needed to filter the speckle interferogram phase image.

3.5 The phase unwrapping technique

The filtering result of Digital Shearography is the wrapped map containing the phase information of the measured object surface. In the graph of the phase distribution, phase value is a discontinuous distribution that appears as a sawtooth shape. When the phase increases to 2π, the phase information of the next pixel jumps to 0 and repeats again. It is necessary to unwrap the phase information to obtain the actual distribution of the first derivative of the surface deformation of the measured object [82, 83]. Figure 3.12 shows the phase value of wrapped and unwrapped map.

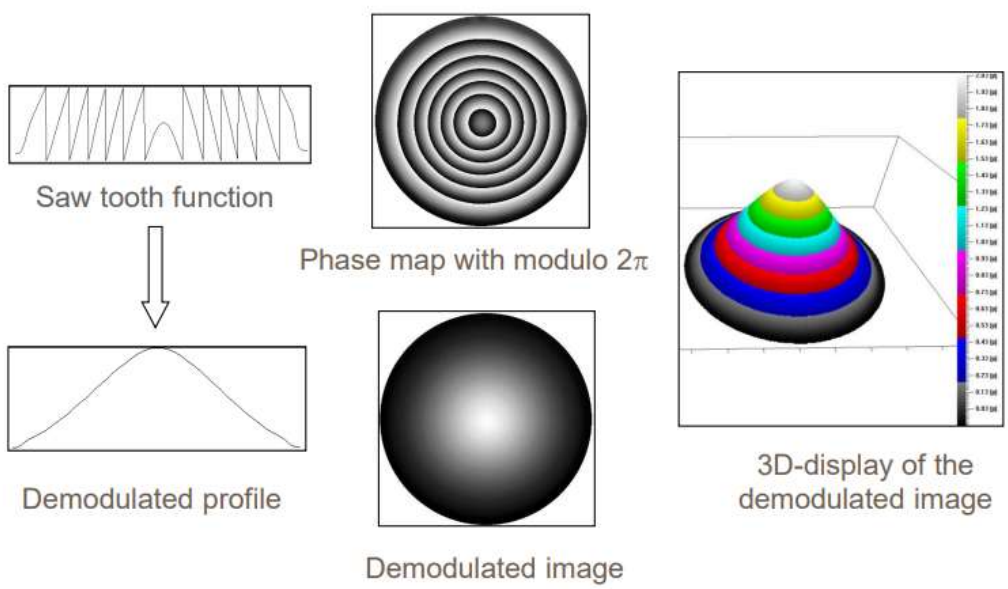

Figure 3.12 The comparison of wrapped and unwrapped phase map

The basic principle of the phase unwrapping technology can be simply summarized as starting from a certain phase point, comparing the phase value information of adjacent pixels, within a range, the phase change is continuous. When the phase difference between adjacent pixels exceeds a certain threshold, it is considered that the phase value has jumped. According to the jump situation, add or subtract an integer 2π on the value of previous pixel to obtain the phase information of the next pixel. In this way, phase information with discontinuous transitions is converted into continuous phase information.

CHAPTER FOUR

MODIFIED MICHELSON INTERFEROMETER BASED DUAL SHEARING DIGITAL SHEAROGRAPHY

4.1 Shearing effect on NDT

Shearing is an essential element of shearography which affects the measurement sensitivity by a shearing amount and shearing direction. In a small shearing amount, the deformation from some minor defects can be revealed, and the fringe patterns represent the gradients of deformation. With the increasing of the shearing amount, the measurement sensitivity is increased. Shearogram represents the deformation instead of gradients while the shearing amount equals to the half size of the defects. Unlike the ESPI whose pattern represents shape and size of deformation, shearograms have the different expressions in different shearing directions. For example, the defect brings a circular deformation on the surface. The shearograms direction will be in accord with the shear direction like the Figure 4.1.

Even though the shearograms of different shearing directions are different, they are from the same defect with the same loading. Such circular defects have less requirement on the shearing directions. However, if the defects have an irregular shape as a crack, the results could be complicated in different shearing direction. For example, Figure 4.2, the crack grows in the horizontal direction. In common sense, the gradients change rapidly in a vertical direction while the gradients change only on the two edges of the cracks in a horizontal direction. Figure 4.2 (a) shows the shearograms in x shearing of the testing.

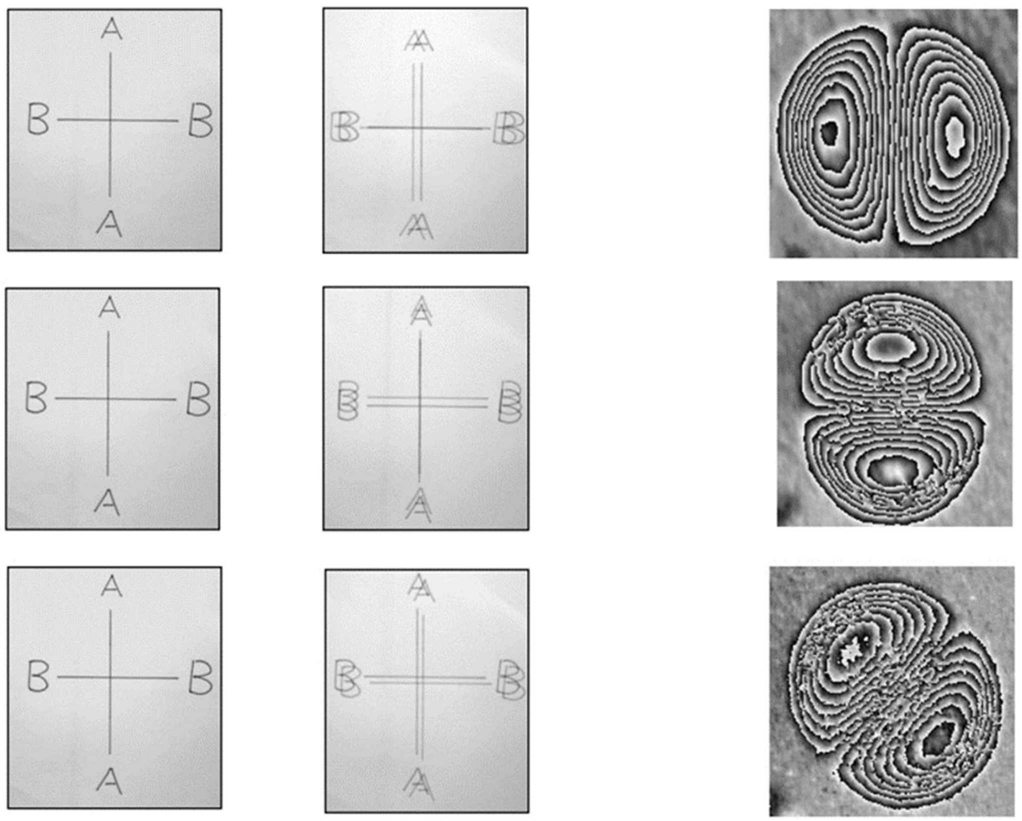

Figure 4.1 Shearograms in different shearing directions

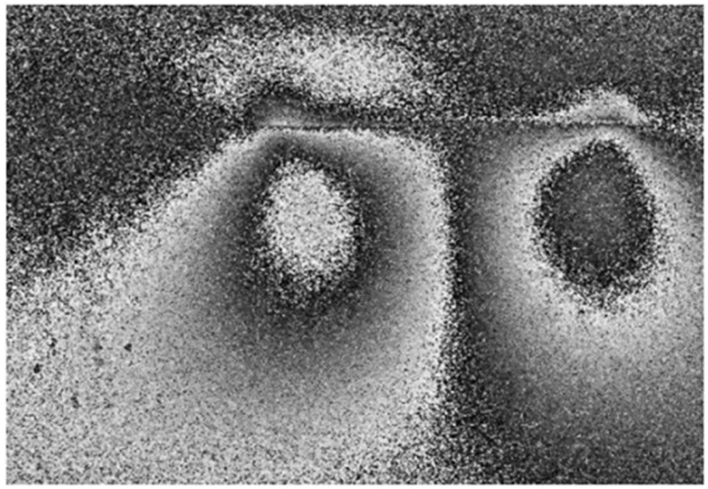

(a)

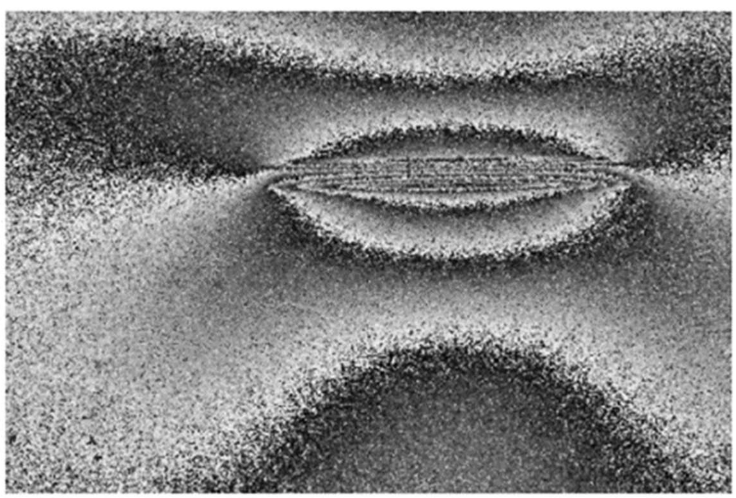

(b)

Figure 4.2 Shearograms of a crack in different shearing directions (a) the shearogram in x shearing direction (b) the shearogram in y shearing direction.

The proposed crack and Figure 4.2(b) shows the shearograms in y shearing direction of the proposed crack. In this case, we can still tell where is the defects on the horizontal shearing directions based on the huge shearograms on the two side of the crack, However, it is hard to tell there is only one defect or two defects if just judged by the shearograms. Only by combining the results of another shearing direction to observe can we reach a conclusion. If the defects are like the rectangle slots shown on the Figure 2.14, the slots could be missed by a single shearing direction measurement.

Two shearing directions measurement is necessary for avoid missing the flaws, which means two times testing at least. However, adjusting shearing directions takes a long time and complicated operation even in the modest setup. To save the labor and cost, improve the testing efficiency, a dual shearing directions measurement is needed to be developed in Digital Shearography.

4.2 The review of dual shearing shearography

4.2.1 Dual shearing shearography of two stacked interferometers

In conjunction with the invention of shearographic technology, people have discovered issues associated with the difficulty of multi-directional measurement. In the past few decades, various developments have been proposed to overcome this problem. However, other problems have resulted from this research, such as high cost, poor image quality, unstable structure and error accumulation.

Steinchen W and Yang L reported the first temporal phase-shift digital shearography system to perform simultaneous dual shearing direction measurement [84]. The system used the temporal phase shift method and required two individual cameras as shown in the Figure 4.3. Basically, it stacks two Michelson interferometer and uses two cameras to record the images with the corresponding shearing direction. In this system, three reflective mirrors are used, one large mirror is used as the PZT mirror which has no shearing and utilized to generating phase shift. Another two mirrors shear in x and y direction respectively. In the configuration of Figure 4.3, the laser is expanded to illuminate the object, then incident into the top and bottom beam splitter separately. Top Michelson interferometer has a y shearing while the bottom beam splitter has the x shearing. Two cameras are connected to the frame grabber and recorded the image at the same time. All the images will be finally transferred to the computer to process with pre-input parameters.

The configuration did solve the dual shearing directions issue and were applied in a long term. It has the advantages of simple structure and good phase map quality due to the PZT based temporal phase shift method. However, the setup also leaves a lot of problems in structure, operation and error analysis.

Since two Michelson interferometer are stacked together, the incident light goes in different angles. In the imaging plane, two images of two channels have different observation angle. If the object is far from the setup, this angle can be neglected. However, in a limited measurement area, two images could present a different surface information especially in the quantitative test. Besides, Beam splitter could be the field diaphragm which reduces the field of view. Siebert and Schmitz later proposed an improved setup, using the polarization effect to resolve the image offset [85]. The new setup puts the interferometers on the same height and uses only one beam splitter to receive the light. This method optimizes the equipment to a certain extent but cannot solve the operation issue of two cameras. Two image acquisition devices not just increase

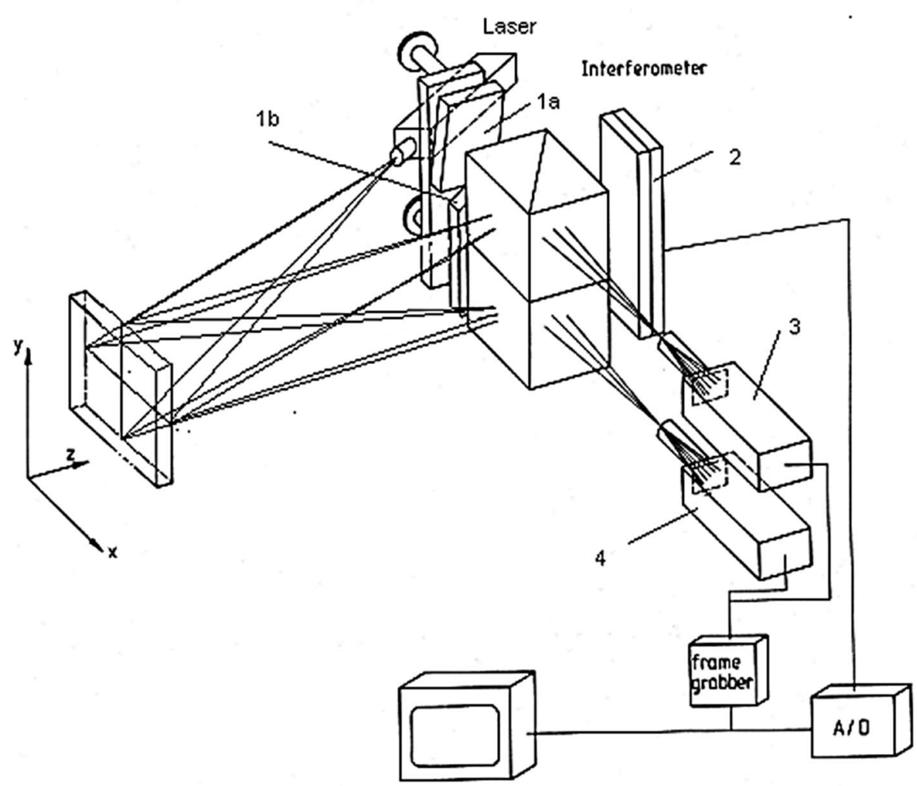

Figure 4.3 The schematic of dual shearing shearography of two stacked interferometers

the cost but also introduce the issue of device consistent. Different cameras have their own characteristic, even triggered at the same time, the system error cannot be avoided. The first thinking is to reduce the image acquisition device amount.

4.2.2 Dual shearing shearography of multiple wavelengths and a color camera

In recent years, with the development of electronic devices and software, RGB color camera grow up. In 2006, Guillaume L. Richoz and Gary S. Schajer proposed a technique using multiple wavelengths and a color camera to do the simultaneous dual shearing measurement [86]. Figure 4.4 is the schematic of the simultaneous two-axis shearographic interferometer using multiple wavelengths and a color camera.

In this arrangement, a color camera views an object illuminated by three coherent laser sources of different wavelengths. A Cyan dichroic filter is installed in front of the mirror in Michelson interferometer. Another mirror is arranged as a PZT mirror which is connected to a PZT driver. Cyan dichroic filter can make the specific light wave reflect on the surface of a filter but let other light waves cross. Based on this characteristic, Blue and Green light waves cross the dichroic filter and are reflected upon the mirror, red light is reflected on the surface on the dichroic filter. A color camera simultaneously records the independent colored signals. An RGB color camera can record three color signals by different sensitivity unit. Each kind of unit only reacts to the color it belongs, which grantees the different color signal will not mix. In this setup, the mirror on the side of dichroic filter tilts in the y-direction, and the Cyan dichroic filter tilts in the x direction. Two pairs of images are formed on the plane of CCD Camera. The two signals are separated by the blue and red channels after the acquisition. Temporal phase shift is used to evaluate the fringes for both blue and red waves.

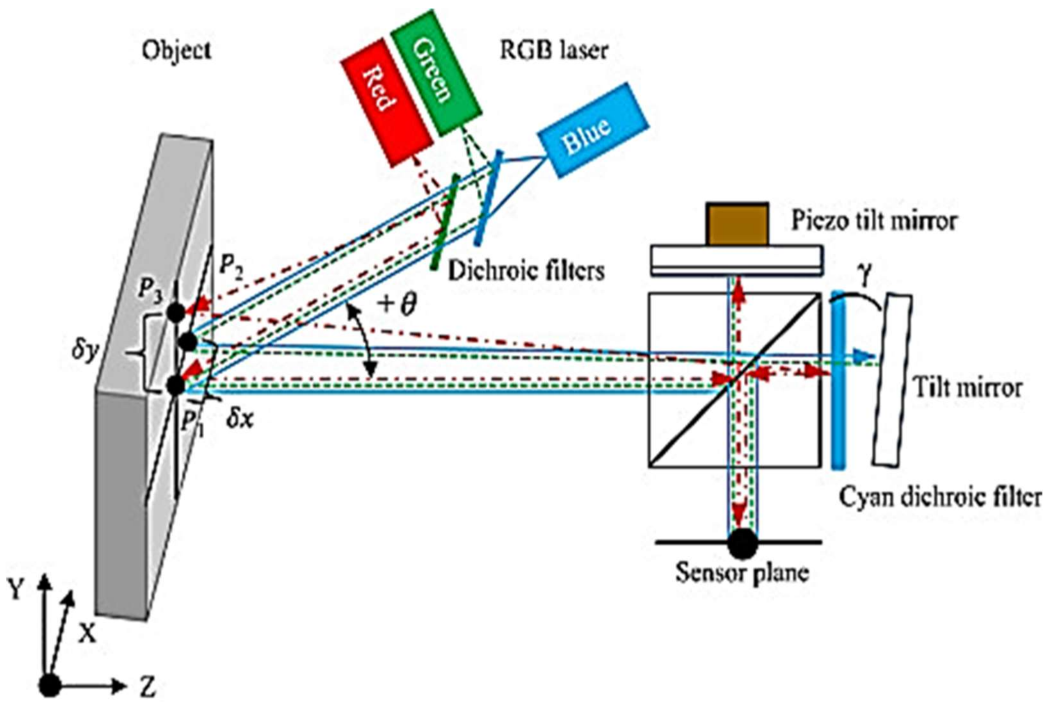

Figure 4.4 The arrangement of simultaneous two-axis shearographic interferometer using multiple wavelengths and a color camera.

The multiwavelength and color camera based shearography only need a single camera to record the images which can reduce the system error between two channels. Single Michelson Interferometer only have one incident port which eliminate the issue of different observing angle between two channels.

However, this technique also introduces some issues. Two shearing components are laterally placed, which makes the optical path of two channel different. Clearly, the amplify ratio of the two shearing directions image are different. Besides, single image lens may project the images on the CCD but cannot get good focus of both. If we choose to adjust the focus to make x shearing image clear, y shearing image could be blur. In opposite, x shearing image could be blur with y shearing image in focus. There is no perfect state for the two channels in this system.

The RGB color camera is an advanced camera, but it still has some disadvantages. First, the color unit does not respond only a single wavelength but a wavelength band. The width of the band depends on the manufacturing quality of the color CCD unit. Standard color cameras have a small area of the different bands overlapped, which could make a cross interference of x shearing and y shearing information. The noise and wrong fringe pattern sometimes will be introduced to the result. Second, this setup saves the utilization of optical components, but need two more lasers with different wavelength. Laser diode can help reduce the cost but may have too large wavelength band. In conclusion, Color camera and dichroic filter method did increase the accuracy of the shearographic system. At the same time, it simplifies the structure and operation. However, blur image and the overlap of the band can be new problems. The next thinking is to use a single gray scale camera to record images.

4.2.3 Dual shearing shearography of multiple wavelengths and spatial phase shift

After the first carrier frequency spatial phase-shift shearography system was reported in 1996 by Pedrini et al, more consideration was given to the use of the spatial phase-shift technique for NDT tests. The spatial phase-shift technique uses the Fourier Transform (FT) to transfer the spectrum to the frequency domain. A single pair of speckle pattern images is required to derive the phase map, making it appropriate for use by most current interferometry techniques due to its inclusivity. In addition, carrier frequencies allow multiple pieces of information to share one image plane. Information with different carrier frequencies have a separate area on the frequency domain, making this another viable means for dual shearing directional measurement. In 2016, Wang et al. introduced a dual shearing directional spatial phase-shift digital shearography system [87].

As shown in the Figure 4.5, the system used multi-wavelength light sources with two optical band-pass filters to separate the wave for two shearing directions and avoid cross interference. An interferometer combining the Mach-Zehnder and Michelson Interferometer was proposed for this system. For this combination, two individual Michelson Interferometers were substituted for the mirrors on the two arms of the Mach-Zehnder interferometer. The Mach-Zender interferometer was used to split and combine waves, while the two Michelson Interferometers were used as the shearing device to create two shearograms, one in the x-shearing direction and one in the y-shearing direction. A single camera recorded the multi-wavelength shearograms in the different shearing directions. This system was the first to achieve simultaneous dual directional

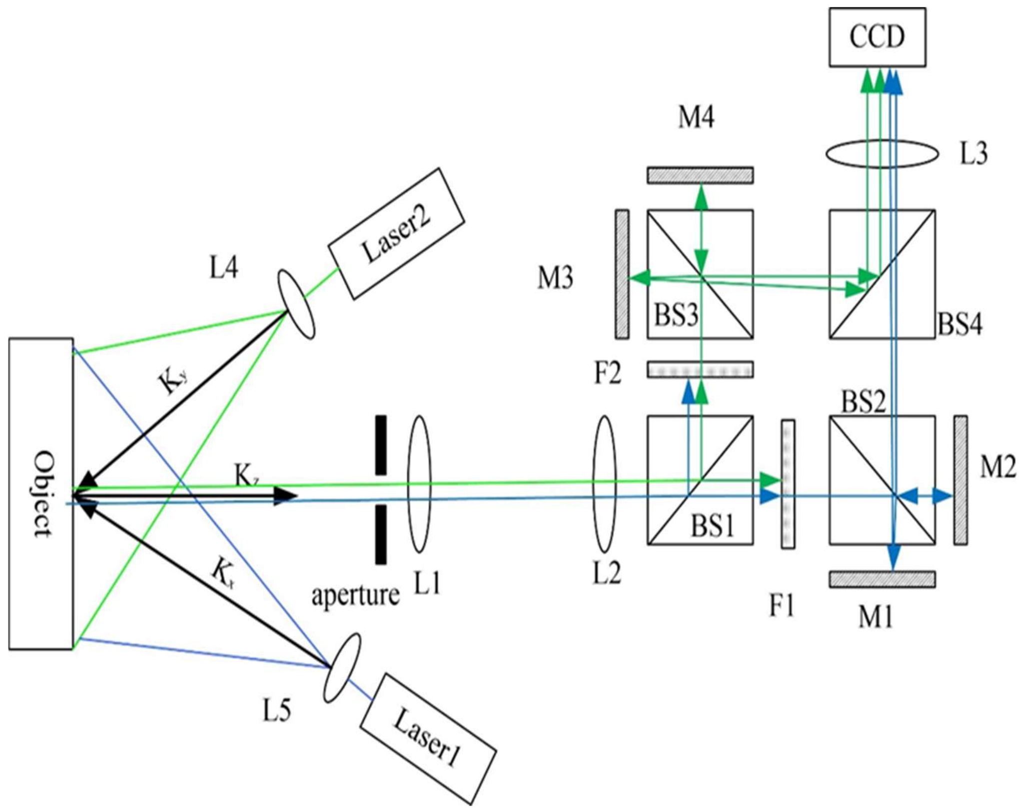

Figure 4.5. The schematic of simultaneous two-axis shearographic interferometer using spatial phase-shift digital shearography and multiple wavelengths

shearographic NDT by the spatial phase shift technique using a single CCD camera. The main limitations of Wang's system were the power loss due to the optical reflection structure and the omission of an optical band-pass filter. Assuming each band-pass filter would absorb half of the light intensity, only 6.25 % of the original light could be used on each shearing direction. Thus, two high power illumination lasers and corresponding laser alignment procedures were necessary, increasing the cost greatly. Multiple wavelengths also increased the computational complexity such that the results for the two shearing directions required arithmetic compensation to maintain consistency. The continuing thinking is to use only a single wavelength laser.

4.2.4 Dual shearing shearography of polarization method and spatial phase shift

Xin et al. investigated the use of a single laser to build a dual shearing direction Shearography system [88]. The laser polarization technique was used instead of multi-wavelength lasers and band pass filters to separate the signals.

The schematic is shown in Figure 4.6. Light that was polarized 90 degrees with each other did not interfere, so two waves with a polarization difference of 90 degrees could be used as the x-shearing and y-shearing component. Two 90-degree polarization difference waves are obtained using a polarized beam splitter. Two sub-Mach-Zehnder Interferometers, which were substituted for the reflection mirrors on the two arms of the main Mach-Zehnder Interferometer, generated the x-shearing and y-shearing. Xin's system reduced the cost (single laser) and increased the light use efficiency (12.5 % for each shearing direction). However, the complicated optical structure, which utilized 6 beam splitters and 4 reflection mirrors, was unstable, making it suitable only in lab environments with good vibration isolation.

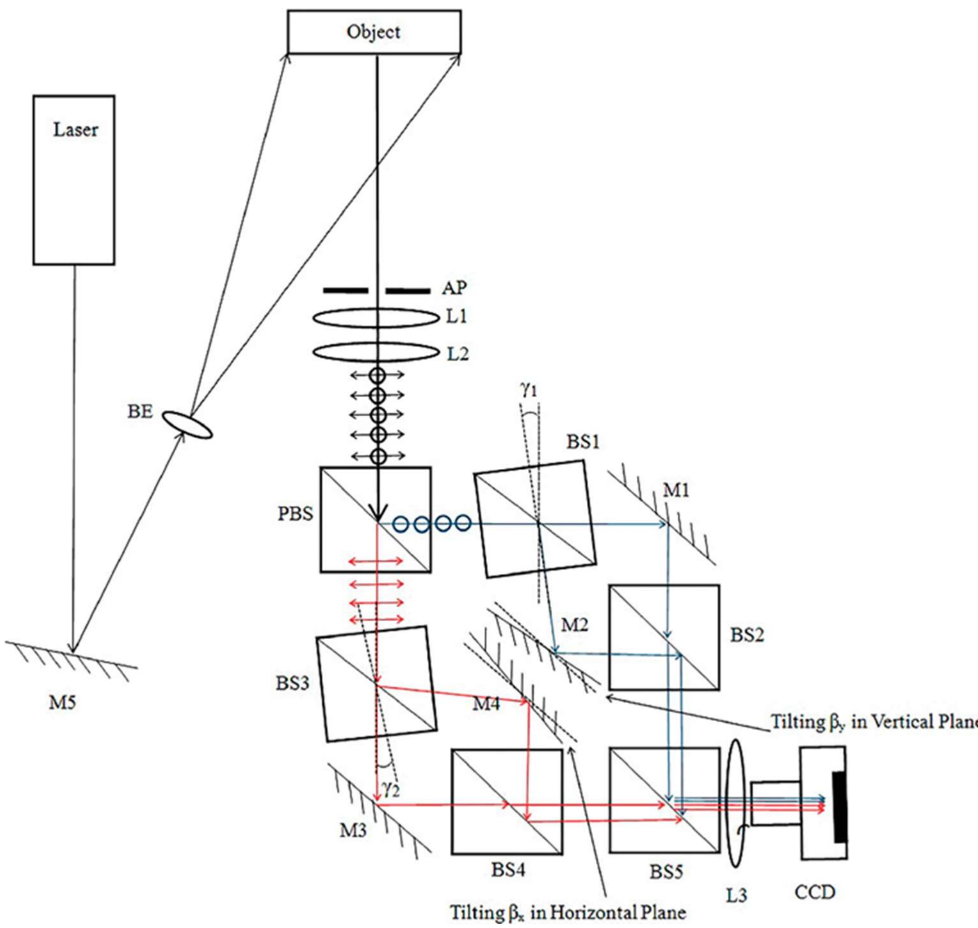

Figure 4.6. The schematic of polarized digital shearography for simultaneous dual shearing directions

Up to now, comparing the four techniques mentioned above, it can be found that dual shearing shearography development is on the following points. 1) There is less requirement of acquisition devices. At the very beginning, at least two cameras are required to record the two shearing directions information respectively. Then, a single-color camera can used to record multiple information. Now, a single gray scale camera can do the same thing based on the spatial phase shift method. 2) The dual shearing measurement becomes simultaneous. PZT driven temporal phase shift method is the basis of the early dual direction shearography which highly limited their measurement not in state. Also, two channels always have a difference in observing angle or amplifying ratio. In recent years, frequency carrier spatial phase shift method becomes the main approach to extract the phase information which only need a single image to calculate the phase value. Thus, the simultaneously measurement become possible. 3) The laser requirement is reduced. To separate two channels, different wavelength lasers are required to avoid the cross interference on the same plane. After the polarized effect applied, a single laser is available to do the test.

Even though the performance of dual shearing shearography has improved a lot, some issues also introduced with the development. 1) The optical structure becomes more and more complicated which reduces the stability of the setup. It increases the challenge of industry application. 2) A single laser can achieve the measurement but need a very high-power illumination because of low light efficiency. It brings the safe issue in application. In the next section, a new shearography system is proposed to solve the problem of simultaneous two directions measurement. This method keeps the benefits of good consistency and low cost. Also, it highly improves the light efficiency and simplify the setup.

4.3 Optical setup

Figure 4.7 shows a schematic of modified Michelson Interferometer based dual shearing direction shearography setup. The setup draws on some of the ideas of Siebert and Schmitz's system and is improved to record the information of two shearing directions on one shot with a single camera. A coherent laser with a 532 nm wavelength is used as a light source, while a λ/4 wave filter is used to transform the laser from linear to circular polarization. Rough surface reflection can turn a good linearly polarized laser to random polarization; however, the majority of the reflection wave would keep the original polarized direction. A λ/4 wave filter guarantees a 50:50 division of the light intensity in each polarized direction when the wave passes the polarized beam splitter.

AP and L1 are the aperture and lens of the imaging system, and L2 and L3 are the lenses of the 4f system used to enlarge the size of view. The wave front reflected from the object is divided into two waves by a normal beam splitter BS. One wave, named channel #R, hits mirror M1 and reflects to the BS then strikes the CCD with no polarization. Another wave enters a polarized Michelson interferometer formed by PBS as shown in the Figure 4.8, M2 and M3, then is divided into two polarized sub-beams. The sub-beam in the ordinary polarized direction hits M2, then is reflected. This sub-beam is named as channel #S. The second sub-beam in the extraordinary polarized direction hits M3 and is named channel #P. Carrier frequencies, shearing directions and the shearing distance are introduced by tilting M2 and M3 individually in the horizontal direction (x-shearing) and vertical direction (y-shearing). To separate the spectrum of the two shearograms on the

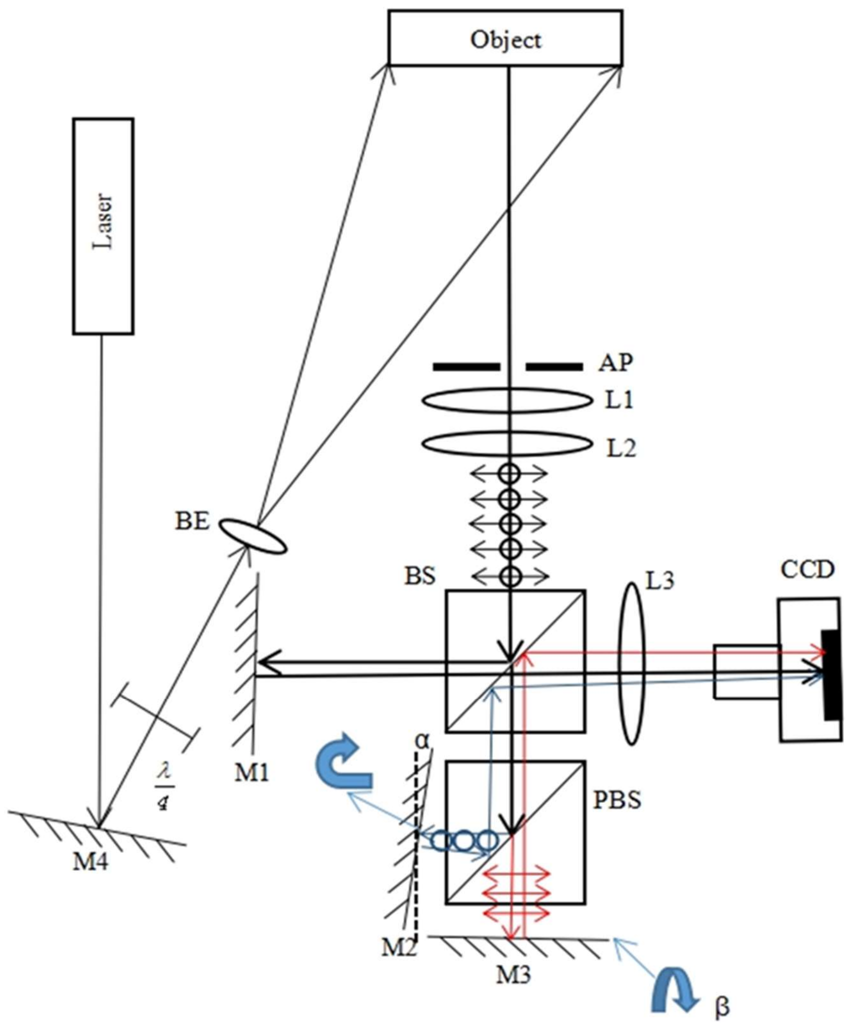

Figure 4.7. The schematic of polarized digital shearography for simultaneous dual shearing directions using modified Michelson Interferometer

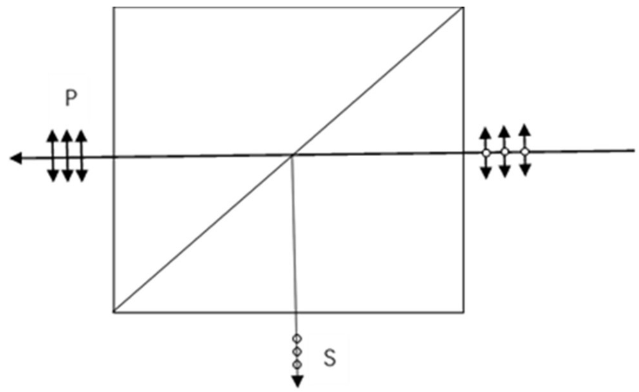

Figure 4.8. The schematic of polarized beam splitter

spatial frequency domain, a circular aperture is used to control the spectrum size while shearograms are evaluated by a Fourier transform method.

The formulas are introduced for better understanding of the whole process. Assuming the illumination and observation plane is in the XOZ plane, the light wave of channel #R shown in Figure 4.7 can be expressed as:

$$u(x,y) = |u(x,y)|exp[i\varphi(x,y)] \tag{4.1}$$

Where, φ(x,y) is the phase value, x is the pixel location and © is the imaginary unit. There is no polarization in the beam of channel #R. However, interference occurs when channel #R and channels #S or #P, with their own polarized directions, mix on the CCD plane. Eq. 4.1 can be rearranged as two equations with the corresponding polarizations.

$$u_x(x,y) = |u_x\,(x,y)|exp[i\varphi_x\,(x,y)] \tag{4.2}$$

$$u_y(x,y) = |u_y(x,y)|exp[i\varphi_y(x,y)] \tag{4.3}$$

u_x represents the part resulting from interference with channel #P and u_y represents the part resulting from interference with channel #S. In the meantime, the propagation direction of the reference wave is perpendicular to the CCD plane, resulting in no carrier frequency. Similarly, the wave going through M2 and M3 can be expressed as:

$$u_1(x, y) = |u_1(x + \Delta x, y)| exp[i\varphi_1(x + \Delta x, y) + 2\pi i f_1 x] \quad (4.4)$$

$$u_2(x, y) = |u_2(x, y + \Delta y)| exp[i\varphi_2(x, y + \Delta y) + 2\pi i f_2 y] \quad (4.5)$$

u_1 is the wave reflected from M2 with horizontal shearing direction (x-shearing direction) in channel #S, and u_2 is the wave reflected from M3 with vertical shear direction (y-shearing direction) in channel #P. Two carrier frequencies (f_1 , f_2) are introduced into the wave fronts by shearing angles α and β, which can be presented as:

$$f_1 = (sin\,\alpha/\lambda) \quad (4.6)$$

$$f_2 = (sin\,\beta/\lambda) \quad (4.7)$$

The angle α is achieved by tilting M2 in the x-shearing direction while the angle β is achieved by tilting M3 in the y-shearing direction. Furthermore, the relationship between the shearing distance and shearing angle can be expressed as:

$$\alpha = tan^{-1}\frac{\Delta x}{l} \quad (4.8)$$

$$\beta = tan^{-1}\frac{\Delta y}{l} \quad (4.9)$$

Here, l is the optical path distance between the mirrors and the CCD. Because orthogonal polarized waves cannot have interference, u_x only interferes with u_1 and u_y

only interferes with u_2. I_x and $I_y$are used to represent the interference intensity of the two polarized directions on the CCD plane.

$$I_x = (u_x + u_1)(u_x^* + u_1^*) \tag{4.10}$$

$$I_y = (u_y + u_2)(u_y^* + u_2^*) \tag{4.11}$$

Where * denotes the complex conjugate. The total recorded intensity I can be expressed as:

$$I = I_x + I_y \tag{4.12}$$

The Fourier transform is used to transform the signals to the frequency domain, which can be represented by:

$$\begin{aligned} FT(I) = {} & U_x(f_x, f_y) \otimes U_x(f_x, f_y)^* + U_1(f_x + f_1, f_y) \\ & \otimes U_1(f_x + f_1, f_y)^* + U_y(f_x, f_y) \\ & \otimes U_y(f_x, f_y)^* + U_2(f_x, f_y + f_2) \\ & \otimes U_2(f_x, f_y + f_2)^* + U_x(f_x, f_y) \\ & \otimes U_1(f_x + f_1, f_y)^* + U_1(f_x + f_1, f_y) \\ & \otimes U_x(f_x, f_y)^* + U_y(f_x, f_y) \otimes U_2(f_x, f_y + f_2)^* \\ & + U_2(f_x, f_y + f_2) \otimes U_y(f_x, f_y)^* \end{aligned} \tag{4.13}$$

The equation can be rearranged as five parts:

$$\begin{aligned} A(f_x, f_y) = {} & U_x(f_x, f_y) \otimes U_x(f_x, f_y)^* + U_1(f_x + f_1, f_y) \\ & \otimes U_1(f_x + f_1, f_y)^* + U_y(f_x, f_y) \otimes U_y(f_x, f_y)^* \\ & + U_2(f_x, f_y + f_2) \otimes U_2(f_x, f_y + f_2)^* \end{aligned} \tag{4.14}$$

$$B(f_x + f_1, f_y) = U_1(f_x + f_1, f_y) \otimes U_x(f_x, f_y)^* \tag{4.15}$$

$$C(f_x - f_1, f_y) = U_x(f_x, f_y) \otimes U_1(f_x + f_1, f_y)^* \tag{4.16}$$

$$D(f_x, f_y - f_2) = U_y(f_x, f_y) \otimes U_2(f_x, f_y + f_2)^* \tag{4.17}$$

$$E(f_x, f_y + f_2) = U_2(f_x, f_y + f_2) \otimes U_y(f_x, f_y)^* \tag{4.18}$$

Where, symbol $\otimes$ is convolution, f_x and f_y are the variables on frequency domain. As Eq. 4.14 to 4.18 show, the phase distribution in the Fourier domain is separated into five components: A, B, C, D, and E. Here, A represents the background information, and the remaining components represent the complex amplitudes of the interferogram. If an appropriate carrier frequency is introduced, the phases can be extracted by separating the five components in the frequency domain. For example, if the value of angle α and β are large enough to completely separate the five spectrums, the phase distribution in the Fourier domain can be achieved as shown in Figure. 4.9.

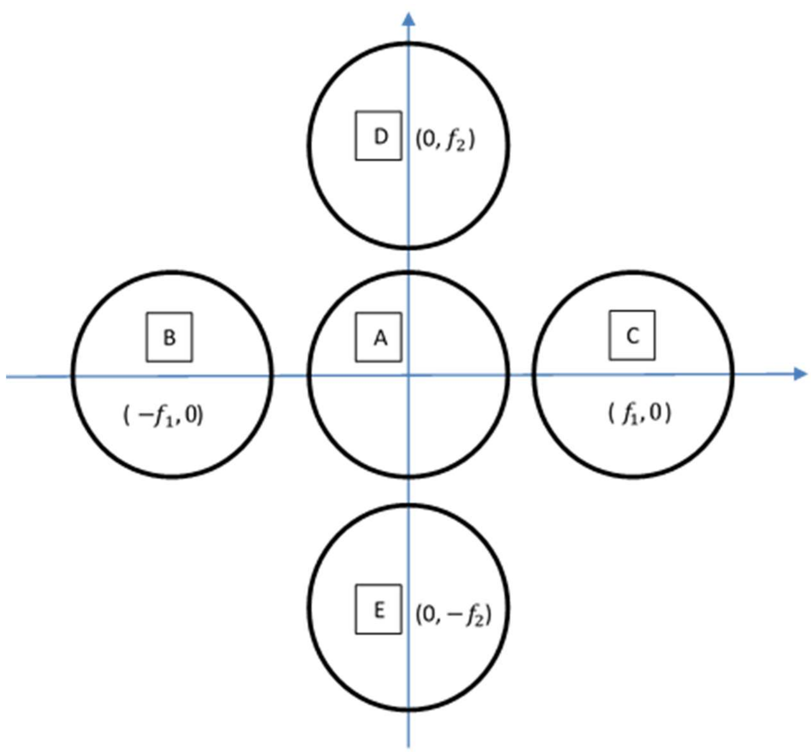

Figure 4.9. The ideal phase distribution in Fourier domain

The inverse Fourier Transform is applied to extract the phase information. The phase of spectrum C and D can be expressed as

$$[\theta_x + 2\pi x f_1] = arctan\frac{Im[u_1 u_x{}^*]}{Re[u_1 u_x{}^*]} \tag{4.19}$$

The phase of Y-direction shearing on spectral C can be expressed as below:

$$[\theta_y + 2\pi y f_2] = arctan\frac{Im[u_2 u_y{}^*]}{Re[u_2 u_y{}^*]} \tag{4.20}$$

Similar, repeating the producer on each image during the test. Then the phase difference caused by the loading can be expressed as:

$$\Delta_{\theta x} = \frac{4\pi\delta x}{\lambda}\frac{\partial w}{\partial x} \tag{4.21}$$

$$\Delta_{\theta y} = \frac{4\pi\delta y}{\lambda}\frac{\partial w}{\partial y} \tag{4.22}$$

4.4 Experimental validation

In Figure. 4.10, a center loaded square metal plate was tested using the proposed new dual directional shearographic setup. A 2453 x 2056-pixel grayscale CCD camera with a pixel size of 3.45 µm in the horizontal direction and 3.45 µm in the vertical direction is used to record the pictures. In this experiment, a Coherent Verdi G5 laser was used, the laser power of 150mW was selected. However, the idea descripted in this paper doesn't need such a highly monochromatic source. We use this laser just because we do not have other 150mW laser available for the time being. In fact, shearographic system can use a relative low cost laser, such as diode lasers, due to the self-referenced system, which has been proved and presented by many papers, books and journals [89]. The aperture size is chosen as 1 mm and the imaging lens is 25 mm (f = 25 mm). The focal

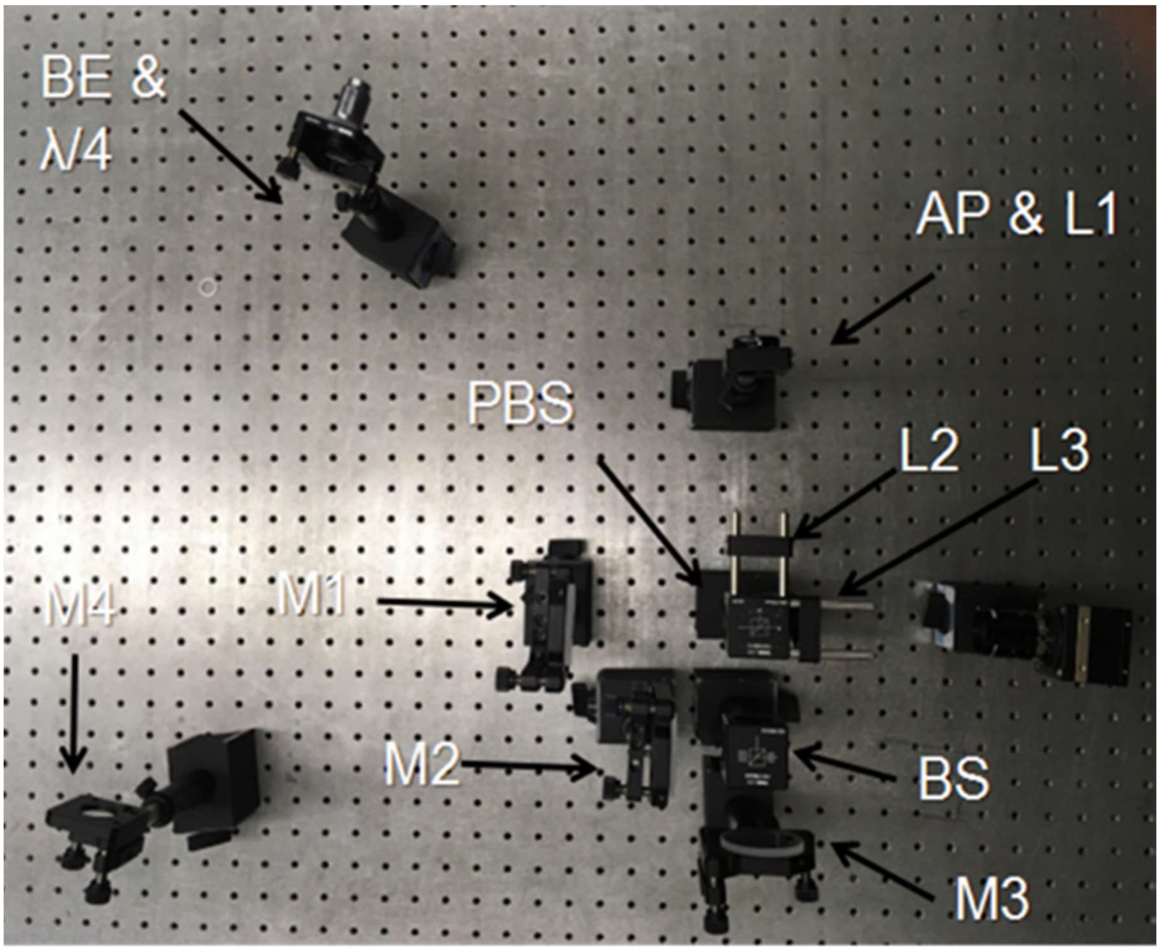

Figure 4.10. The real setup of the dual directional shearography using modified Michelson Interferometer

lengths of L2 and L3 are f = 100 mm. The split ratios of the normal beam splitter and polarized beam splitter both are 50:50. The shearing amounts in both directions are 5mm. The speckle size in the image can be achieved by the equation：

$$\Delta S = \frac{\lambda f}{D} \tag{4.23}$$

Where D is the aperture size and f is the focal length of image lens. The result is 13.3 µm in the test condition.

Figure. 4.11 presents the frequency spectrum of the recorded speckle image after Fourier transform, with the five components marked. The center part is a low-frequency region that contains background information. B or C are extracted by a Window Inverse Fourier Transform method to obtain the deformation gradients in the x-shearing direction, while the gradients of the y-shearing direction can be obtained from either components D or E. Care must be given with respect to the crossover area of the high and low frequency areas when creating the mask. The inclusion of too much low frequency information decreases the quality of the phase map

The wrapped and unwrapped phase maps in the x-shearing direction after calculation are presented in Figure. 4.12 (a)-(b), and the wrapped and unwrapped phase maps in the y-shearing direction after calculation are presented in Figure. 4.12 (c)-(d). Even though the 4f system and spatial phase shift technique degrade the phase map quality, the raw phase map quality in Figure. 4.12 is still much better compared to other dual directional spatial phase shift shearography methods. This advantage brings a lot of potential development which requires the high quality phase map, especially on the quantitative measurement.

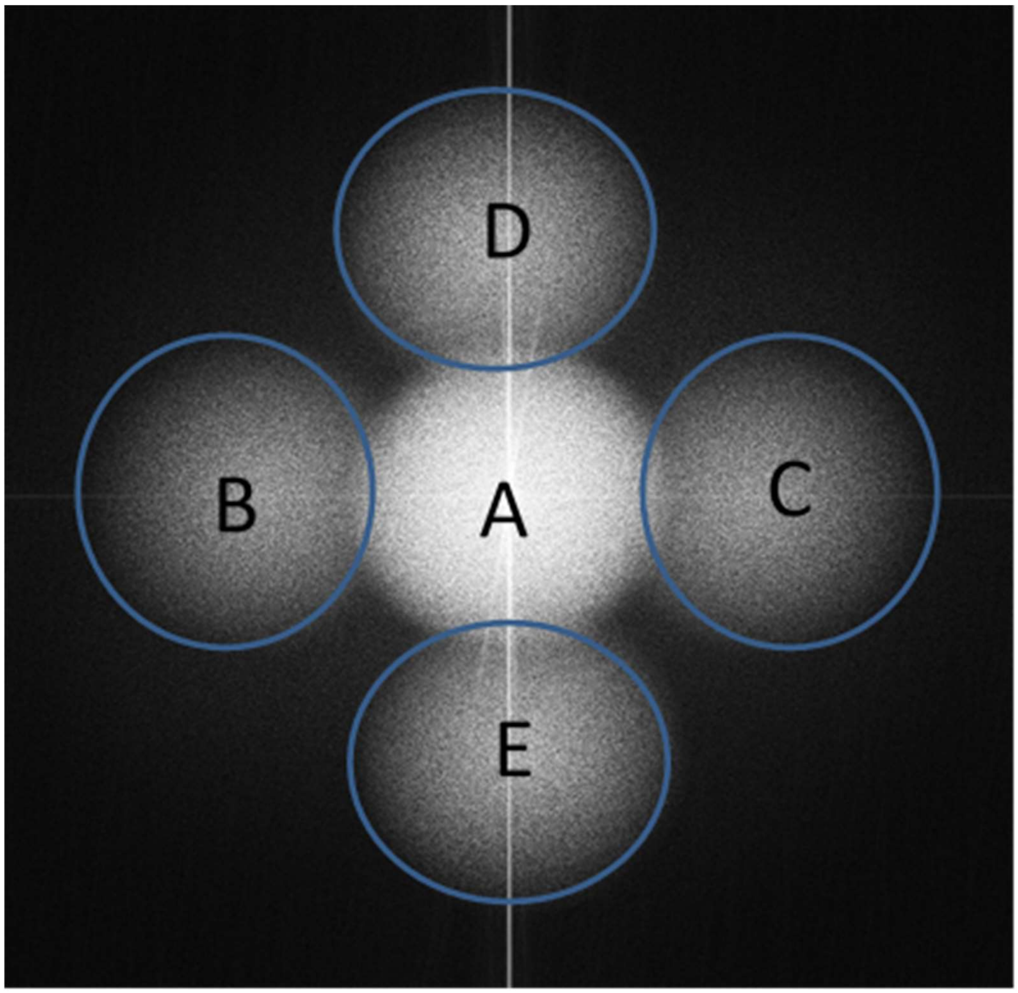

Figure 4.11. The frequency spectrum distribution

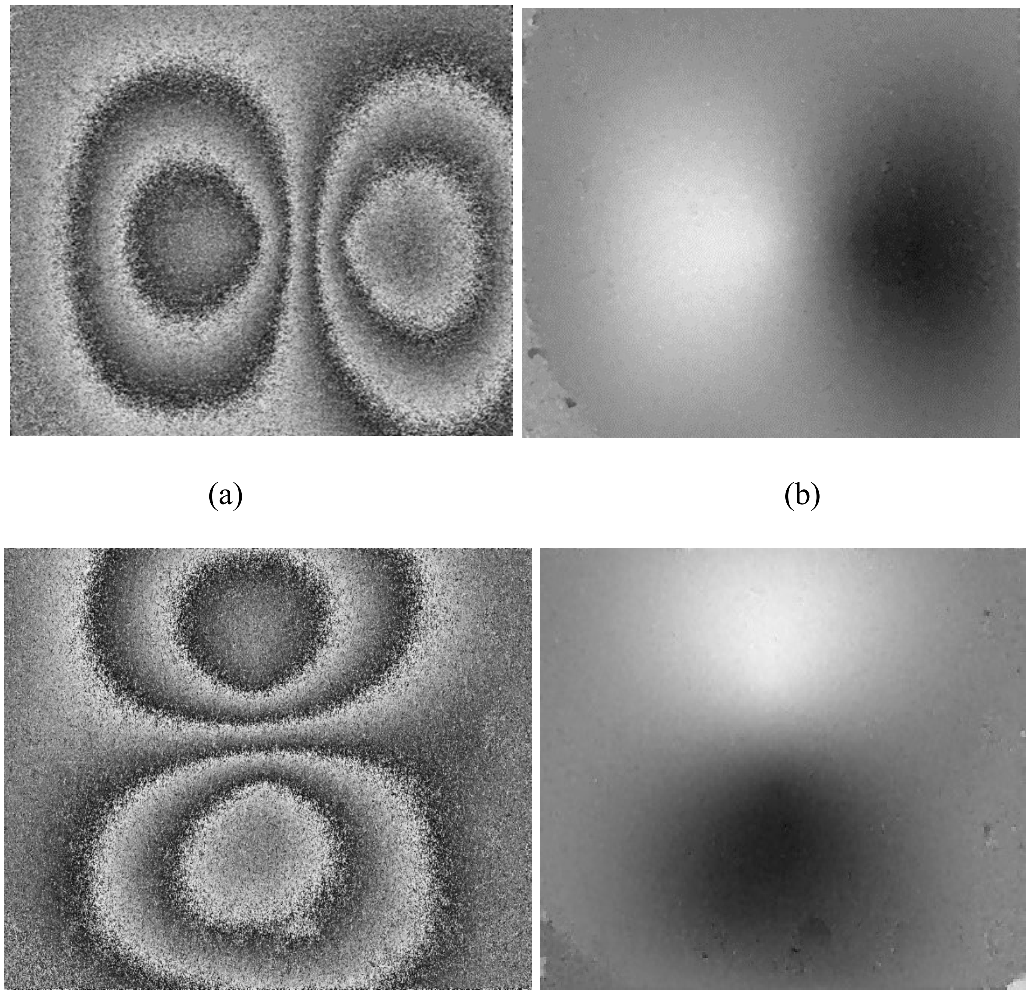

(a) (b) (c) (d)

Figure 4.12. The wrapped and unwrapped phase map in x-direction and y-direction: (a) wrapped phase map of x shearing direction; (b) unwrapped phase map of x shearing direction; (c) wrapped phase map of y shearing direction; (d) unwrapped phase map of y shearing direction

An application of NDT for a rectangle plastic board was taken to verify the functionality of the technique proposed in this paper. A 5 mm thick plastic board with three slit defects under the surface was designed as a sample. Two slits, designed to be 2mm wide and 3mm depth and 40mm long, were mutually perpendicular. The other slit was 2mm wide and 3 mm thick and oriented at a 45 degree angle to the other two slits. The sample was tested under heat loading and the camera took a series of images during the cooling process. A normal heat gun which can heat the object to 50 degree centigrade in 10 seconds was used. To remove the effect of vibration, the continuous acquisition was taken after 5 seconds of the heating stop. Total 50 images were saved with acquisition rate of 10 HZ. To obtain the defect information, two recorded speckle images were picked to perform the Fourier Transform. Two wrapped phase maps in the x- and y-shearing directions are presented in Figure 4.13 (a-b), respectively. In Figure 4.13 (a), the vertical and 45 degree defects are clear. However, it is hard to define the horizontal defects because digital shearography is sensitive to its shearing direction. Conversely, Fig. 4.13 (b) reveals that the vertical slit can barely be found compared to the horizontal slit.

Defects whose growing direction is the same as the shearing direction can be overlooked on the conventional digital shearography system, but it can be easily and precisely obtained by the modified Michelson interferometer based spatial digital shearography system. The results indicate the system works well in real applications.

The second application is a composite material consisted of two aluminum plates stuck together which has three different sizes of defects inside. The material is sensitive to the pressure change, so a vacuum loading is adopted.

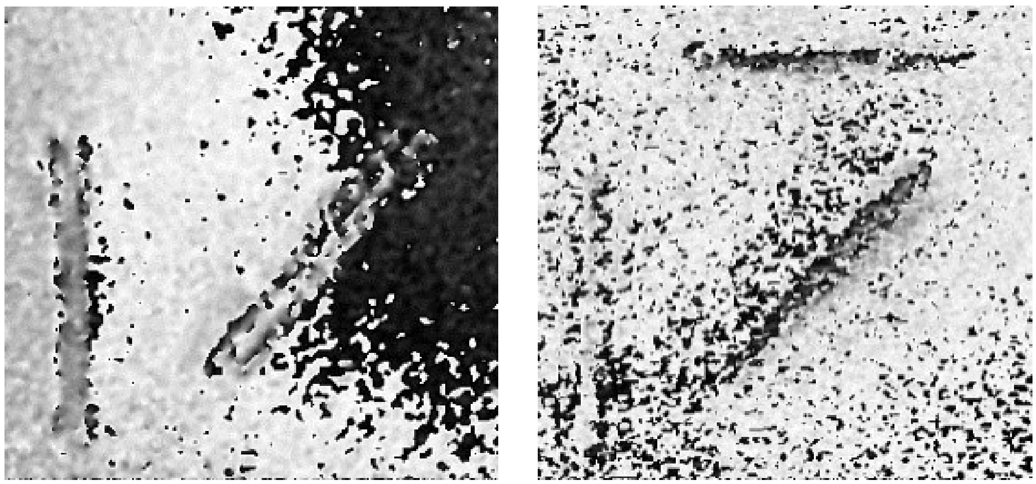

(a) (b)

Figure 4.13. The wrapped phase map of slit defects: (a) wrapped phase map of x shearing direction; (b) wrapped phase map of y shearing direction

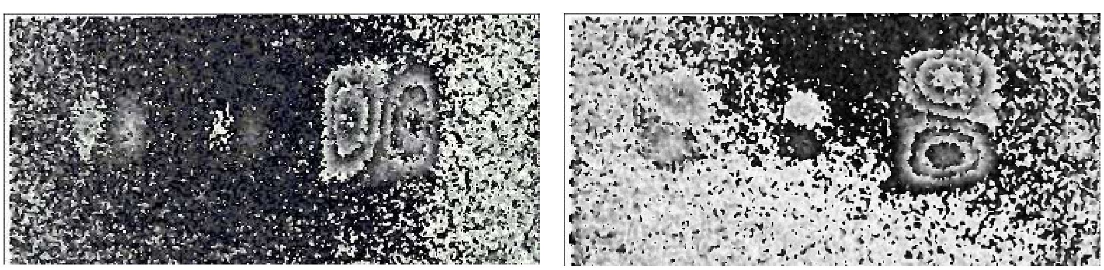

(c) (d)

Figure 4.14. The wrapped phase map of defects in a honeycomb structure: (a) wrapped phase map of x shearing direction; (b) wrapped phase map of y shearing direction

The continuous acquisition was taken as the valve open. Total 50 images were saved with acquisition rate of 10 HZ. Two wrapped phase maps in the x and y shearing directions are presented in Figure 4.14 (a-b). The applications illustrated above show the capability of the reported modified Michelson Interferometer based dual directional measurement shearography system to find both directional and non-directional shaped defects.

4.5 Chapter summary

Laser techniques are limited by safety issues and industrial costs, especially when high-power lasers and penetrable lasers are required. The cost of isolation and laser usage training also becomes a burden in production. People prefer a cheaper and safer approach, even if there is a better laser solution. Conventional digital shearography has the advantages of anti-vibration and relatively low cost, making it well-received in industry even when dual directional shearography is needed for a comprehensive and accurate test. To realize simultaneous dual directional measurement but keep the original advantages of the conventional shearography system, a low power loss, low cost and stable structure setup is required.

The key to reducing the cost is to use common optical instruments instead of special devices like high power lasers or high resolution RGB cameras. Additionally, optical component quantities also affect the assembly, integration and material cost. The price of optics is very high, and the economics of the system can be greatly improved for every device saved. The economics of the proposed setup is the best of all techniques introduced in the paper because it uses the least number of optics, requiring only a regular laser and a grayscale camera and no additional special devices.

The spatial phase shift technique requires high light usage efficiency for a good phase map quality, which is significant for improving the signal to noise ratio. Light usage efficiency is mainly determined by the times for combination and reflection of wave fronts. A square beam splitter is used as an optical combiner, where half of the light intensity can be lost because of half reflection and half transmission. Reducing wave combination times can increase the light usage efficiency. For the setup proposed, only two beam splitters are used, one of them being a polarized beam splitter for which the coating results in a very small power loss when waves combine. Thus, only 50% incident light is lost, if only considering the loss of combination, and each shearing channel can obtain 25% of the incident light, which is much larger than the two previous methods introduced (12.5% and 6.25%).

Many laser technologies, which have a strong ability to solve problems, are limited to lab environments due to their high sensitivity to vibration. Bad interference occurs when a relative vibration happens between optical components. Digital shearography is welcomed in industry due to its anti-turbulence. If the system is strengthened functionally, but has weakened stability, it will not pay off. Reducing optical components can decrease the error accumulation and increase its anti-turbulence ability. In addition to the necessary components of the imaging system and 4f system, the modified Michelson Interferometer based dual directional measurement shearography only has 5 extra parts (3 reflection mirrors and two beam splitters). Compared with other two techniques (8 components and 10 components), the setup is more robust.

However, as a Michelson Interferometer based setup, the proposed approach has an issue with the inflexibility of the introduced carrier frequency. Tilting angles of reflection mirror affect both shearing distance and carrier frequency. Generally speaking, small shearing distances are good for detecting minor defects, while small carrier frequencies result in a mix of background information and useful information on the frequency domain. A balance between shearing distance and carrier frequency needs to be achieved.

CHAPTER FIVE

SPATIAL LIGHT MODULATOR BASED DUAL SHEARING DIRECTION SHEAROGRAPHY

In the previous Chapter, Michelson interferometer based dual shearing direction shearography overcomes many issues of the earlier development which has been discussed in details. Basically, it improves the optical structure to enhance the stability of the system and reduced the energy leakage. However, for the spatial phase shift technology, low image quality and stringent equipment requirements are problems that have always limited its practical application.

First and foremost, the most important characteristics of the dual shearing direction shearography system should be identified. The shearography system is well known for its stability; thus, the optical structure needs to be simple. Additionally, only safe and harmless low-power lasers can be used in order to deploy the technique for industrial production. This necessitates the need to reduce energy leakage in the system. To obtain credible results, S/R (signal to noise ratio) is another concern, as high-precision quantitative measurements can only be obtained using a decent phase map.

The conventional shearing device needs to be improved to satisfy the stated requirements. In 2019, Fangyuan Sun proposed a shearography system based on a spatial light modulator (SLM) which is used as a shearing device and phase shifter [90]. An SLM simplifies the setup and improves the efficiency due to its high integration and digital nature. The details of SLM theory will be discussed in the next section. This paper proposes a dual shearing direction shearography system that combines a simple modified

Michelson Interferometer, SLM and temporal phase shift method. A conventional Michelson interferometer is applied, while the SLM is used as a substitute for the mirror of one arm. Here, the SLM plays the role of the shearing device, which allows for accurate adjustment of the shearing direction as well as provides a phase shift generator capable of performing a fast temporal phase shift. A 4f system is embedded to enlarge the field of view [91]. The theory, equation derivation, feasibility study and nondestructive testing application results are presented in this paper.

5.1 The theory of Spatial Light Modulator

The spatial light modulator (SLM) can modulate a certain parameter of the light field using liquid crystal molecules. Its modulation includes modulating the amplitude of the light field, the phase by the refractive index, and the polarization state through the rotation of the polarization plane. This enables certain information to be written into the light wave for the purpose of light wave modulation. It is the core device of computing systems for real-time optical information processing.

According to the order of the spatial arrangement of liquid crystal molecules, liquid crystals can be divided into twisted nematic, smectic, cholesteric and disc liquid crystals [92]. Among them, twisted nematic liquid crystal is one of the most commonly used liquid crystals, and its molecular shape is elongated rod shape [93, 94].

The model of the spatial light modulator used in the Digital Shearography system is: XY phase series spatial light modulator [87]. The twisted nematic liquid crystal used in the spatial light modulator is uniformly arranged in the liquid crystal screen. Liquid crystal molecules are optically anisotropic substances, which correspond to the refraction of laser light, and the vertical and horizontal directions of a certain axis of the liquid crystal molecules are different. When the polarization direction of the incident polarized light is parallel to the long axis of the liquid crystal molecules and the liquid crystal molecules rotate, the refractive index of the polarized light refracted by the liquid crystal molecules will change, resulting in a phase change. By inputting different voltages to control the deflection of liquid crystal molecules, the situation of controlling the input light phase can be achieved.

Figure 5.1 shows a simplified side view of the liquid crystal layer in the spatial light modulator. When no voltage is applied to the liquid crystal molecules, the liquid crystal molecules are parallel to the YOZ plane. In this case, there will be the greatest difference in refractive index between extraordinary light and ordinary light, which means that there will be a maximum phase retardation. When a voltage is applied to the liquid crystal molecules, the liquid crystal molecules will tilt. The refractive index difference between the extraordinary light and the ordinary light can be changed to a minimum value close to zero, which means that there will be a minimum phase delay. It can be seen that the phase retardation can be controlled by changing the voltage applied to the liquid crystal molecules.

The spatial light modulator modulates the input light wave signal based on a functional relationship between the control signal and light input. Eq. (5.1) describes the relationship between input light and output light.

$$O(x, y) = C(x, y, t)I(x, y) \tag{5.1}$$

Here, O is the light output and I is the light input. C is the control signal, which includes the space coordinate and time variables. For most cases, (x,y) represents the controlling unit, named in this case as pixels. The SLM can change one or multiple

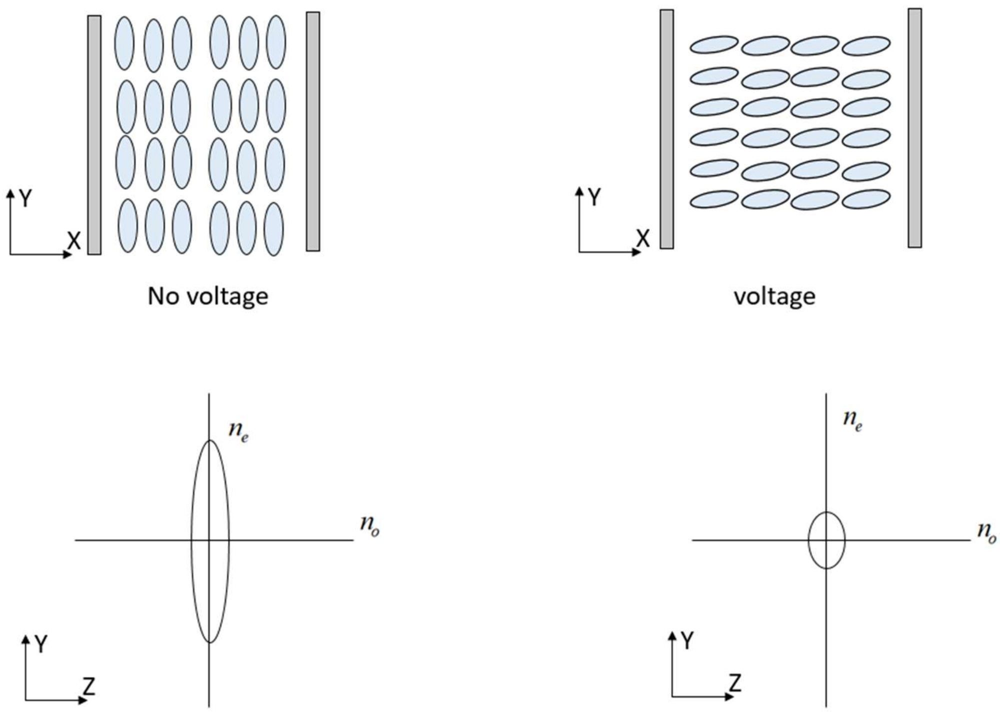

Figure 5.1. Side view of liquid crystal layer of spatial light modulator

optical parameters that may be changed include amplitude, phase, polarization state, wavelength, and coherence. Changes in these parameters can cause various transformations of light wave characteristics.

5.2 SLM based Digital Shearography

Fangyuan Sun's system is capable of applying on the Digital Shearography. The schematic of the setup is shown on the Figure. 5.2. The speckles information on the surface of the measured object respectively pass through the imaging lens, diaphragm, polarizer and glass slide, and then undergo the Fourier transform of the lens to be projected on the surface of the spatial light modulator in the form of parallel light. Due to the birefringence effect of the liquid crystal molecules, the spatial light modulator can only modulate the polarized light whose polarization direction is parallel to the long axis of the liquid crystal molecule, but has no modulating effect on the polarized light whose polarization direction is parallel to the short axis of the liquid crystal molecule. The light reflected into the system will have various polarization states due to the diffuse reflection of the rough surface. Therefore, in order to obtain light with a certain polarization direction, a polarizer is placed in front of the lens to polarize the speckle light from the surface of the object to be measured. The polarization direction is changed to 45 degree to the length of the liquid crystal molecules. By this way, the modulated polarized light and the unmodulated polarized light will have the same intensity, which has a better contract interference. In order to make full use of the Fourier transform characteristics of the lens, the spatial light modulator is placed on the Fourier transform surface of the lens. By adjusting the control signal of the spatial light modulator, the liquid crystal molecules are deflected on the Fourier changing surface, and the polarized light whose polarization

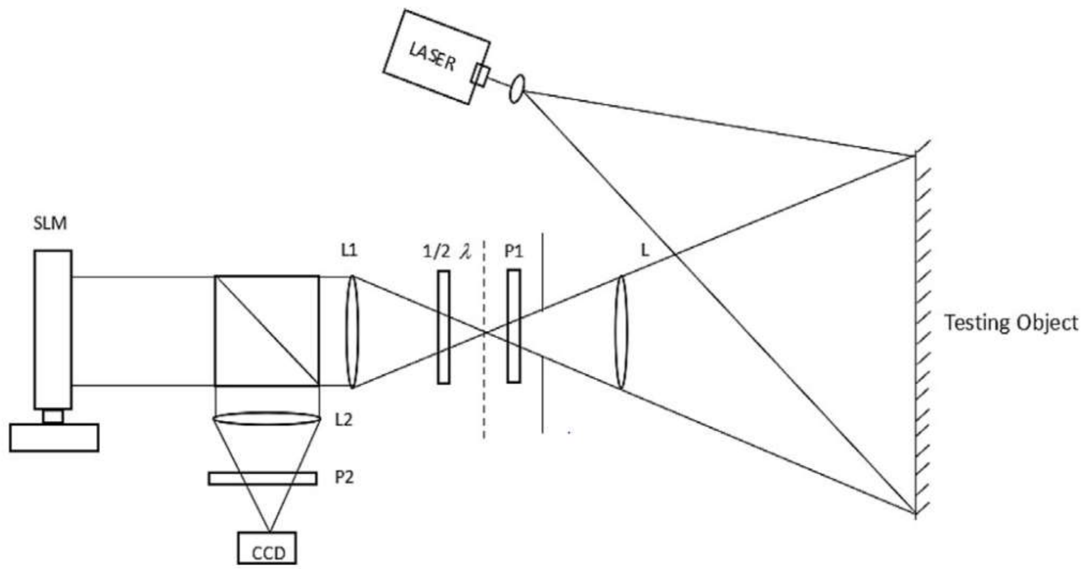

Figure 5.2. The schematic diagram of Digital Shearography with SLM

direction is parallel to the long axis of the liquid crystal molecules is modulated, and a phase shift is introduced in the frequency domain. After the action of the inverse Fourier transform of the lens, the phase shift in the frequency domain is converted into a shearing.

After the modulation of the spatial light modulator is completed, the modulated light and the unmodulated light are reflected by the dichroic prism, and are imaged on the target surface of the CCD through the Fourier transform effect of the lens. The angle between the polarization direction of the polarizer and the long axis of the liquid crystal molecules is also 45°. In this way, the modulated light and the unmodulated light whose polarization directions are perpendicular to each other will interfere on the CCD target surface after passing through the polarizer to form a speckle interferogram.

Sun's setup uses polarizer to adjust the contrast which reduces the light efficiency. A new setup with less optical components and higher light efficiency is introduced in the next chapter to realize the dual shearing shearography.

5.3 Optical setup

Figure 5.3 shows a schematic of the SLM based dual shearing direction shearography setup. A coherent laser with a 532 nm wavelength is used as a light source to illuminate the object by the expander. The aperture and L1 form the imaging system, while the 4f system used to adjust the field of view is made up of L2 and L3. A 50:50 normal beam splitter divides the reflection waves to two channels. A pair of laterally sheared images of the tested object is generated on the image plane of the CCD camera through SLM modulation of the Michelson interferometer. Compared to the classic SLM shearography system, the proposed system is simpler that only use one regular polarizer while has a half energy leakage.

Prior to entering the 4f system, the light can be expressed as $\mathrm{U_0(x, y)}$. After the original wave passes through the beam splitter and is separated to two channels, channel #S represents the wave that strikes the SLM and channel #M represents the wave that goes to the normal mirror. The SLM is placed on the Fourier plane of L2 and L3 and it is a reflective mode. Both two light beams will be reflected to the beam splitter and combined to project on the CCD plane of the camera. During the process, the light beam has been modulated by the optical components multiple times which can be represent by equations. The wave of channel #S on the SLM before modulation can be written as:

$$U_2(f_x, f_y) = \frac{1}{2} C\mathcal{F}\{U_0(x, y)\} \tag{5.2}$$

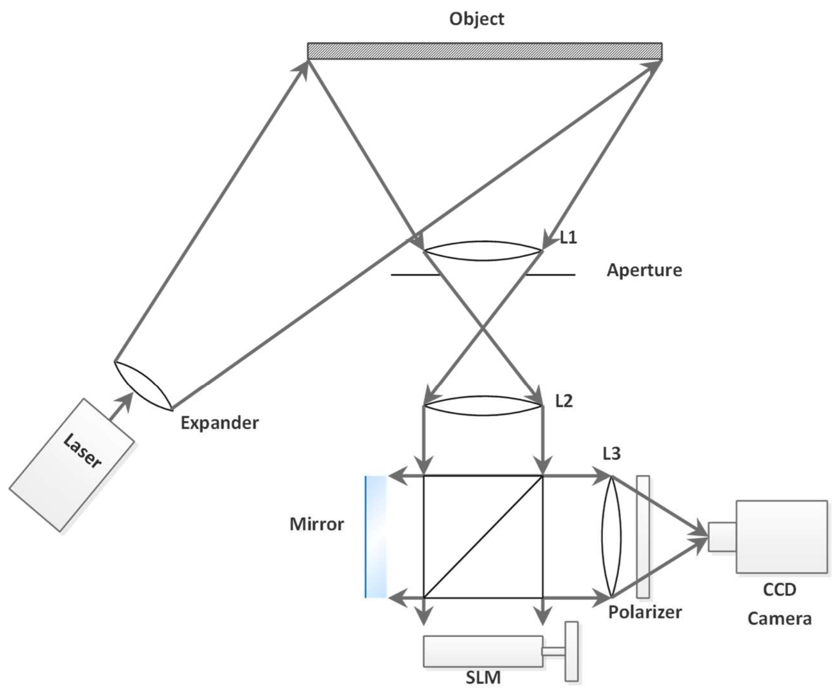

Figure 5.3. The schematic of SLM based dual shearing directional shearography.

Where C is a constant factor and $\mathcal{F}$ represents the Fourier transform process. The ordinary portion of U_2 is $U_{2,o}$ and the extraordinary portion is $U_{2,e}$. Because the phase shift in the frequency domain can result in displacement in space domain to occur in Channel #M, the modulated extraordinary light can be described as:

$$U_S(f_x, f_y) = U_{2,e}(f_x, f_y)t_{SLM} \tag{5.3}$$

Here $t_{SLM}(f_x, f_y) = t_{\emptyset} * \exp[-j2\pi(f_x, f_y)]$ is a modulated factor, and $t_{\emptyset} = \exp[j\emptyset]$ is a constant phase. There is no modulation in Channel #M, if we only concern extraordinary light, the U_M can be written as:

$$U_M(f_x, f_y) = U_{2,e}(f_x, f_y) \tag{5.4}$$

A polarizer which filters a beam of ordinary light is placed behind L3. Extraordinary light can pass through the polarizer while ordinary light is blocked. The CCD is placed on the focal plane of Lens L3. So, the extraordinary light of the two channels passing through L3 will undergo another Fourier transform, which can be denoted respectively as:

$$U_{3,S}(x, y) = C\mathcal{F}\{U_S(f_x, f_y)\} \tag{5.5}$$

$$U_{3,M}(x, y) = C\mathcal{F}\{U_M(f_x, f_y)\} \tag{5.6}$$

The result has the same form as the original function after performing a Fourier transform on the function twice in succession. However, the coordinates are reversed, which is equivalent to the lateral magnification V=-1. The interference of $U_{3,S}(x, y)$ and $U_{3,M}(x, y)$ can be expressed as:

$$U_4 = -\frac{1}{2}R[U_0(-x, -y) + \exp(j\emptyset) * U_0(-x, -y)] \tag{5.7}$$

Here, R is the percentage of extraordinary light in total light.

The shearing amount and shearing directions can be adjusted precisely by programming the SLM. The modulation term t_{SLM} determines the shearing directions and shearing amount. To obtain information in two directions, x-shearing and y-shearing need to be applied separately. Based on the translation properties of Fourier transform, the linear phase shift on frequency domain can obtain the image displacement. For x-shearing, the phase shift term f_a will be added to t_{SLM}. $t_{SLM,x}$ for x-shearing can be expressed as:

$$t_{SLM,x}(f_x, f_y) = t_{\emptyset} * \exp[-j2\pi(f_x f_a, f_y)] \tag{5.8}$$

The x-shearing interference speckle pattern with shearing amount f_a can then be written as:

$$U_{4,x} = -\frac{1}{2}R[U_0(-x, -y) + \exp(j\emptyset) * U_0(-x + f_a, -y)] \tag{5.9}$$

It is similar in y shearing direction with shearing amount $f_b$that $t_{SLM,y}$ can be expressed as:

$$t_{SLM,x}(f_x, f_y) = t_{\emptyset} * \exp[-j2\pi(f_x, f_y f_b)] \tag{5.10}$$

The y-shearing interference speckle pattern with shearing amount f_a can then be written as:

$$U_{4,y} = -\frac{1}{2}R[U_0(-x, -y) + exp(i\emptyset) * U_0(-x, -y + f_b)] \tag{5.11}$$

Compared with conventional dual shearing direction shearography system, shearing amount can be accurately modulated without considering the control problems of mirror translation and rotation. Even if the x-shearing and y-shearing cannot be operated at the same time, the current SLM on the market can reach a working frequency of hundreds of Hz which is far exceeded the sampling frequency of commonly used industrial cameras. The dynamic measurement speed is mainly limited by the frame rate of the camera. Qualitative measurement can be done in two directions within 4 shots. The specific workflow is as Figure 5.4.

A temporal phase shift algorithm is introduced to extract the phase information. Several algorithms, such as the three step method with a phase step of 120 degrees and the four step method with a phase step of 90 degrees, have been popular phase calculation because of their fast and easy calculation As we known, t_{SLM} is the term to modulate the shearogram. The fixed-step phase shift can be achieved by adjusting $\exp(j\emptyset)$ in t_{SLM}.

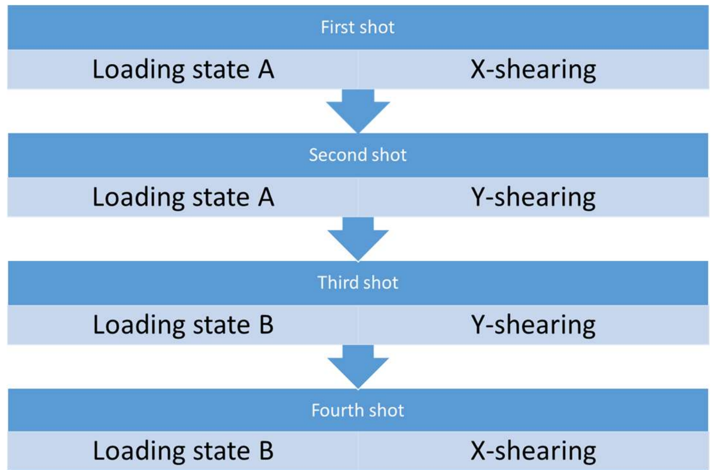

Figure 5.4. The workflow of qualitative measurement of dual shearing directions.

In this case, the four steps method is adopted and the modulation process can be written as:

$$U_{S,0}(f_x, f_y) = exp(j\emptyset) * exp[-j2\pi(f_a f_x + f_y)]U_{2,e}(f_x, f_y) \tag{5.12}$$

$$U_{S,1}(f_x, f_y) = exp\left(j(\emptyset + \frac{\pi}{2})\right) * exp[-j2\pi(f_a f_x + f_y)]U_{2,e}(f_x, f_y) \tag{5.13}$$

$$U_{S,2}(f_x, f_y) = exp(j(\emptyset + \pi)) * exp[-j2\pi(f_a f_x + f_y)]U_{2,e}(f_x, f_y) \tag{5.14}$$

$$U_{S,3}(f_x, f_y) = exp\left(j(\emptyset + \frac{3\pi}{2})\right) * exp[-j2\pi(f_a f_x + f_y)]U_{2,e}(f_x, f_y) \tag{5.15}$$

And the interference can be denoted as:

$$U_{4,0} = -\frac{1}{2}R[U_0(-x, -y) + exp[j\emptyset] * U_0(-x + f_a, -y)] \tag{5.16}$$

$$U_{4,1} = -\frac{1}{2}R[U_0(-x, -y) + exp\left[j(\emptyset + \frac{\pi}{2})\right] * U_0(-x + f_a, -y)] \tag{5.17}$$

$$U_{4,2} = -\frac{1}{2}R[U_0(-x,-y) + exp[j(\emptyset + \pi)] * U_0(-x + f_a, -y)] \tag{5.18}$$

$$U_{4,3} = -\frac{1}{2}R[U_0(-x,-y) + exp\left[j\emptyset(\emptyset + \frac{3\pi}{2})\right] * U_0(-x + f_a, -y)] \tag{5.19}$$

The phase can be calculated as:

$$\varphi = arctan\frac{U_{4,3} - U_{4,1}}{U_{4,0} - U_{4,2}} \tag{5.20}$$

The similar process will be applied in each shearing and loading condition. When all the phase value is obtained, the shearogram can be calculated as the normal phase subtraction between two states.

5.4 Experimental validation

A real dual direction shearography system is shown in Figure 5.5. For the first test, a defect-free aluminum plate with a size of Φ150 was used to verify the feasibility of the SLM for fast shearing direction changes. The plate was clamped all around and loaded at the center by a screw micrometer as shown in the Figure 5.6. A 1600 ×1200-pixel grayscale CCD camera with a pixel size of 3.45 μm in the horizontal direction and 3.45 μm in the vertical direction was used to record the pictures. The imaging lens was 50 mm (f = 50 mm), and the focal lengths of L2 and L3 were f = 150 mm.

In the first step, the SLM was programmed for an x-shearing direction and captured four images with different phases. Keeping in step with phase shifting, the system was adjusted to the y-shearing direction and another four step phase shift was applied. By the two steps above, $\emptyset_x$ and $\emptyset_y$, which respectively are the x-shearing and y-shearing phases before loading, could be calculated. $\emptyset'_y$ and $\emptyset'_x$, which are the phases after loading, were then obtained by applying a phase shift in the y-shearing direction first, then switching to the x-shearing direction. The shearographic phase map can then be formed by taking the difference of the phases before and after loading, or $\emptyset_x' - \emptyset_x$ and $\emptyset_y' - \emptyset_y$. Figure 5.7 shows the phase map of the proposed verification test.

An application of NDT for a rectangular plastic board was performed to verify the functionality of the technique proposed in this paper. A 5 mm thick plastic board with two slit defects under the surface was designed as the test sample. Two mutually perpendicular slits, designed to be 2 mm wide, 3 mm deep and 50 mm long, were cut. The sample was then tested under heat loading. A normal heat gun with the capability to

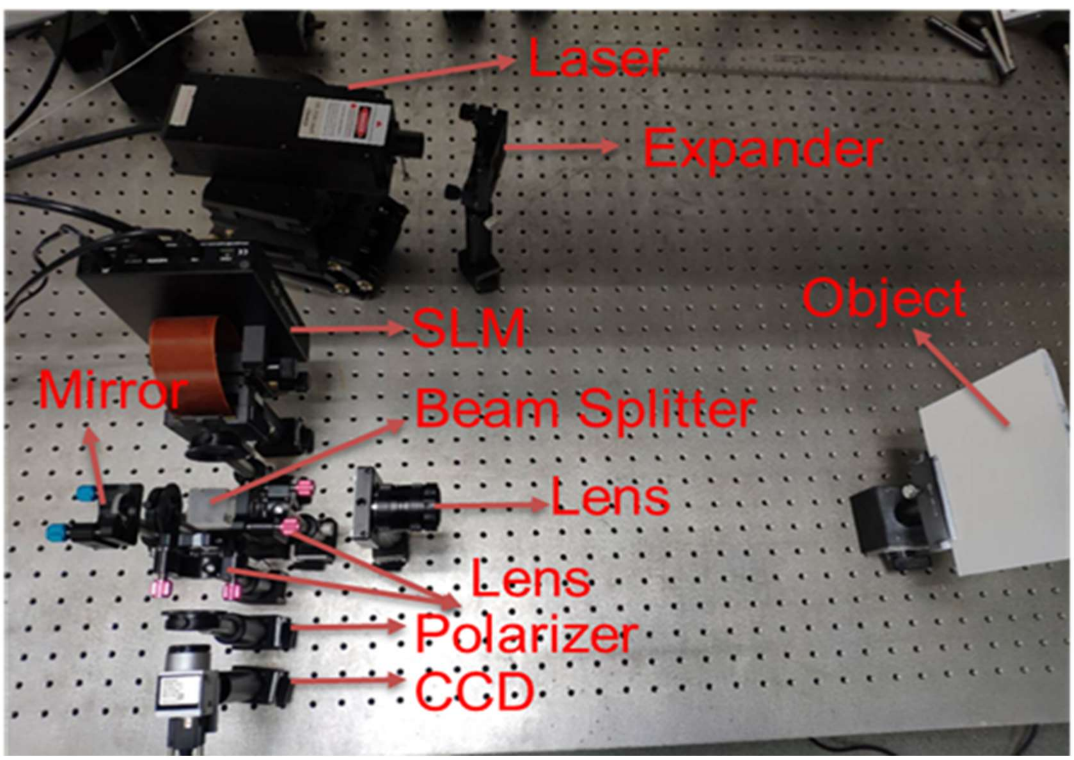

Figure 5.5. The real setup of the SLM based dual shearing directional shearography.

heat an object to 50 degrees Centigrade in 10s was used for the test. To remove the effects of vibration, acquisition was taken 5s after heating was stopped.

The interval between the first and second set of pictures is 10 seconds. Two phase maps in the x- and y-shearing directions are presented in Figure 5.8 (a-b), respectively. In Figure 5.7 (a), the vertical defect is clear, but the horizontal defect is not because digital shearography is sensitive on its shearing direction. Figure 5.8 (b) shows the opposite, where the vertical slit is barely visible compared with the horizontal slit.

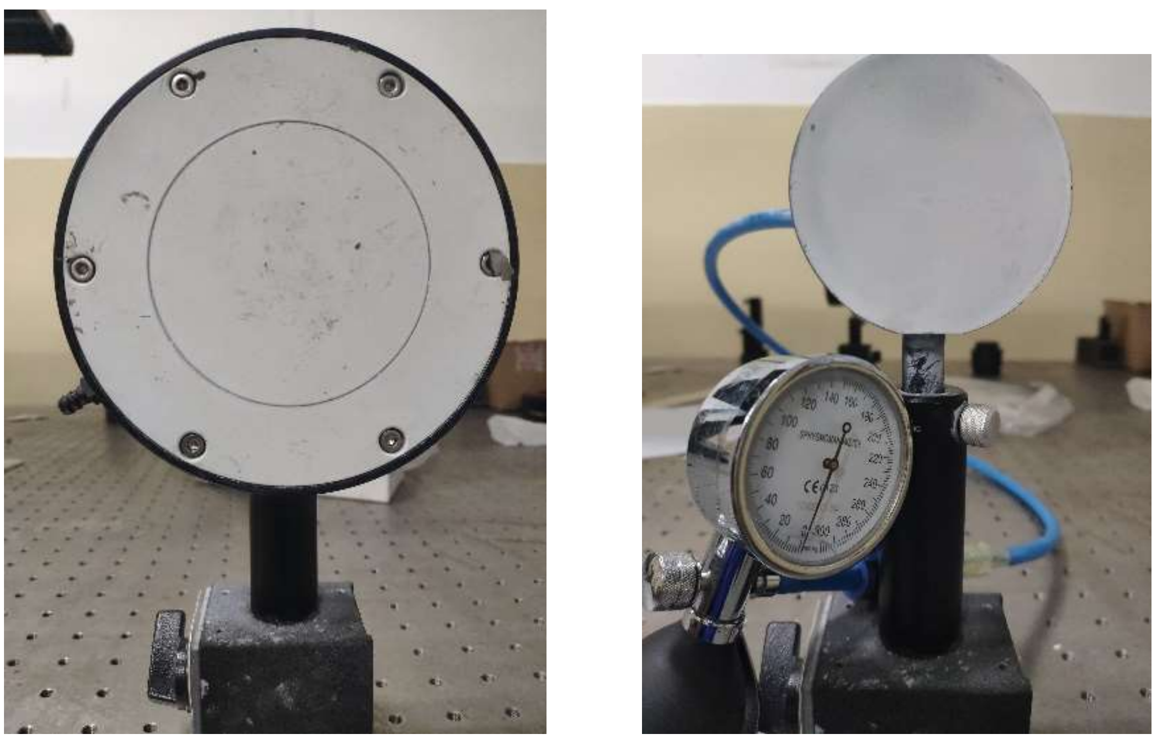

(a) (b)

Figure 5.6. The setup and object to be tested: (a) The round plate to be tested; (b) The vacuum system

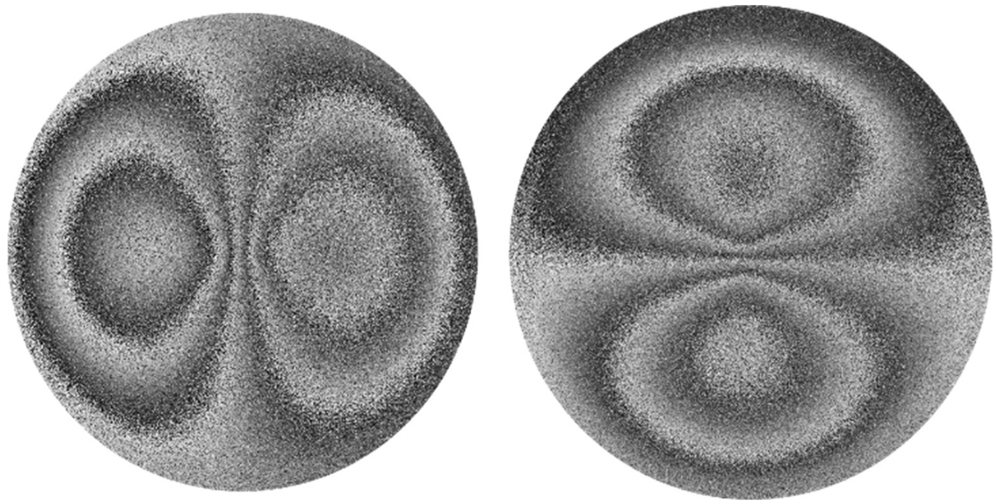

(a) (b)

Figure 5.7. The phase map in x and y shearing directions of the round aluminum plate: (a) phase map of x shearing direction; (b) phase map of y shearing direction

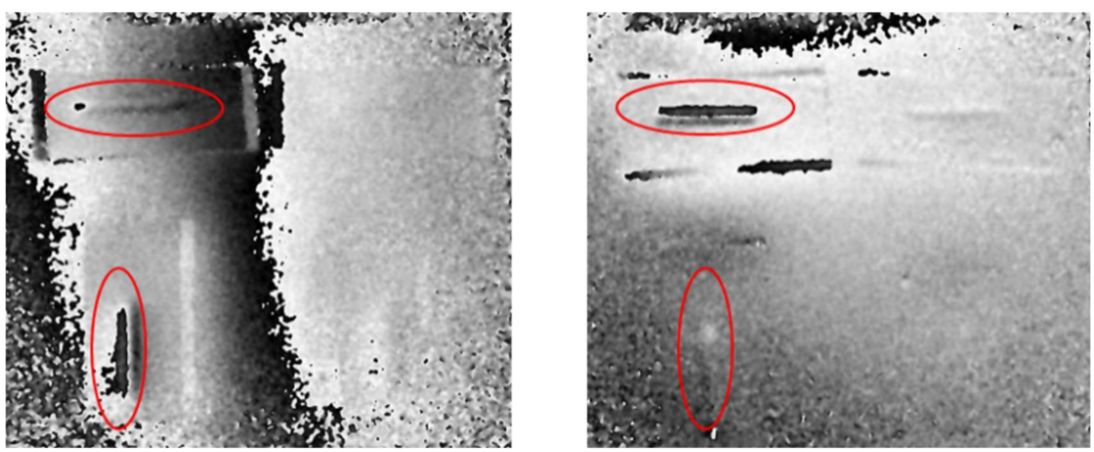

(c) (d)

Figure 5.8. The phase map in x and y shearing directions of the rectangle plastic board: (a) phase map of x shearing direction; (b) phase map of y shearing direction

5.5 Chapter summary

The technique of shearography in multiple shearing directions has long been a topic that people are committed to solving. Complicated optical structure and expensive equipment initially had to be used, making this type of application unavailable. After the carrier frequency spatial phase shift technology was proposed, one could achieve complete simultaneous measurement of dual shearing directions through a simple optical path. However, carrier frequency spatial phase shift technology had and still has significant image quality, shearing amount control and energy loss issues. After reviewing the main problems faced by the past approaches, the technology proposed has successfully achieved several of the most important goals of dual shearing directional shearography.

For the interference techniques, the relative motion of the two optical paths will have a huge impact on the quality of the interference. This makes it necessary to deploy part of the interference technology on a platform completely isolated from vibration. Shearography is a dual beam system as well, but the technical advantage is that two coherent beams will interfere within a short distance after generating. Many dual shearing direction shearography technologies have greatly increased the propagation distance of coherent light and placed a lot of optical components on the optical path, thus reducing the stability greatly. Based on the versatility of the SLM, there is no requirement for multiple shearing devices to change shearing directions, and the entire optical structure returns to its simplest and most efficient form. SLM based dual shearing directional shearography has a simpler and more stable optical structure compared with the previous technology.

Energy leakage refers to the energy lost between the final available light on the CCD and the incident light. There are several reasons for the energy leakage, such as transmittance of optical components, aperture size and the design of the optical structure. Recently proposed dual shearing direction shearography systems, which mainly rely on the spatial phase shift technique, requires limiting the aperture size to avoid aliasing of the spectrum pattern on the frequency domain. The needed aperture leads to a measurement light intensity loss of typically more than 97 percent, which greatly reduces the intensity depth resolution and, therefore, the longitudinal result quality. The proposed dual shearing direction shearography system does not have a strict aperture size requirement because of its use of the temporal phase shift technique. Compared with other dual shearing direction shearography systems, energy leakage of the SLM based dual shearing direction shearography system is not serious. Besides, Conventional SLM shearography system uses multiple polarizers to transform the ordinary light and extraordinary to reach the interference. Assuming the object reflection light has the uniform polarization direction. The classic setup filters the reflection light into single polarization direction then transform 45 degrees to modulate. After modulation, the light would be polarized again to interfere. 75% of incident light are lost without concerning other leakage. In the same condition, 50% of incident light can be kept by the proposed setup while using less optical components.

Temporal phase shift technology can bring better image quality, but also brings a difficult problem that makes it impossible to achieve simultaneous measurement on two shearing directions. Unlike spatial phase shift technology, which can extract multiple sets of information from a single picture, temporal phase shift technology requires at least three phase shift steps to obtain the phase in one state [6]. In the static measurement, the temporal phase shift technique performs well. However, for dynamic measurements, each collected picture is in a different state. If using a mechanical phase shift device during a rapid continuous loading, the picture will lose its relevance and fail to obtain the phase information. Fortunately, the working frequency of SLM can reach hundreds of HZ, which is able to handle slow dynamic loading measurements. Therefore, the use of SLM-based dual directional shearography is acceptable in continuous measurements.

An SLM based dual shearing direction shearography system is proposed in this research. The system, which uses an SLM as both the shearing device and phase shift generator, has the advantage of precise shearing amount control and fast phase shift speed, thus enabling dynamic measurements within a certain range. Its simple and stable optical structure, low energy leakage and decent phase map quality makes the system more competitive compared to other dual shearing direction shearography systems.

CHAPTER SIX

POLARIZED DIGITAL SHEAROGRAPHY FOR SIMULTANEOUS DUAL SENSITIVE MEASUREMENT

Nowadays, most of the image acquisition based optical inspection system is a single-camera configuration with a fixed field of view, which is simple and effective when measuring the limited area of a certain object. However, the problem of low resolution may be encountered while testing the object with unknown internal defects. The minor defects information could be missed due to the small amount of data and poor signal to noise ratio. It happens in digital shearography as well, for example, the surface of a fuselage suffered by hail, a pipe used for many years with multiple cracks and a honeycomb structure mis made resulting in delamination. Some examples are shown in the Figure 6.1 and Figure 6.2 [20]. In general, if the deformed surface area is much smaller than the field of view, the fringes could be unobservable, which may cause by small size or the large depth of the defect. In addition, a suspicious stress concentration area could be buried in the large surface deformation. To solve the issue, a high-resolution small field of view can help observe it, but would lost the full field information if only testing in a small field of view.

The most straightforward way is to perform measurements in multiple times with large field and small field. It is necessary to prepare several sets of equipment or customize it with a variable field of view. The solution increases time and labor costs while induces the complicated operation. There is no solution to work with two different

Figure 6.1. The shearograms on the airplane surface of different size of defects

resolutions simultaneously under experimental conditions that cannot be repeated in digital shearography.

The equipment must have two channels to implement dual resolution measurement in single device. The two channels digital shearography has recently been widely discussed in the application dual shearing directions test. The first dual shearing direction temporal phase-shift digital shearography system was reported by Steinchen W and Yang L [84,85]. The essence of this system is to bind the two interferometric systems together with two cameras. The two channels are independent but can be synchronized triggered by external command. Theoretically, two different resolutions acquisition can be achieved by adjusting the focus length of cameras. The system structure is simple and easy operated. However, Michelson interferometers are placed in front of the image lens,

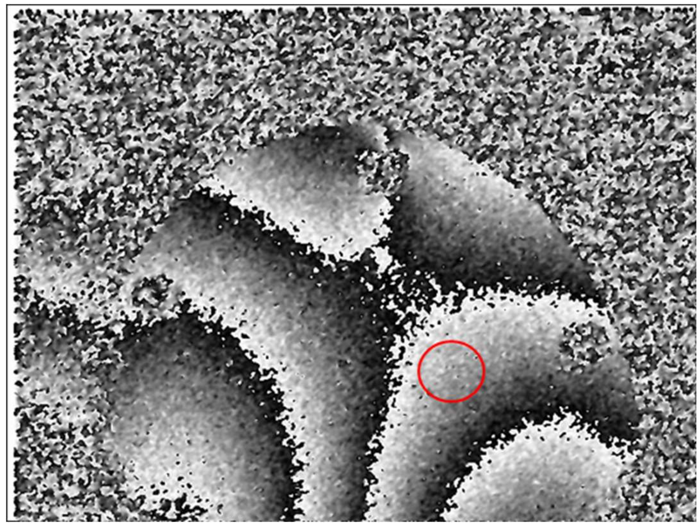

(a)

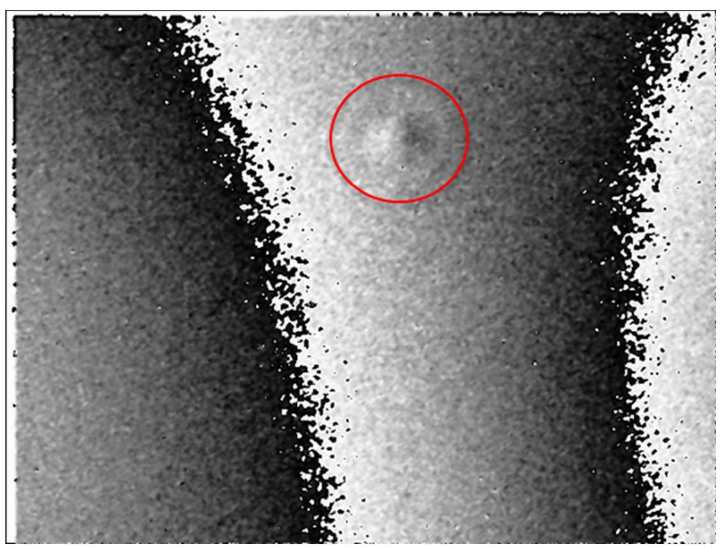

(b)

Figure 6.2. The small shearogram in different field of view. (a) Large field of view (b) Small field of view

which determines that the field of view is limited by the frame size of Michelson interferometers. It is inconvenient in application, as it requires high-quality calibration to achieve accuracy close to that of two channels. Besides, double cameras increase the cost of the whole device. The ideal architecture owns the free filed of view with single camera.

Based on the carrier frequency spatial phase-shift shearography first reported by Pedrini et al. in 1996, information that overlapped on the CCD plane can be separated with different carrier frequencies. In recent years, some two channels' systems based on carrier frequency method are proposed. The biggest challenge of the two channels structure is how to avoid cross interference between the two signals on the CCD plane. In 2016, Wang et al. introduced a Michelson interferometer based spatial phase-shift digital shearography system [87]. The system uses two wavelength illumination lasers with wavelength filters to form the two channels because the different wavelength light beams have no cross interference. Another method proposed by Xin et al. is to use a single-wavelength laser with a polarizer to form two channels whose polarization directions are perpendicular to each other. This method can also avoid the problem of cross interference [88]. Considering that two wavelength laser beams need to be compensated for the wavelength difference in the later calculation, the method using polarized effect is a better way to construct dual channels. However, current optical setups are not available for dual resolution measurement because two channels are designed for the same field of view.

This chapter introduce a novel dual senstitve shearography system based on the carrier frequency spatial phase shift and polarization effect. A Sagnac Interferometer is applied and first time used in the digital shearography while a modified Michelson interferometer is used as a substitute for one of the mirrors in Sagnac interferometer. The two sets of interferometers each form a channel but are not completely independent. The theory, schematic, equation derivation and nondestructive testing application results are presented.

6.1 Sagnac Interferometer

The Sagnac interferometer is first proposed in 1913 by Georges Sagnac. Since it is extremely sensitive to rotations, the most common application is ring laser gyroscope [96-97]. The schematic of Sagnac interferometer is shown as Figure. 6.3. A beam of light is split by a beam splitter and the two beams are made to follow the same path but in opposite directions. When the light returns to the point of entry, an interference pattern is obtained.

Optical fibers are usually used as the light carrier in conventional Sagnac interferometer. In digital shearography application, what is transmitted is the object light with complex signals, mirror is used to construct the optical path. It is a common design to use three or more mirrors to form a loop, and at least two mirrors are required. The amount of reflection mirrors used could have impact on the shearing function in the application. If the reflection mirror amount is even, tilting mirror will not generate shearing. In opposite, the reflection mirror amount is odd, shearing will be generated by tilting any mirrors. The special structure can satisfy the requirement of dual resolution measurement. In addition, the two light path which are going to interfere keep staying on the same optical components, which means the relative movement of two light path is cancel out. Using Sagnac interferometer as a shearing component has a better disturbance

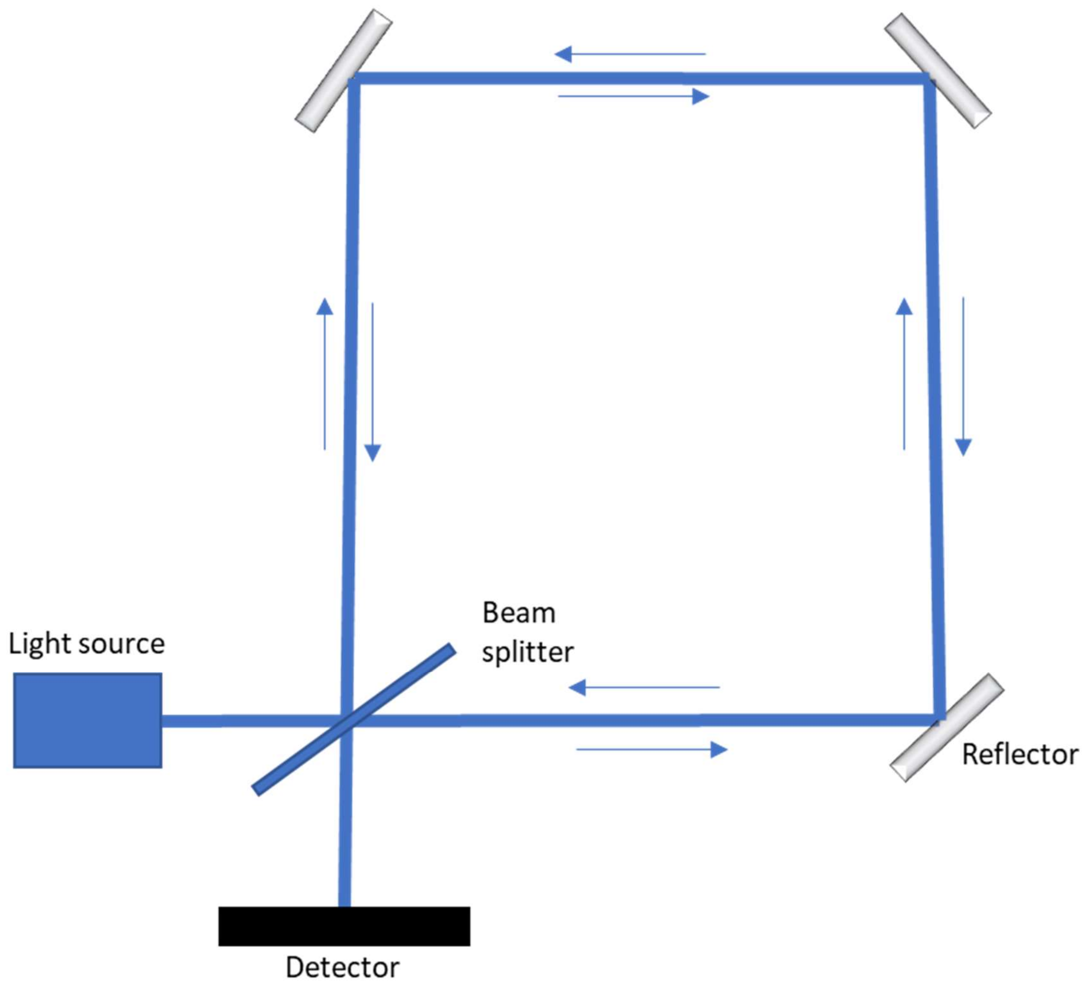

Figure. 6.3. The schematic of Sagnac interferometer.

resistance than other interferometers whose light paths are independent.

In a Sagnac interferometer based digital shearography, the laser is expanded to illuminate the object with diffuse reflection. The wave passes through the beam splitter (BS) and is separated into two waves equally. M represents the regular flat mirror. The green beam goes counterclockwise and meets mirror 1, mirror 2 and mirror 3 follow a sequence while the red beam goes clockwise in opposite marked as green beams. Two beams are combined in beam splitter and interfere on the CCD plane of the camera.

By tilting M2, the shearing will be obtained. Although Sagnac interferometer has a strong disturbance resistance, it has limitations in phase shift technology. Common phase shift technologies include temporal phase shift and spatial phase shift technology. The most of temporal phase shift technologies requires to modulate the single beam independently to obtain interferograms with a phase difference. The conventional temporal phase shift approach is not applicable in the application of Sagnac interferometer. For example, if a PZT driven mirror is used to do the temporal phase shift, there would be no phase difference because the displacement of two beams is the same. In opposite, the carrier frequency spatial phase shift method achieves the phase information through the carrier frequency difference which is directly related to the spatial angle between two beams. When M2 rotates an angle α, the angle between two beams will be 2α and the carrier frequency would be Eq. 6.1.

$$f = (sin2\,\alpha/\lambda) \tag{6.1}$$

Where f is carrier frequency, and λ is the wavelength of the laser. Sagnac interferometer has a big potential on the digital shearography application based on the carrier frequency spatial phase shift. It is the main structure of the proposed dual resolution digital shearography system.

6.2 Optical setup

6.2.1 Optical layout

Figure 6.4 shows a schematic of the polarized dual sensitive shearography setup. L represents the ideal convex lens. A coherent laser with a 532 nm wavelength is used as a light source to illuminate the object by the expander. The aperture and L1 form the imaging system. A 50:50 normal beam splitter divides the reflection waves to two beams marked in blue. M2 and M3 are placed in 45-degree tilting to the horizontal direction to transmit the two beams to the polarized beam splitter. A polarizing beam splitter can transform a non-polarized wave to two waves with a 90 degrees polarized angle difference. The dielectric coating along the diagonal interface of the polarized beam splitter reflects s-polarized light while transmitting p-polarized light. When a beam goes along the direction from BS to M3 to PBS, it will be separated into two beams. The reflected one is marked as red which goes to M2 and back BS. Another one which is marked as green will pass through the PBS and reflected back by M5, then follow the same way back to BS. In opposite, when a beam goes along the direction from BS to M2 to PBS, it will be separated as well. The reflected one is marked as red which goes to M3 and back BS. Another one which is marked as green will pass through the PBS and reflected by M4, then follow the same way back to BS. All the red beams form the channel #Red while all the green beams form the Channel # Green, which is shown in the Figure 6.5. Red channel represents the regular field of view. If we only look at the red

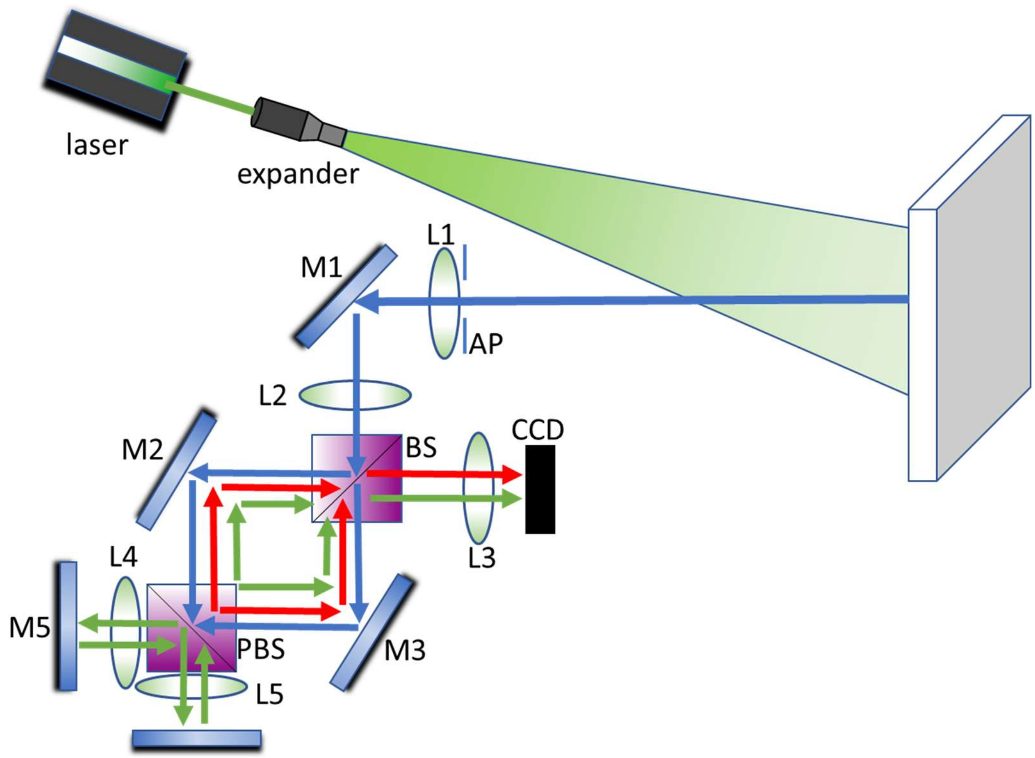

Figure. 6.4. The schematic of Digital Shearography for simultaneous dual sensitivity measurement

channel, it is a typical Sagnac interferometer. Green channel represents the small filed of view or called high sensitive view.

6.2.2 Image formation

The final imaging position of the single-camera system is on the CCD plane. For the traditional single imaging system, we only need to pay attention to how to configure the lens parameters to obtain the desired magnification and it is mainly based on the Gauss formula as the Eq. (6.2)

$$\frac{1}{f} = \frac{1}{u} + \frac{1}{v} \tag{6.2}$$

Here f is the focal length of the lens, u is the object distance and v is the image distance. The magnification can be represented as:

$$m = \frac{v}{u} \tag{6.3}$$

In a multi-channel system, multiple images are formed on one image plane, and each channel needs to have the same or similar optical configuration. However, in the dual sensitivity Digital Shearography system, the two channels need to obtain different magnifications, the optical configuration must be different, and at the same time, two images can be captured at the same place of the CCD plane. To determine the magnification between two channels, the final image distance can be recognized as a constant value V_f. Then, the optical parameters of red channel can be calculated. During the research, we found the object distance of L3 must be a negative value for a dual channel imaging, so the following requirement can be obtained.

$$f_1 + 2\, f_2 > D_{L1-L2} > f_1 + \ f_2 \tag{6.4}$$

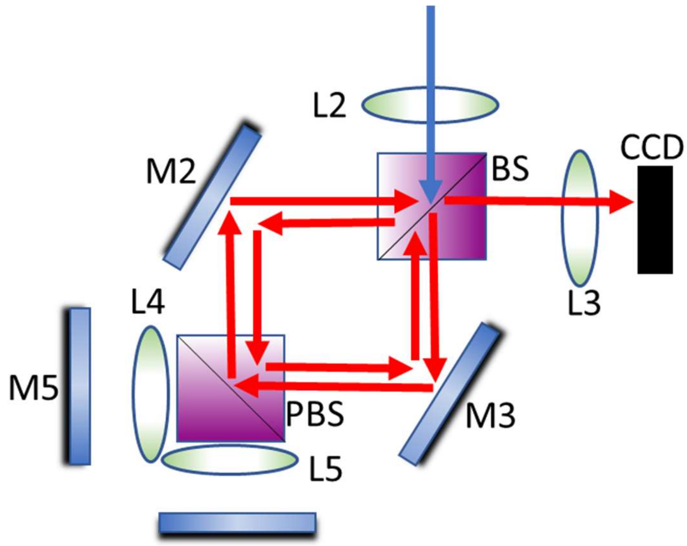

(a)

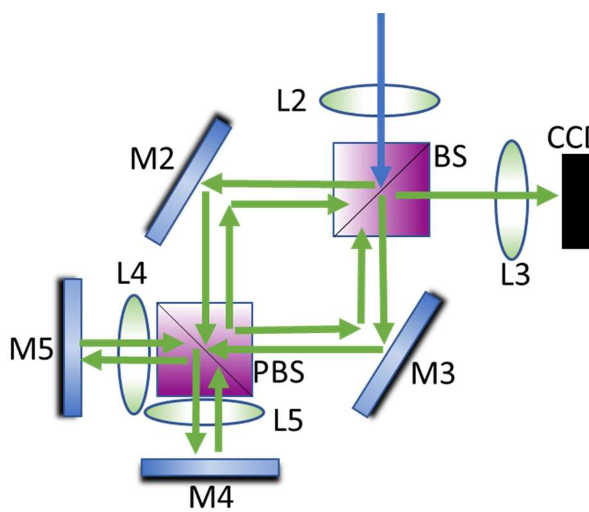

(b)

Figure. 6.5. The schematic of red and green channels: (a) Red channel (b) Green channel

$$V_2 > D_{L_2-L_3} \tag{6.5}$$

Here, f_1, f_2 are the focal lens of $L1$ and $L2$ respectively. D_{L1-L2} is the distance from $L1$ to $L2$. D_{L2-L3} is the distance from $L2$, M2, PBS, M3 to BS. The distance between lens and beam splitter is neglected. L1 determines the regular filed of view which can be adjusted based on the requirement.

To figure out the magnification between two channels, the following derivative is present

$$\frac{1}{f_3} = \frac{1}{U_3} + \frac{1}{V_f} \tag{6.6}$$

Here, f_3 is the focal lens of L3 and U_3 are the object distance of f_3. So the image distance V_2 of L2 can be calculated as

$$V_2 = -U_3 + D_{L2-L3} \tag{6.7}$$

Based on the gaussian formula, V_2 is directly related to the object distance of L4 and L5. L4 and L5 lie in the same optical configurations, so we only focus on a channel L4. Since, the light goes through the L4 twice, to separate the parameters, 4^1 and 4^2 represents the related variables. The variable with 4^1 is the light first time goes through the L4 whose direction is from L4 to M4. The variable with 4^2 is the light next goes through the L4 whose direction is from M4 to L4. As the V_2 is known, U_{4^1} can be calculated as:

$$U_{4^1} = 0.5D_{L2-L3} - V_2 = U_3 - 0.5D_{L2-L3} \tag{6.8}$$

Then, V_{4^1} can be written as:

$$\frac{1}{f_4} = \frac{1}{U_{4^1}} + \frac{1}{V_{4^1}} \tag{6.9}$$

At the meantime, to achieve the same final image position, V_{4^2} must be:

$$V_{4^2} = -U_3 + 0.5D_{L2-L3} \tag{6.10}$$

So U_{4^2} will be:

$$\frac{1}{f_4} = \frac{1}{U_{4^2}} + \frac{1}{V_{4^2}} \tag{6.11}$$

If we put $-U_3 + 0.5D_{L2-L3}$ as a constant value D, the magnification of $L4^1$ is:

$$M^1 = \frac{V_{4^1}}{-D} = \frac{-f_4}{f_4 + D} \tag{6.12}$$

the magnification of $L4^2$ is:

$$M^2 = \frac{D}{U_{4^2}} = \frac{D - f_4}{f_4} \tag{6.13}$$

The Total magnification of green channel is :

$$M_g = M^1 M^2 = \frac{D - f_4}{D + f_4} \tag{6.14}$$

From the Eq. (6.13), we can find the final magnification is determined by the red channel configuration and focus length of L4. Usually, the configuration of red channel is hard to adjust, but the magnification can be modified by change the lens L4 and L5.

6.2.3 Spatial phase shift analysis

Assuming the illumination and observation plane is in the XOZ plane, the light wave entering the shearing system can be expressed as:

$$u(x, y) = |u(x, y)| exp[i\varphi(x, y)] \tag{6.15}$$

Where, φ(x, y) is the phase value, (x, y) is the pixel location and i is the imaginary unit. The two channels are expected to have the half equal intensity of the whole incidence wave. Thus, Channel #Red and Channel #Green can be expressed as the following equations with horizontal shearing direction.

$$u_{r1}(x,y) = |u_r(x,y)|exp[i\varphi_r(x,y)] \quad (6.16)$$

$$u_{r2}(x,y) = |u_r(x+\Delta x_r,y)|exp[i\varphi_r(x+\Delta x_r,y) + 2\pi i f_1 x] \quad (6.17)$$

$$u_{g1}(x,y) = |u_g(x,y)|exp[i\varphi_g(x,y)] \quad (6.18)$$

$$u_{g2}(x,y) = |u_g(x+\Delta x_g,y)|exp[i\varphi_g(x+\Delta x_g,y) + 2\pi i f_2 x] \quad (6.19)$$

u_{r1} and u_{r2}represent the two beams of Channel #Red while u_{g1} and u_{g2} represent the two beams of Channel #Green. Δx_r and Δx_g are the shearing amount of two channels respectively. Two carrier frequencies $(f_1\ , f_2)$ are introduced into the wave fronts by shearing angles α and β. I_r and $I_g$are used to represent the interference intensity of the two channels on the CCD plane.

$$I_r = (u_{r1} + u_{r2})(u_{r1}^* + u_{r2}^*) \quad (6.20)$$

$$I_g = (u_{g1} + u_{g2})(u_{g1}^* + u_{g2}^*) \quad (6.21)$$

Where * denotes the complex conjugate. The total recorded intensity I can be expressed as:

$$\mathrm{I} = I_r + I_g \quad (6.22)$$

Currently, multiple information is overlapping on the CCD camera. Even the signals of two channels will not have interference due to the polarization angle of two beams of 90 degree, the phase cannot be extracted directly on the spatial domain. To separate the information, spatial phase shift method is induced. The Fourier transform is used to transform the signals from the spatial domain to the frequency domain, which can be represented by:

$$FT(I) = U_{r1}(f_x, f_y) \otimes U_{r1}(f_x, f_y)^* + U_{r2}(f_x + f_1, f_y) \otimes U_{r2}(f_x + f_1, f_y)^* + U_{g1}(f_x, f_y) \otimes U_{g1}(f_x, f_y)^* + U_{g2}(f_x + f_2, f_y) \otimes U_{g2}(f_x + f_2, f_y)^* + U_{r1}(f_x, f_y) \otimes U_{r2}(f_x + f_1, f_y)^* + U_{r2}(f_x + f_1, f_y) \otimes U_{r1}(f_x, f_y)^* + U_{g1}(f_x, f_y) \otimes U_{g2}(f_x + f_2, f_y)^* + U_{g2}(f_x + f_2, f_y) \otimes U_{g1}(f_x, f_y)^* \tag{6.23}$$

The equation can be rearranged as five parts:

$$A(f_x, f_y) = U_{r1}(f_x, f_y) \otimes U_{r1}(f_x, f_y)^* + U_{r2}(f_x + f_1, f_y) \otimes U_{r2}(f_x + f_1, f_y)^* + U_{g1}(f_x, f_y) \otimes U_{g1}(f_x, f_y)^* + U_{g2}(f_x + f_2, f_y) \otimes U_{g2}(f_x + f_2, f_y)^* \tag{6.24}$$

$$B(f_x + f_1, f_y) = U_{r1}(f_x, f_y) \otimes U_{r2}(f_x + f_1, f_y)^* \tag{6.25}$$

$$C(f_x - f_1, f_y) = U_{r2}(f_x + f_1, f_y) \otimes U_{r1}(f_x, f_y)^* \tag{6.26}$$

$$D(f_x - f_2, f_y) = U_{g1}(f_x, f_y) \otimes U_{g2}(f_x + f_2, f_y)^* \tag{6.27}$$

$$E(f_x + f_2, f_y) = U_{g2}(f_x + f_2, f_y) \otimes U_{g1}(f_x, f_y)^* \tag{6.28}$$

Where, symbol $\otimes$ is convolution, f_x and f_y are the variables on frequency domain. As Eq. (4.14-4.18) show, the phase distribution in the Fourier domain is separated into five components: A, B, C, D, and E. Here, A represents the background information, and the remaining components represent the complex amplitudes of the interferogram. If an appropriate carrier frequency is introduced, the phases can be extracted by separating the five components in the frequency domain.

The inverse Fourier Transform is applied to extract the phase information. The phase of spectrum C and D can be expressed as:

$$[\varphi_{r1}(x,y) - \varphi_{r2}(x+\Delta x_r, y) + 2\pi x f_1] = tan^{-1}\frac{Im[u_{r2}u_{r1}^*]}{Re[u_{r2}u_{r1}^*]} \tag{6.29}$$

$$[\varphi_{g1}(x,y) - \varphi_{g2}(x+\Delta x_g, y) + 2\pi x f_2] = tan^{-1}\frac{Im[u_{g1}u_{g2}^*]}{Re[u_{g1}u_{g2}^*]} \tag{6.30}$$

where Im and Re denote the imaginary and real parts, respectively. Then, assuming that the illumination angle is zero, the phase difference caused by the loading can be expressed as:

$$\Delta_{\theta r} = \frac{4\pi\delta x_r}{\lambda}\frac{\partial w}{\partial x} \tag{6.31}$$

$$\Delta_{\theta g} = \frac{4\pi\delta x_g}{\lambda}\frac{\partial w}{\partial x} \tag{6.32}$$

6.3 Experimental validation

A real dual resolution shearography system utilized a 2453 x 2056-pixel grayscale CCD camera with a pixel size of 3.45 μm in the horizontal direction and 3.45 μm in the vertical direction. The imaging lens was 35 mm (f = 35 mm). The focal lengths of L2 and L3 were 100mm (f =100 mm) while the focal lengths of L4 and L5 were 150mm (f=150mm). A Coherent Verdi G5 laser was used, the laser power of 150mW was selected. The split ratios of the normal beam splitter and polarized beam splitter both are 50:50. The real setup is shown on the Figure 6.6.

For the first test, a defect-free aluminum plate with a size of Φ150 was used to verify the feasibility of the dual resolution shearography. The plate was clamped all around and loaded at the center by a screw micrometer. The first image was taken without any loading. After rotating the screw micrometer, the second image was recorded. As the result in Figure 6.7, the proposed system can obtain the two resolution results with only two images in different state.

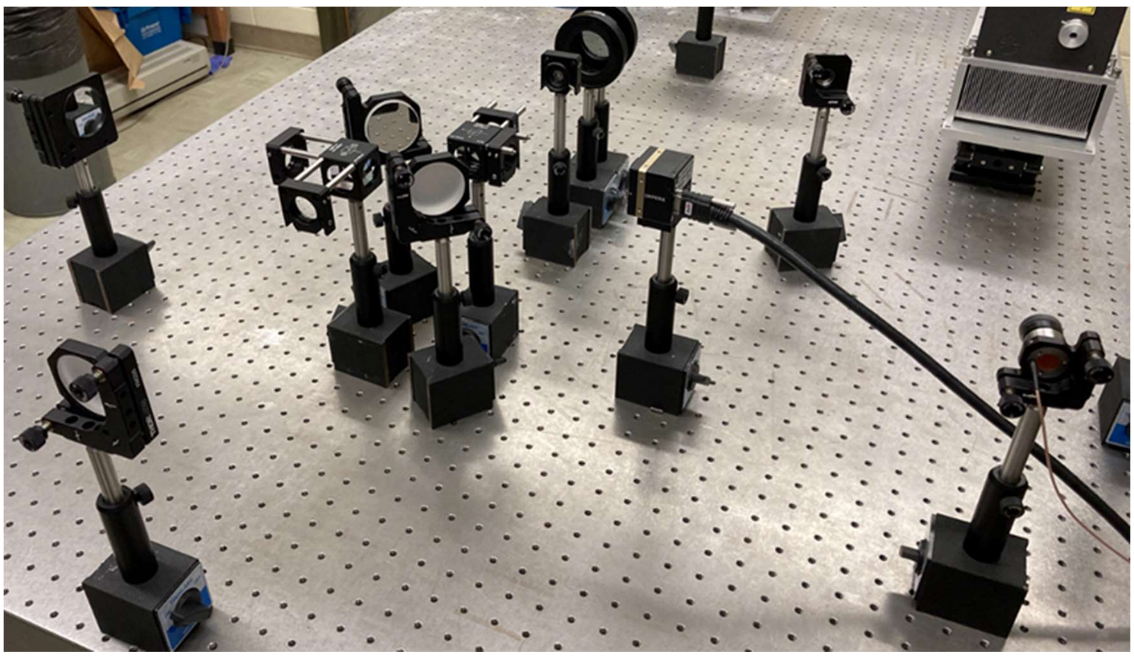

Figure. 6.6. The real setup of the dual sensitive shearography

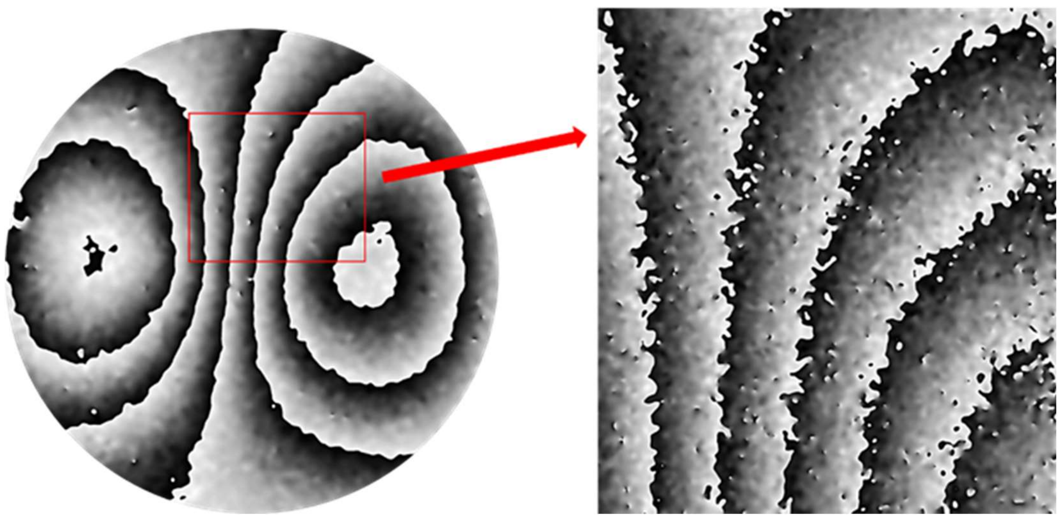

Figure. 6.7. The phase map of two sensitive results of an aluminum plate.

An application of NDT for a round aluminum plate with two different size defects was performed to verify the functionality of the technique proposed in this paper. The plate is 10 mm thick and mounted on a sealed chamber which connected to a vacuum. The first defect is a round shape with 8mm diameter and 0.5mm thick to the surface. The second defect is a round shape with 12mm diameter and 0.5 mm thick to the surface. When the inner pressure was reduced to negative 40 kpa, the valve was released to let the air in while the cameras took the pictures with the acquisition rate of 5 HZ.

As shown in the Figure. 6.8, there are three pairs of results on different loading state. Figure 6.8 (a) presents the large field of view and corresponding small field of view results focusing on the 12 mm defects under 10 kpa pressure difference. In large filed of view window, only a slight pattern can be observed which is hard to separate it from the noise. While, the shearogram is clear in the small filed of view due to the high resolution. It can tell that when the gradients of the deformation are smaller than a single fringe, large filed view result can hardly determine the place of the defects while it is clearly observed on the small field of view. In the Figure 6.8 (b), the loading is 20 kpa difference. The defects can be observed on the large field of the view while a much clear pattern can be found on the small filed view. Continuing to increase the pressure difference to 30 Kpa, the second defect of 8mm diameter is appearing in Figure 6.8 (c), but the surface deformation is too large whose fringe patterns cover the 8mm defect information in large filed of the view because of the weak signal. By changing the zone to the 8 mm filed, small filed view result still can capture this defect which shows the more details of the pattern.

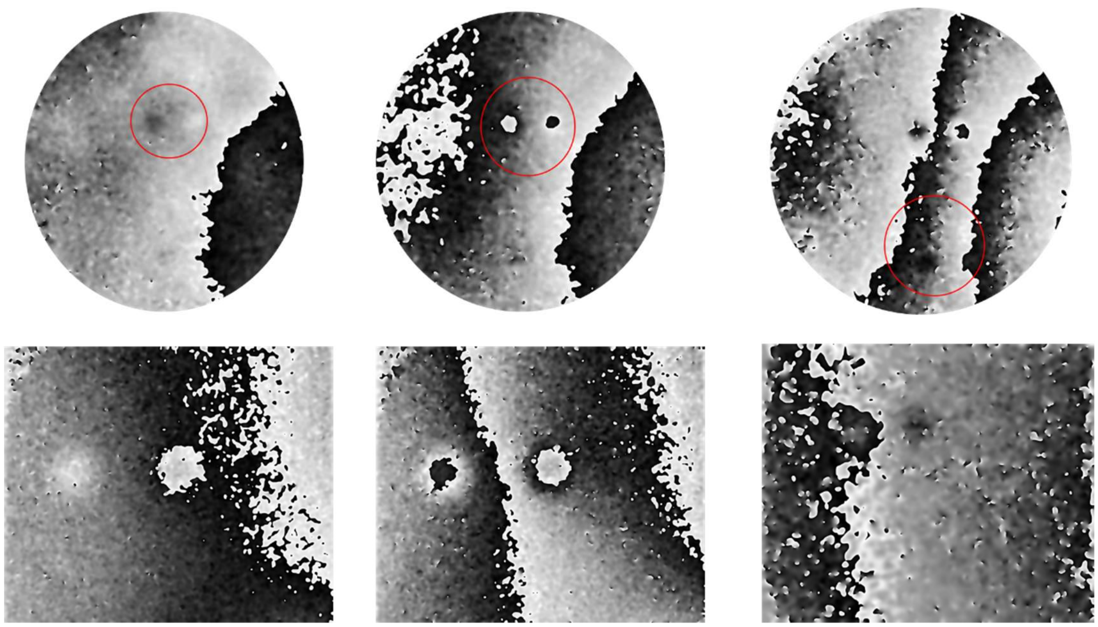

Figure. 6.8. The testing results of a round aluminum plate. (a) 12 mm defect in 10kpa pressure difference. (b) 12 mm defect in 20 kpa pressure difference. (c) 8 mm defect in 30 kpa pressure difference.

6.4 Chapter summary

The proposed system is capable of doing the dual shearing measurement. The difference is that the two channels have different optical configurations. Thus, the x shearing, and y shearing results cannot be consistent because of the different magnification. But the function is still useful for some specials conditions, especially, the defects is unpredictable and in large amount. The Figure 6.9 shows the results of dual sensitivity Digital Shearography in dual shearing measurement application.

The defects are the same as the application in Figure 6.8. Its size is 12 mm, and the testing is under the 15 kpa pressure difference. From the results, it can be proved that dual shearing application can be achieved in dual sensitivity Digital shearography. The large field of view measured the x shearing direction while the small filed of view measure the y shearing direction.

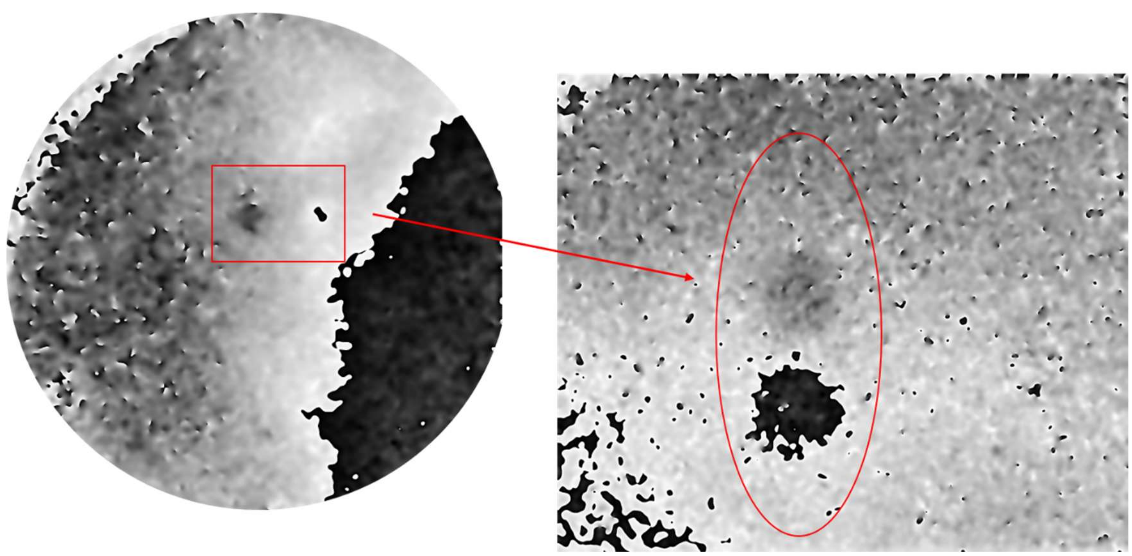

Figure. 6.9. The dual shearing application in dual sensitivity Digital Shearography

The spatial phase shift spectrum needs to be concerned in this application. The cutoff spatial frequency is given as below:

$$f_c = D/2\lambda f \tag{6.23}$$

Where f_c is the cutoff spatial frequency, D is the aperture diameter on the focus plane, λ is the wavelength and f is the focus length of the image lens. In conventional Digital Shearography, usually, only a single image lens existed. However, dual sensitivity Digital Shearography has a different lens pair in two channels. As the schematic in Figure 6.4, L1 is the major image lens but it is not the final image lens of the whole system. In red channel, L1, L2 and L3 forms a complete image lens pair. L2 and L3 play a little influence on the image formation, so the focus length of red channel can be reorganized as the focus length of L1. Green channel has one more lens L4 or L5 than red channel. This lens plays the important role in image formation which adjusts the magnification. So the final focus length of green channel is affected by the L1 and L4. This would make the spectrum size in Fourier domain different of two channels. It requires the cautious choose of aperture size and the lens usage.

A polarized Digital Shearography for dual sensitive measurement is proposed in this research. The system relies on the polarization effect to separate the channels and the spatial phase shift method to extract the phase. Special optical configuration enables the two channels with different sensitive. It has the advantage of enabling simultaneously dynamic measurements in two sensitive filed, which saves the time and labor cost on the application and highly improve the potential of Digital Shearography.

CHAPTER SEVEN

CONCLUSION

Digital Shearography is becoming more and more popular in the application of industry. The basic shearography technology has many limitations which requires various kind of development. Especially, defects inspection is the major task of Digital Shearography. Defects size and shape can play a serious effect on the quality of measurement. Thus, a series developments are proposed to solve the issue.

The research work of this article mainly includes the following contents: 1) Modified Michelson interferometer based dual shearing digital shearography. 2) Spatial light modulator based dual shearing direction shearography. 3) Polarized digital shearography for simultaneous dual sensitive measurement.

With the combination of polarized effect and spatial phase shift, it is capable of doing the dual shearing measurement simultaneously in a dynamic loading with a single laser and single camera. Based on the SLM, dual shearing Digital Shearography is improved in phase map quality and precise shearing amount Dual shearing system solves the issue of incomplete measurement of the narrow crack. With the special optical configuration design, the dual sensitivity measurement is enabled which makes Digital Shearography detect the minor defects in a large field of view.

The core of above research is the development of dual channel system. This concept has potential to spread to other optical system who have the same issue. Based on such developments, Digital Shearography can be more and more industrialized. In the future, Digital shearography can be the prior choice and solution of many NDT inspection and measurement task.

REFERENCE

[1] Bar-Cohen, Y., A.K. Mal, and Z. Chang, Composite material defect characterization using leaky Lamb wave dispersion data. Proceedings of SPIE - The International Society for Optical Engineering, 2011. 3396(2): p. 309-318.

[2] Paolo, et al., Defect and damage analysis of advanced discontinuous carbon/epoxy composite materials. Composites Part A Applied Science & Manufacturing, 2010. 41(7): p. 888-901.

[3] Xu, L., J. Han, and X. Zhang, Defect and its Influence on Mechanical Property of Titanium Diboride-Copper Matrix Composite. Key Engineering Materials, 2007. 336-338(Pt2): p. 1414-1416.

[4] Jiao, J., et al., Vibro-modulation and Guided wave techniques for contact defect detection in plate. Shengxue Xuebao/acta Acustica, 2011. 34(3): p. 242-248.

[5] Scalea, F.L.d., et al., Non-contact ultrasonic inspection of rails and signal processing for automatic defect detection and classification. Or Insight, 2005. 47(6): p. 346-353.

[6] Di Scalea, F.L., et al., Laser-Air-Coupled Hybrid Noncontact System for Defect Detection in Rail Tracks: Status of FRA Prototype Development at University of California-San Diego. Transportation Research Record Journal of the Transportation Research Board, 2006. 1943(1): p. 57-64.

[7] Leendertz, J.A. and J.N. Butters, An image-shearing speckle-pattern interferometer for measuring bending moments. Journal of Physics E Scientific Instruments, 1973. 6(11): p. 1107.

[8] Safarabadi M, Shokrieh MM. Non-destructive Testing (NDT) Techniques in the Measurement of Residual Stresses in Composite Materials: an Overview. Residual Stress Composite materials. Wood head Publishing Limited, 2014.p. 58–75

[9] Santos F, Vaz M, Monteiro J. A new set-up for pulsed digital shearography applied to defect detection in composite structures. Opt Lasers Eng, 2004. 42 (2):131–40.

[10] Krupka R, Walz T, Ettemeyer A. Industrial applications of shearography for inspection of aircraft components. E-J Nondestruct Test, 2003. 8 (2): 476–9.
[11] Hung, Y.Y., A speckle-shearing interferometer: A tool for measuring derivatives of surface displacements. Optics Communications, 1974. 11(2): p. 132-135.
[12] Burch J.M., Leendertz J.A. Speckle pattern and holographic techniques in engineering metrology. Optics and Laser Technology, 1971, 3(1): 26-30.
[13] Nakadate S., Yatagai T., Saito H. Electronic speckle pattern interferometry using digital image processing techniques. Applied Optics, 1980, 19(11): 1879-1883.
[14] Creath K. Phase-shifting speckle interferometry. Applied Optics, 1985, 24(18): 3053-3058.
[15] Hung Y.Y. A speckle-shearing interferometer: a tool for measuring derivatives of surface displacements[J]. Optics Communications, 1974, 11(2): 132-135.
[16] Hung Y.Y. Shearography: a new optical method for strain measurement and nondestructive testing[J]. Optical Engineering, 1982, 21(3): 391-395.
[17] Hung Y.Y. Applications of digital shearography for testing of composite structures[J]. Composites Part B-Engineering, 1999, 30(7): 765-773.
[18] Xu, N., Xie, X., Harmon, G., Gu, R. et al., "Quality Inspection o f Spot Welds using Digital Shearography," SAE Int. J. Mater. Manf.,2012, 5(1): 96-101.
[19] L.X. Yang, F. Chen, W. Steinchen, Y.Y. Hung, "Digital Shearography for Nondestructive Testing: Potentials, Limitations and Applications," J. Holography Speckle, 2004, 1(2): 69 - 79.
[20] Francis, D., R.P. Tatam, and R.M. Groves, Shearography technology and applications: a review. Measurement Science & Technology, 2010. 21(10): p. 102001.
[21] Takai, N. and T. Asakura, Statistical properties of laser speckles produced under illumination from a multimode optical fiber. JOSA A, 1985. 2(8): p. 1282-1290.

[22] Moore, A.J. and J.R. Tyrer, An Electronic Speckle Pattern Interferometer for Complete in Plane Displacement Measurement. Measurement Science & Technology, 1999. 1(10): p. 1024.

[23] Jingbo and Zhang, Two-dimensional in-plane electronic speckle pattern interferometer and its application to residual stress determination. Optical Engineering, 1998. 37(8): p. 2402-2409.

[24] Santos, F., M. Vaz, and J. Monteiro, A new set-up for pulsed digital shearography applied to defect detection in composite structures. Optics & Lasers in Engineering, 2004. 42(2): p. 131-140.

[25] Yang, L., Digital Shearography: Theory and Application of Digital Speckle Pattern Shearing Interferometry. 2003.

[26] Gould, R. Gordon. "The LASER, light amplification by stimulated emission of radiation." In The Ann Arbor conference on optical pumping, the University of Michigan, 1959.15(128): p. 92.

[27] Okwuashi, Chionye J. "Molecular Dynamics Simulation of Nanoindentation and Nanoscratch of Silicon Wafer." PhD diss., Saint Louis University, 2020.

[28] Maiman, T. H. "Optical and microwave-optical experiments in ruby." Physical review letters, 1960. 4(11), p. 564.

[29] Zhang, Keqian, Dejie Li, Keqian Chang, K. Zhang, and D. Li. Electromagnetic theory for microwaves and optoelectronics. Berlin: Springer, 1998.

[30] Akcay, Ceyhun, Pascale Parrein, and Jannick P. Rolland. "Estimation of longitudinal resolution in optical coherence imaging." Applied optics, 2002. 41(25), p. 5256-5262.

[31] Ackermann, Gerhard K., and Jürgen Eichler. Holography: a practical approach. John Wiley & Sons, 2007.

[32] Shipman, James, Jerry D. Wilson, Charles A. Higgins, and Bo Lou. An introduction to physical science. Cengage Learning, 2020.

[33] Sim, C. W., F. S. Chau, and S. L. Toh. "Vibration analysis and non-destructive testing with real-time shearography." Optics & Laser Technology, 1995. 27(1), p. 45-49.

[34] Ettemeyer, A. "Shearografie-ein optisches Verfahren zur zerstörungsfreien Werkstoffprüfung/Shearography-an optical method for nondestructive testing." tm-Technisches Messen, 1991. 58(6), p. 247-252.

[35] Hung, Y. Y., HuaiMin Shang, and Lian Xiang Yang. "Unified approach for holography and shearography in surface deformation measurement and nondestructive testing." Optical engineering, 2003. 42(5), p. 1197-1207.

[36] Steinchen, W., L. Yang, G. Kupfer, and P. Mäckel. "Non-destructive testing of aerospace composite materials using digital shearography." Proceedings of the Institution of Mechanical Engineers, Part G: Journal of Aerospace Engineering, 1998. 212(1), p. 21-30.

[37] Blain, Pascal, Fabrice Michel, Yvon Renotte, and Serge Habraken. "Using a Savart plate in optical metrology." In Interferometry XV: Applications, International Society for Optics and Photonics, 2010. 779107.

[38] Blain, Pascal, Pierre Piron, Yvon Renotte, and Serge Habraken. "An in-line shearography setup based on circular polarization gratings." Optics and Lasers in Engineering, 2013. 51(9), p.1053-1059.

[39] Blain, Pascal, Fabrice R. Michel, Pierre Piron, Yvon L. Renotte, and Serge Habraken. "Combining shearography and interferometric fringe projection in a single device for complete control of industrial applications." Optical Engineering, 2013. 52(8), p. 084102.

[40] Viotti, Matias R., Walter Kapp, and Armando Albertazzi G Jr. "Achromatic digital speckle pattern interferometer with constant radial in-plane sensitivity by using a diffractive optical element." Applied optics, 2009. 48(12), p. 2275-2281.

[41] Viotti, Matias R., Armando Albertazzi G Jr, and Walter A. Kapp. "Mechanical stress measurement by an achromatic optical digital speckle pattern interferometry strain sensor with radial in-plane sensitivity: experimental comparison with electrical strain gauges." Applied optics, 2011. 50(7), p. 1014-1022.

[42] Viotti, Matias R., Armando Albertazzi Jr, Danilo Bonomo, and Filipe Fontana. "Radial in-plane digital speckle pattern interferometer combined with instrumented indentation." Optics and Lasers in Engineering, 2015. 71, p.1-8.

[43] Kohler, Christian, Matias R. Viotti, and G. Armando Albertazzi Jr. "Measurement of three-dimensional deformations using digital holography with radial sensitivity." Applied optics, 2010. 49(20), p. 4004-4009.

[44] Viotti, Matias R., and Armando Albertazzi G Jr. "Robust speckle metrology for stress measurements outside the lab." In Optical measurement systems for industrial inspection IX, International Society for Optics and Photonics, 2015. 9525, p. 95250T.

[45] Baker, R. Jacob. CMOS: mixed-signal circuit design. john Wiley & sons, 2008.

[46] Fossum, Eric R., and Donald B. Hondongwa. "A review of the pinned photodiode for CCD and CMOS image sensors." IEEE Journal of the electron devices society, 2014.

[47] Xie, Xin, Lianxiang Yang, Xu Chen, Nan Xu, and Yonghong Wang. "Review and comparison of temporal-and spatial-phase shift speckle pattern interferometry for 3D deformation measurement." In Sixth International Symposium on Precision Mechanical Measurements, International Society for Optics and Photonics, 2013. 8916, p. 89160D.

[48] Furukawa, T., K. Ishida, and E. Fukada. "Piezoelectric properties in the composite systems of polymers and PZT ceramics." Journal of Applied Physics, 1979. 50(7) p. 4904-4912.

[49] Panda, P. K., and B. Sahoo. "PZT to lead free piezo ceramics: a review." Ferroelectrics, 2015. 474(1), p. 128-143.

[50] Savakus, H. P., K. A. Klicker, and R. E. Newnham. "PZT-epoxy piezoelectric transducers: a simplified fabrication procedure." Materials Research Bulletin, 1981. 16(6), p. 677-680.

[51] Kothiyal, Mahendra P., and Claude Delisle. "Rotating analyzer heterodyne interferometer: error analysis." Applied optics, 1985 24(15), p. 2288-2290.

[52] Gerrard, Anthony, and James M. Burch. Introduction to matrix methods in optics. Courier Corporation, 1994.

[53] Helen, S. Suja, M. P. Kothiyal, and R. S. Sirohi. "Achromatic phase shifting by a rotating polarizer." Optics Communications 1998.154 (5), p. 249-254.

[54] Murukeshan, V. M., Ong Lin Seng, and A. Asundi. "Polarization phase shifting shearography for optical metrological applications." Optics & Laser Technology, 1998. 30(8), p. 527-531.

[55] Kreis, Thomas M., Ralf Biedermann, and Werner PO Jueptner. "Evaluation of holographic interference patterns by artificial neural networks." In Interferometry VII: Techniques and Analysis, International Society for Optics and Photonics, 1995. 2544, p. 11-24

[56] Creath, Katherine. "Phase-shifting speckle interferometry." Applied Optics, 1985. 24(18), p. 3053-3058.

[57] Hung, M. Y. Y., K. W. Long, and J. Q. Wang. "Measurement of residual stress by phase shift shearography." Optics and Lasers in Engineering, 1997. 27(1), p.61-73.

[58] Zhu, Lianqing, Yonghong Wang, Nan Xu, Sijin Wu, Mingli Dong, and Lianxiang Yang. "Real-time monitoring of phase maps of digital shearography." Optical Engineering, 2013. 52(10), p. 101902.

[59] Xie, Xin, Lianxiang Yang, Xu Chen, Nan Xu, and Yonghong Wang. "Review and comparison of temporal-and spatial-phase shift speckle pattern interferometry for 3D deformation measurement." In Sixth International Symposium on Precision Mechanical Measurements, International Society for Optics and Photonics, 2013. 8916, p.89260D.

[60] Yang, L. X., W. Steinchen, M. Schuth, and G. Kupfer. "Precision measurement and nondestructive testing by means of digital phase shifting speckle pattern and speckle pattern shearing interferometry." Measurement, 1995. 16(3), p. 149-160.

[61] Takeda, Mitsuo, Quan Gu, Masaya Kinoshita, Hideaki Takai, and Yosuke Takahashi. "Frequency-multiplex Fourier-transform profilometry: a single-shot three-dimensional shape measurement of objects with large height discontinuities and/or surface isolations." Applied optics,1997. 36(22), p. 5347-5354.

[62] Kolenovic, Ervin, Wolfgang Osten, Reiner Klattenhoff, Songcan Lai, Christoph von Kopylow, and Werner Jüptner. "Miniaturized digital holography sensor for distal three-dimensional endoscopy." Applied optics, 2003. 42(25), p. 5167-5172.

[63] Gong, X. L., and S. Toyooka. "Investigation on mechanism of plastic deformation by digital speckle pattern interferometry." Experimental mechanics, 1999. 39(1), p. 25-29.

[64] Restivo, Gaetano, Gary L. Cloud, Rob M. Beaudry, and Basavaraju B. Raju. 3-D Strain fields using embedded DSPI: pilot study. ARMY TANK AUTOMOTIVE RESEARCH DEVELOPMENT AND ENGINEERING CENTER WARREN MI, 2004.

[65] Baik, Sung-Hoon, Seung-Kyu Park, Cheol-Jung Kim, and Soo-Yong Kim. "Two-channel spatial phase shifting electronic speckle pattern interferometer." Optics communications, 2001. 192(3), p. 205-211.

[66] Fu, Yu, Min Guo, and Huan Liu. "Determination of instantaneous curvature and twist by digital shearography." Optical Engineering, 2012. 51(8), p. 083602.

[67] Pedrini, G., Y. L. Zou, and H. J. Tiziani. "Quantitative evaluation of digital shearing interferogram using the spatial carrier method." Pure and Applied Optics: Journal of the European Optical Society Part A, 1996. 5(3), p. 313.

[68] Pedrini, Giancarlo, Wolfgang Osten, and Mikhail E. Gusev. "High-speed digital holographic interferometry for vibration measurement." Applied optics, 2006. 45(15), p. 3456-3462.

[69] Bhaduri, Basanta, N. Krishna Mohan, M. P. Kothiyal, and R. S. Sirohi. "Use of spatial phase shifting technique in digital speckle pattern interferometry (DSPI) and digital shearography (DS)." Optics express, 2006 14(24), p. 11598-11607.

[70] Bhaduri, Basanta, Nandigana Krishna Mohan, and Mahendra Prasad Kothiyal. "Simultaneous measurement of out-of-plane displacement and slope using a multiaperture DSPI system and fast Fourier transform." Applied optics, 2007. 46(23), p. 5680-5686.

[71] Pedrini, G., Y-L. Zou, and H. J. Tiziani. "Simultaneous quantitative evaluation of in-plane and out-of-plane deformations by use of a multidirectional spatial carrier." Applied optics, 1997. 36(4), p. 786-792.

[72] Pedrini, G., Y. L. Zou, and H. J. Tiziani. "Quantitative evaluation of digital shearing interferogram using the spatial carrier method." Pure and Applied Optics: Journal of the European Optical Society Part A, 1996. 5(3), p. 313.

[73] Pedrini, Giancarlo, Wolfgang Osten, and Mikhail E. Gusev. "High-speed digital holographic interferometry for vibration measurement." Applied optics, 2006. 45(15), p. 3456-3462.

[74] Kohler, Christian, Matias R. Viotti, and G. Armando Albertazzi Jr. "Measurement of three-dimensional deformations using digital holography with radial sensitivity." Applied optics, 2010. 49(20), p. 4004-4009.

[75] Bhaduri, Basanta, Nandigana Krishna Mohan, and Mahendra Prasad Kothiyal. "Simultaneous measurement of out-of-plane displacement and slope using a multiaperture DSPI system and fast Fourier transform." Applied optics, 2007. 46(23), p. 5680-5686.

[76] Xie, Xin, Nan Xu, Jianfei Sun, Yonghong Wang, and Lianxiang Yang. "Simultaneous measurement of deformation and the first derivative with spatial phase-shift digital shearography." Optics Communications, 2013. 286, p. 277-281.

[77] Schedin, Staffan, Giancarlo Pedrini, Hans J. Tiziani, and Fernando Mendoza Santoyo. "Simultaneous three-dimensional dynamic deformation measurements with pulsed digital holography." Applied optics, 1999. 38(34), p.7056-7062.

[78] X. Xie, L. X. Yang, N. Xu, and X. Chen. "Michelson interferometer based spatial phase shift shearography." Appl. Opt, 2013. 52(17), p.4063-4071.

[79] Tang, C., et al., Denoising by coupled partial differential equations and extracting phase by backpropagation neural networks for electronic speckle pattern interferometry. Applied Optics, 2007. 46(30): p. 7475-84.

[80] Aebischer, H.A. and S. Waldner, Simple and effective method for filtering speckle-interferometric phase fringe patterns. Optics Communications, 1999. 162(4): p. 205-210.

[81] Da′ vila and Abundio, Scale-space filter for smoothing electronic speckle pattern interferometry fringes. Optical Engineering, 1996. 35(12): p. 3549-3554.

[82] Bone, D.J., Fourier fringe analysis: the two-dimensional phase unwrapping problem. Applied Optics, 1991. 30(25): p. 3627-32.

[83] Flynn, T.J., Two-dimensional phase unwrapping with minimum weighted discontinuity. Journal of the Optical Society of America A, 1997. 14(10): p. 2692-2701.

[84] Steinchen W, Yang L.: Digital shearography: theory and application of digital speckle pattern shearing interferometry. Bellingham, USA: SPIE Press, 2003.

[85] Siebert, T., Schmitz, B.: New shearing setup for simultaneous measurement of two shear directions. Proc. SPIE, 1999. 3637, p. 225-231.

[86] G. L. Richoz, G. S. Schajer, "Simultaneous two-axis shearographic interferometer using multiple wavelengths and a color camera," Opt Lasers Eng. 2016; 77, p. 143-53

[87] Wang, Y., Gao, X., Xie, X., Wu, S., Liu, Y., Wang, L.: Simultaneous dual directional strain measurement using spatial phase-shift digital shearography. Opt. Laser Eng, 2016. 87, p. 197-203.

[88] Xie, X., Lee, C. P., Li, J., Zhang, B., Yang, L.: Polarized digital shearography for simultaneous dual shearing directions measurements. Rev. Sci. Instrum, 2016. 87(8), 083110.

[89] Malacara, Daniel, ed.: Optical shop testing. Vol. 59. John Wiley & Sons, 2007.

[90] F. Sun, et al, "The application of SLM in shearography detecting system." Optics and Lasers in Engineering, 2019. 114 p.90-94.

[91] S. Wu, X. He, and L. Yang, "Enlarging the angle of view in Michelson-interferometer-based shearography by embedding a 4f system," Appl. Opt, 2011. 50, p. 3789.

[92] Richmond, T.J., Crystal structure of the nucleosome core. Nature, 1998. 12(8): p. A1313.

[93] Schadt, M. and W. Helfrich, VOLTAGE‐DEPENDENT OPTICAL ACTIVITY OF A TWISTED NEMATIC LIQUID CRYSTAL. Applied Physics Letters, 1971.

[94] Lien and A., Extended Jones matrix representation for the twisted nematic liquid-crystal display at oblique incidence. Applied Physics Letters, 1990. 57(26): p. 2767-2769.

[95] Hornbeck, L.J., Spatial light modulator and method. 1987.

[96] Schreiber, Karl Ulrich, T. Klügel, J-PR Wells, R. B. Hurst, and A. Gebauer. "How to detect the chandler and the annual wobble of the earth with a large ring laser gyroscope." Physical Review Letters, 2011. 107(17), p. 173904.

[97] Simonelli, Andreino, Jacopo Belfi, Nicolò Beverini, Giorgio Carelli, Angela Di Virgilio, Enrico Maccioni, Gaetano De Luca, and Gilberto Saccorotti. "First deep underground observation of rotational signals from an earthquake at teleseismic distance using a large ring laser gyroscope." arXiv preprint arXiv, 2016.1601, p. 05960.